



LEVEL #

12

SACLANTCEN Report  
SR - 42 ✓

SACLANT ASW  
RESEARCH CENTRE  
REPORT

AD A095018

SEISMIC INTERFACE WAVES IN COASTAL WATERS: A REVIEW

by

DIETER RAUCH

DTIC  
ELECTE  
FEB 13 1981

A

15 NOVEMBER 1980

NORTH  
ATLANTIC  
TREATY  
ORGANIZATION

This document has been approved  
for public release and sale; its  
distribution is unlimited.

LA SPEZIA, ITALY

This document is unclassified. The information it contains is published subject to the conditions of the legend printed on the inside cover. Short quotations from it may be made in other publications if credit is given to the author(s). Except for working copies for research purposes or for use in official NATO publications, reproduction requires the authorization of the Director of SACLANTCEN.

FILE COPY

This document is released to a NATO Government at the direction of the SACLANTCEN subject to the following conditions:

1. The recipient NATO Government agrees to use its best endeavours to ensure that the information herein disclosed, whether or not it bears a security classification, is not dealt with in any manner (a) contrary to the intent of the provisions of the Charter of the Centre, or (b) prejudicial to the rights of the owner thereof to obtain patent, copyright, or other like statutory protection therefor.

2. If the technical information was originally released to the Centre by a NATO Government subject to restrictions clearly marked on this document the recipient NATO Government agrees to use its best endeavours to abide by the terms of the restrictions so imposed by the releasing Government.



14

SACLANTCEN ~~REPORT~~ -SR-42

NORTH ATLANTIC TREATY ORGANIZATION

SACLANT ASW Research Centre  
Viale San Bartolomeo 400, I-19026 San Bartolomeo (SP), Italy

tel: national 0187 560940  
international + 39 187 560940

telex: 271148 SACENT I

12 106

(1) SEISMIC INTERFACE WAVES IN COASTAL WATERS: A REVIEW

by

(1) Dieter/Rauch

(11) 15 November 1980

This report has been prepared as part of Project 05.

✓  
APPROVED FOR DISTRIBUTION

*B.W. Lythall*  
B.W. LYTTHALL  
Director

A  
210150

TABLE OF CONTENTS

	<u>Page</u>
ABSTRACT	1
LIST OF SYMBOLS AND ABBREVIATIONS	3
INTRODUCTION	5
1 THEORETICAL ASPECTS OF SEISMIC WAVE PROPAGATION IN THE SEA FLOOR	9
1.1 Basic Types of Seismic Body and Interface Waves	9
1.2 Elementary Relations for an Idealized Plane Harmonic Scholte Wave	13
1.3 Wave-front Pattern of a Point Source Close to an Interface	24
1.4 Sound Propagation in a Stratified Oceanic Lithosphere and a Wedge-shaped Water Layer on Top	32
1.5 Some Analytic Approaches and Model Experiments Regarding Annular Scholte-wave Pulses	40
2 EXPERIMENTAL ASPECTS OF SEISMIC SENSING AT THE OCEAN BOTTOM	47
2.1 Geophones as Standard Transducers for the Detection of Seismic Signals	47
2.2 Some Essential Features of Sea-floor Acoustics	49
2.3 Acoustic and Seismic Ambient Noise Data from Shallow-Water Areas	57
2.4 Field Experiments Concerning Seismic Detection of Waterborne Infrasound	61
3 MODELLING OF SEISMIC WAVE PROPAGATION IN THE SEA-FLOOR	67
3.1 Characteristics of the Thomson-Haskell Matrix Method	67
3.2 Some Preliminary Results from the Fast-Field Program	71
CONCLUSIONS AND PROPOSALS FOR FUTURE RESEARCH PROGRAMMES	77
REFERENCES	81
APPENDIX A POST-1978 WORK AT SACLANTCEN	95

List of Figures

1. Particle displacements, their resulting orbits, and energy flux densities, for a monochromatic Scholte wave at a water/sediment interface.	20
2. Primary (T) and secondary traces (T') as the results or origins of different wave-front patterns at the interface of two solids.	26
3. The most complicated wave-front pattern at the interface of two solids.	31
4. Dispersion curves for the symmetric ( $s_v$ ) and antisymmetric ( $a_v$ ) propagation modes in a free plate.	33
5. Phase-velocities of the lowest modes in shallow water over a liquid-like or rock-like bottom.	34

TABLE OF CONTENTS (Cont'd)	Page
6. Typical reflection coefficients at a very soft sedimentary sea floor (A) and at a very hard rock-bottom (B).	36
7. Phase-velocities of the lowest modes in shallow water over a relative "soft" rock-bottom.	38
8. Comparison of Strick's modelling results with the laboratory measurements by Roeber and Vining.	43
9. Frequency dependence of the attenuation coefficient $\alpha_p$ for compressional waves in sediments.	53
10. Depth dependence of the attenuation factor $K_p$ for compressional waves in sediments.	55
11. Sound-pressure spectrum levels for different noise sources in the sea.	58
12. Averaged vertical and horizontal velocity spectrum levels on the sea floor in shallow water.	60
13. Averaged vertical velocity spectrum levels for different sites on land and on the sea floor in shallow and deep water.	60
14. Range dependence of the acoustic and seismic transmission loss for a 10 Hz source over different thick sand layers.	72
15. Range dependence of the acoustic and seismic transmission loss for a 10 Hz source over different thin sand layers.	73
16. Range dependence of the seismic transmission loss for a 10 Hz source over and on a thin sand layer.	74
17. Range dependence of the acoustic and seismic transmission loss for a 10 Hz source in different water columns over a thin sand layer.	75
18. Frequency dependence of the acoustic and seismic transmission loss at a fixed range of 10 km for a 10 Hz source over a thin sand layer.	76
A1 Installation of the sensor package on the sea floor and mooring of its radio buoy in shallow water	95
A2 Electronic block-diagram.	97
A3 The operational area off the Versilian coast (Italy) with the two chosen OBS-positions.	98
A4 Line-printer plot of the signals from the four basic sensors.	99
A5 Radial and vertical particle velocity of the interface wavelet in Fig. A4 with the resulting hodographs.	100
A6 (a) Stacking of the vertical particle-velocity for an acoustic run over a layered sediment-bottom.	101
A6 (b) Stacking of the radial particle-velocity for the same acoustic run as in A6(a).	102
Table 1 Classification of the basic interface-waves, with an estimation of their phase-velocities.	11
Table 2 Classification of different wave-front patterns at the interface of two solids.	28
Table 3 Densities $\rho$ , velocity ratios $n$ , and attenuation factors $K$ , for typical bottom layers.	52

## SEISMIC INTERFACE WAVES IN COASTAL WATERS: A REVIEW

by

Dieter Rauch

ABSTRACT

↙ The basic elements of seismic wave propagation in the upper sea floor are presented, special emphasis being devoted to the often-neglected interface phenomena (Scholte- and Stoneley waves). The most important theoretical approaches to the seismic sensing of waterborne sound are discussed briefly and a great deal of the pertinent field work since World War II is reviewed. Some guidelines are given for future research activities in this interdisciplinary field, which combines the low-frequency regime of underwater acoustics and the high-frequency regime of seismology. An extensive bibliography is provided.

↑

LIST OF SYMBOLS AND ABBREVIATIONS

$a_v, A_v$	Index or prefix for "asymmetric" or "acoustic"
$A_{n,m}$	Amplitude-factors
$\mathcal{A}_m = (a_{\mu\nu})_m$	(4x4)-layer-matrix of the m-th layer
$\mathcal{A}_{\text{syst}}$	(4x4)-system-matrix of a stack of layers
$B_n$	Amplitude-factors
$c, c_o, c_v$	Phase-velocities
$C( ) ; D( )$	Weighting-functions ("excitation"; "response")
$E$	Young's modulus
$E_v$	Amplitude-factors of the energy density
$f, f_v$	Frequencies
$F( ) ; G( )$	Period- resp. response function of the system
$H$	Density ratio
$h ; H_n = L$	Vertical distance; layer thicknesses
$k, k_v$	Wave numbers
$K_v$	Attenuation factors
$\hat{\mathcal{A}}_m$	(4)-field-vector of the m-th layer
$\bar{m}, \underline{m}$	Top- resp. bottom of the m-th layer
$m, q, s$	Transverse wave numbers (decay constants)
$M, Q, S, Y$	Amplitude factors
$n ; n_v$	Index resp. factors
$N, R, X$	Velocity ratios
$p, s ; P-, S-$	Index resp. prefix for "compressional" or "shear"
$p_v ; \hat{p}_v$	Pressures resp. pressure-amplitudes
$r$	Horizontal distance (range)
$S_o ; R_o$	Source resp. receiver

$\vec{s} = (u, v, w)$	Displacement vector
$\hat{u}, \hat{v}, \hat{w}$	Amplitudes of the displacement components
$s_v$	Index or prefix for "symmetric" or "seismic"
$S_v$	Abbreviations
$\mathcal{S}_0$	(4)-source-vector
$t; T, T_0$	Time variable resp. constant time periods
$T_v; T_{\mu\nu}$	Traces of wave fronts resp. amplitude factors
$\mathcal{T}$	(3x3)-stress-tensor
$v_v$	Trace velocities of the wave fronts
$w$	Index for "water"
$(x, y, z)$	Space variables (Cartesian coordinates)
$\bar{\alpha}_v$	Plane wave attenuation coefficients
$\beta_v; \gamma_v = \frac{\pi}{2} \beta_v$	Grazing angles resp. angles of incidence
$\delta, \mu$	Lamé's constants
$\vec{\varepsilon} = (\xi, \zeta, \eta)$	Vector of the energy flux density
$\Gamma_v$	Total energy fluxes
$\kappa$	Modulus of compressibility
$\lambda$	Wavelength
$\mu, \nu$	Indices
$\rho$	Mass density
$\sigma$	Poisson's modulus
$\tau_{\mu\nu}$	Stress components
$\phi, \psi$	Displacement potentials
$\chi_0$	Source pulse
$\omega = 2\pi f$	Angular frequency
$\Omega_v$	Phase angles



## INTRODUCTION

The purpose of this report is to give an introduction to the physics of seismic wave propagation in the sea-floor and to present the state of knowledge on seismic sensing of waterborne sound according to the open literature published before 1979. Due to this twofold task, the report has both to deal with different, highly-specialized fields and to attempt to synthesize them in a way that may serve as a starting point for future interdisciplinary studies. As a result, many pertinent aspects of underwater acoustics and seismology can be discussed only in a quite superficial way; however, the interested reader is furnished with an extensive reference list to compensate for these unavoidable restrictions.

For the same reason, the presentation of mathematical derivations is restricted to some basic but quite instructive considerations in Sects. 1.2 and 3.1. The reader who is more interested in the phenomenological or experimental aspects of seismic sensing of the sea floor may simply skip those chapters without interrupting the context.

The sound field radiated by a water-borne source and propagating in shallow water or from deep to shallow water over a sloping bottom [1] is strongly affected by the acoustic properties of the sea floor. The ocean bed has to be considered not only as a lossy boundary but also as a quite complicated liquid/solid structure that can support a great variety of wave-propagation phenomena. From this seismic point of view it is obvious that the acoustic energy penetrating into the sea floor may sometimes contribute considerably to medium-range and long-range acoustic transmission. One of the most drastic examples of this is the existence of a low-frequency cut-off for the first mode in shallow water. For all frequencies below this limit the sound field ducted by the water column is in-phase and exponentially evanescent, so that the liquid layer loses its wave-guide character. The affect of a very unfavourable sound-speed profile is much less spectacular, of course, but it may be quite obstructive to the propagation of higher frequencies as well and thus shade off shallow-water areas from a source in deep water.

Under these restrictions, even medium-range propagation of infrasonic energy (frequency band of about 1 to 30 Hz) can happen only along seismic

channels. During the enormous progress of underwater acoustics since World War II there has been a constant but rather moderate interest in these aspects of seismic propagation of waterborne sound. Being at the low-frequency end of classical sonar activity and at the high-frequency end of seismic research, the propagation of infrasonic energy was tackled only sporadically and incoherently. Due to a more systematic study of sea-floor acoustics and to important improvements in the theoretical means (computer-models) and experimental tools (Ocean-Bottom Seismometers and Seismic Arrays) available during the last two decades, this interdisciplinary field seems now to be receiving much more interest. During a recent workshop at the U.S. Office of Naval Research, Washington D.C. [2] the experts complained of the existing lack of knowledge and recommended the study of two potential infrasonic detection methods: either the deployment of ocean-bottom seismometers to probe the marginal portion of the seismic wave-field and/or the installation of rather deeply buried seismic arrays (e.g. in boreholes) to scan its shallow-refracted portion.

For operational reasons (to initiate a relatively inexpensive and very flexible system) this report puts emphasis on the theoretical and practical aspects of the former project (ocean-bottom seismometers), which moreover fits perfectly into SACLANTCEN's current sea-floor studies. Because of their efficient excitation and minimal geometrical spreading, the only seismic wave-types in the marginal zone that are of interest are those that are well trapped within the top layers of the ocean bed or are well-guided along a boundary at or just below the water/bottom interface. In spite of this strong guidance the waves chosen should be governed by the least possible dispersion (minimized multipath propagation or almost no interaction with other nearby boundaries) and no radiation losses should occur in favour of other wave types. This report will show that apart from horizontally-polarized shear waves – the Love waves – only the genuine interface waves of the Stoneley or the Scholte type meet all these requirements from the theoretical point of view. Accordingly we will discuss their physics, examine the existing experimental data, and give some modelling results by using SACLANTCEN's Fast Field Program (FFP).

The propagation-loss curves presented are calculated with realistic (plane wave) attenuation coefficients but they do not yet account for parameter profiles within the layers, and even our advanced model will never be able to take into account spatial variations of the layers or inhomogeneities.

These latter features alone render the real-world propagation conditions much more complex by creating a favourable upward refraction, and simultaneously, very detrimental dispersion and scattering effects. Thus all field signals will strongly depend on the specific terrain traversed. Accordingly, the corresponding receiver configuration (single OBS-station, distributed OBS-system, or OBS-arrays) will have to undergo an extensive calibration procedure before it can be used for surveillance purposes. Concerning the sensors, the use of the ocean bottom for sound transmission will require a feasibility study of seismometers, alternately called geophones, instead of, or together with, the commonly-used hydrophones. The basic characteristics of these motion-detectors will therefore be discussed and the ambient-noise background in the sea will be compared with that attributable to the rather unexplored movements of the sea-floor in shallow-water areas.

Certainly this and other seismic detection methods will never replace the highly-developed sonar techniques but in coastal waters they may offer a valuable support, or the only acoustic alternative, if the classical listening techniques lose accuracy or even fail.

## 1 THEORETICAL ASPECTS OF SEISMIC WAVE PROPAGATION IN THE SEA FLOOR

### 1.1 Basic Types of Seismic Body and Interface Waves

Due to its latticed microstructure, a solid medium can support two basic types of elastic waves: the compressional or P-wave (sometimes also called "density" wave) having a particle deflection parallel to the direction of propagation, and the shear or S-wave having a particle deflection normal to this direction. In a boundless, non-absorbing, homogeneous and isotropic solid these two "body" or "bulk" waves propagate independently of each other with their characteristic phase velocities of  $c_p$  and  $c_s = nc_p$ , with  $0 < n < 0.717$ . These fundamental sound speeds (dealing with isotropic media, we will understand the terms "velocity" and "speed" as synonyms and therefore use them interchangeably) are related to the mass-density  $\rho$  and to the elastic constants  $\delta$  and  $\mu$  (Lamè's constants) or  $\sigma$  and  $E$  (Poisson's and Young's modulus) by

$$c_p = \left[ \frac{\delta + 2\mu}{\rho} \right]^{\frac{1}{2}} = \left[ \frac{(1-\sigma)E}{\rho(1+\sigma)(1-2\sigma)} \right]^{\frac{1}{2}} \quad (\text{Eq. 1a})$$

$$c_s = \left[ \frac{\mu}{\rho} \right]^{\frac{1}{2}} = \left[ \frac{E}{2\rho(1+\sigma)} \right]^{\frac{1}{2}} = \left[ \frac{1-2\sigma}{2(1+\sigma)} \right]^{\frac{1}{2}} c_p, \quad (\text{Eq. 1b})$$

with  $0 < \sigma < 0.5$  for all materials. Another often-used constant combining the pair  $(\delta, \mu)$  or  $(\sigma, E)$  is the modulus of compressibility

$$\kappa = \frac{3}{3\delta + 2\mu} = \frac{3(1-2\sigma)}{E}. \quad (\text{Eq. 2})$$

Non-absorbing liquids have no shear rigidity ( $\mu=0$ ) and can accordingly support no shear waves.

Before passing over to more complicated wave types in homogeneous, isotropic media we would like to clarify some often-used notations. In the field of elastic and electromagnetic wave propagation the shortened terms "plane wave", "cylindrical wave", or "spherical wave" are generally used for the so-called "homogeneous" waves. These are wave fields in which the surfaces of constant phase do not only have the denoted geometry but are

also identical to the surfaces of constant amplitude. Hence we will in general apply the same nomenclature, but the reader should keep in mind that we do it on the tacit understanding that we are dealing with those homogeneous waves that are characterized by a constant amplitude on a given phase surface. In practice almost all fields are, strictly speaking, "non-homogeneous", having surfaces of constant phase and constant amplitude that do not coincide. Accordingly these non-homogeneous waves are provided with a more or less irregular distribution of the amplitude on a given phase surface, such as those due to the radiation pattern of a real source, for example. It has to be remembered that the present report is essentially concerned with "inhomogeneous" waves representing propagation phenomena that have very regular and well-defined deviations from homogeneity.

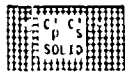

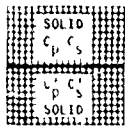
As soon as "pure" body waves impinge on a free surface of a solid, or on a marginal interface with another medium, they are partly converted into each other and their coupling may create "mixed" wave types in the immediate vicinity of the interface. This splitting of the bulk waves, both in the reflected ("inner refraction") and in the refracted field, is an immediate consequence of the specific boundary – or transition – conditions that have to be fulfilled there. In addition to these conditions, their coupling in the form of different interface waves requires incoming plane or cylindrical waves with complex angles of incidence or, in other words, the grazing incidence of inhomogeneous plane or cylindrical waves with an exponential amplitude decay for growing distance from the interface. At first glance, these additional requirements seem to be quite extraordinary, but the mathematical treatment of realistic field patterns reveals that the occurrence of such inhomogeneous field components is due to the more complicated (higher-degree) curvature of the incoming homogeneous wave-fronts or the finite width (amplitude-shading) of the incident beams. In the simple case of incoming cylindrical or spherical waves we can see this immediately from the well-known Sommerfeld integral [3 to 8] or Weyl integral [5 to 9], which break those fields down into an infinite sum of inhomogeneous plane or cylindrical contributions.

The most important interface phenomena are the so-called "free" interface waves that propagate along the surface between two media without subsequent delivery of energy from sources outside the interface. We have already mentioned that their existence demands the combined action of compressional

and shear waves, which is why at least one of the two media has to be a solid while the other may be a solid, a liquid, or a vacuum. Accordingly, no interface wave can be excited at the surface between two liquids, except that in conditions of high viscosity there may occur a non-linear propagation phenomenon analogous to the electro-magnetic Zenneck wave [10] at the interface of two dielectric media.

We have to be yet more precise about the indispensable shear contribution to the synthesis of more complicated elastic fields. Only that component of the shear deflection that is polarized vertically to the given boundary – the so-called SV-wave – can participate in the formation of such mixed wave types propagating with characteristic trace velocities (= resulting phase velocities) along the respective wave guide. When there are two adjacent, homogeneous half-spaces (or sufficient high frequencies), "genuine" interface waves and/or their so-called "generalized" or "pseudo" versions may exist. The genuine interface waves have a constant phase velocity that is always smaller than that of the slowest bulk wave occurring in both the media, and their amplitudes decay exponentially on both sides of the common surface with increasing distance from it. Thus they represent in general the slowest non-dispersive field component that suffers no radiation loss in favour of other wave-types and restricts its energy flux completely to the immediate vicinity of the guiding interface.

Following a suggestion of Cagniard [11] the genuine interface waves go by the name of the scientists associated with them: Rayleigh [12], Scholte [13 to 15], and Stoneley [16]. These are listed in Table 1, together with an estimate of their respective phase velocities:

CLASS OF INTERFACE	TYPE OF FREE INTERFACE WAVE
VACUUM 	<u>RAYLEIGH WAVE</u> $C_R \approx n' C_S$ $0.873 \cdot n' \sim 0.956$
LIQUID 	<u>SCHOLTE WAVE</u> $C_{Sch, min} \left\{ \begin{matrix} C_p \\ C_s \end{matrix} \right\}$
SOLID 	<u>STONELEY WAVE</u> $\min \left\{ \begin{matrix} C_R \\ C_R \end{matrix} \right\} \sim \min \left\{ \begin{matrix} C_p \\ C_s \end{matrix} \right\}$

**TABLE 1** CLASSIFICATION OF THE BASIC INTERFACE-WAVES, WITH AN ESTIMATION OF THEIR PHASE-VELOCITIES

The simplest type of interface wave is the well-known Rayleigh wave, which can always propagate along the free surface of a solid and has a "penetration depth" of about only one wavelength [11, 17 to 21]. Similarly, there are no restrictions on the existence of a Scholte wave at a liquid/solid interface and its decay inside the solid is comparable with that of the Rayleigh wave. The penetration depth inside the liquid remains equally small if the adjacent solid is acting as a "very slow" or "soft" boundary ( $c'_s \ll c_p$ ; as, for example, in most water/unconsolidated-sediment combinations), but it can be much bigger if the solid is "extremely fast" or "hard" ( $c'_s > c_p$ ; as, for example, in all water/rock combinations) [6, 22 to 26]. The most complicated type of interface wave is the well-known Stoneley wave, which can occur at the common surface of two solids for only very limited combinations of parameters; it penetrates into each solid in a similar way to the Rayleigh wave [27 to 31].

Concerning the mathematics, all these genuine interface waves result from a real (or almost real) pole on the physically-relevant sheet of the pertinent Riemann surface ("top-sheet"), which means that their velocities correspond to the only real (or almost real) root of the pertinent equation. For a liquid/solid or a solid/solid interface there may be some contribution to the wave-field from an additional or sometimes vicarious complex pole on a physically less relevant Riemann sheet ("lower sheet") equivalent to an additional or sometimes unique complex root of the velocity equation with physical meaning. This special singularity can entail a generalized or pseudo-interface wave belonging to the more extensive class of "leaking" interface waves [32]. These waves are so called because they continuously radiate energy into the "slower" or "softer" medium, which may then be considered as a kind of perturbation of its "faster" or "harder" counterpart. Because of their radiation loss these wave types are highly attenuated and show apparently an increasing amplitude/distance characteristic on the side of the "slower" medium. A well-known example is the pseudo-Rayleigh wave propagating along a liquid/solid interface with a phase velocity practically identical to that of the genuine Rayleigh wave [23]. For a great many water/solid combinations the existence of this leaking wave has been demonstrated with the aid of seismic records or tests in the laboratory. However, if the liquid is relatively "fast" and the adjacent solid not "hard" enough (as, for

example, in the case of most water/unconsolidated-sediment combinations) this pseudo-Rayleigh wave is completely suppressed in favour of the genuine Scholte wave (see also Sect. 1.5). Much less known, and quite unexplored, is the pseudo-Stoneley wave that occurs at the common surface of two solids and might be an alternative to overcome the restrictions imposed on the existence of the genuine Stoneley wave. Unfortunately, the nomenclature concerning these interface phenomena is still not yet standardized and many authors call all of them Rayleigh waves or distinguish merely between Rayleigh and Stoneley waves. This has created considerable confusion and misunderstandings about the variety of wave types described above.

Finally, we should discuss briefly the neglected component of the shear deflection that is polarized parallel to a given interface — the so called SH-wave. This type occupies a special position in so far as it needs no other wave to fulfil the boundary or transition conditions. As a self-consistent modification of the shear wave it creates the only "pure" propagation modes (see Sect. 1.4) within solid layers, which are named Love waves. Because they are perfectly reflected or guided by a free surface or a liquid/solid interface these Love waves represent an important factor in seismic wave propagation and are often included with the interface phenomena [5.29,33,34].

To give examples of seismic interface waves and to show their integration into the physical background we will refer several times within this report to the medium or microscopic scale of elastic, electro-magnetic, and optical phenomena; that is, to the very high frequency regime. Just recently the existence of piezoelectric acoustic boundary waves has been proved [35,36], and some years ago even more elementary analogues have been discovered in quantum mechanics: surface-spin waves in semi-infinite ferromagnetic crystals [37].

## 1.2 Elementary Relations for an Idealized Plane Harmonic Scholte Wave\*

To give some insight into the physics of the interface problem this section presents a brief mathematical description of a plane, monochromatic Scholte

---

\*This section is based on a SACLANTCEN internal working paper (IN-461) that was originally written in December 1975 and later reproduced as SACLANTCEN Memorandum SM-138 in June 1980.



wave propagating along the adjacent surface of two homogenous, isotropic, and non-dissipative half spaces. The results give a clear idea of the pertinent propagation mechanism, but they are not suitable for the treatment of a realistic sea-floor environment where parameter gradients, inhomogeneities, stratifications, and material losses, for instance, provoke serious modifications.

We choose Cartesian coordinates  $(x,z)$  for range and depth and distinguish between water ( $z < 0$ ) and solid bottom ( $z > 0$ ) by the use of the subscript "w" for all terms relating to the liquid half-space. If we consider the simplest disturbance — a plane, monochromatic wave of angular frequency  $\omega = 2\pi f$  propagating in the  $+x$  direction — our problem becomes two-dimensional ( $\frac{\partial}{\partial y} = 0$ ). Therefore the vector of particle displacement is reduced to  $\vec{s} = (\underline{u}, 0, \underline{w})$  and the time-dependence to  $e^{-i\omega t}$ . (Here and throughout this discussion, all underlined symbols represent complex terms according to the definition:  $\underline{a} = a + ia'$  and derivatives with respect to time  $t$  are, as usual, denoted by a dot).

If we remain in the framework of linear elasticity, neglect superimposed body forces, and introduce the displacement potentials  $\underline{\phi}$  and  $\underline{\psi}$  according to:

$$\begin{aligned} \vec{s} &= (\underline{u}, 0, \underline{w}) = \text{grad} \underline{\phi} + \text{rot} \underline{\psi}, \\ &\text{with} \\ \underline{\psi} &= (0, \underline{\psi}, 0), \end{aligned} \quad (\text{Eq. 3})$$

the above-mentioned potentials have to fulfill the wave equations:

$$\text{water:} \quad \Delta \underline{\phi}_w + k_w^2 \underline{\phi}_w = 0 \quad \text{with} \quad k_w = \frac{\omega}{c_w} \quad (\text{Eq. 4a})$$

$$\begin{aligned} \text{bottom:} \quad \Delta \underline{\phi} + k_p^2 \underline{\phi} &= 0 & \text{with} \quad k_p &= \frac{\omega}{c_p} \\ \Delta \underline{\psi} + k_s^2 \underline{\psi} &= 0 & \text{with} \quad k_s &= \frac{\omega}{c_s} \end{aligned} \quad (\text{Eq. 4b})$$

For their solutions we can calculate the non-vanishing components of the stress-tensor  $\mathcal{T}$  according to:

$$\text{water: } \tau_{xx_w} = \tau_{xx_w} = -p = \delta_w \left( \frac{\partial^2 \phi_w}{\partial x^2} + \frac{\partial^2 \phi_w}{\partial z^2} \right) \quad (\text{Eq. 5a})$$

$$\tau_{xz_w} = 0$$

$$\tau_{xx} = \delta \left( \frac{\partial^2 \phi}{\partial x^2} + \frac{\partial^2 \phi}{\partial z^2} \right) + 2\mu \left( \frac{\partial^2 \phi}{\partial x^2} - \frac{\partial^2 \psi}{\partial x \partial z} \right)$$

$$\text{bottom: } \tau_{xz} = \mu \left( 2 \frac{\partial^2 \phi}{\partial x \partial z} + \frac{\partial^2 \psi}{\partial x^2} - \frac{\partial^2 \psi}{\partial z^2} \right) \quad (\text{Eq. 5b})$$

$$\tau_{zz} = \delta \left( \frac{\partial^2 \phi}{\partial x^2} + \frac{\partial^2 \phi}{\partial z^2} \right) + 2\mu \left( \frac{\partial^2 \phi}{\partial z^2} + \frac{\partial^2 \psi}{\partial x \partial z} \right)$$

In our case the transition conditions for the sound field at the interface (three boundary conditions for three force-free potentials) are given by:

$$\underline{w}_w = \underline{w} \quad (\text{Eq. 6})$$

$$z = 0 \quad \underline{p} = \tau_{zz}$$

$$\tau_{xz} = 0$$

If we assume displacement potentials of the form:

$$\text{water: } \underline{\phi}_w = M e^{mz} e^{i(kx - \omega t)} \quad (z \leq 0) \quad (\text{Eq. 7a})$$

$$\underline{\phi} = Q e^{-qz} e^{i(kx - \omega t)}$$

$$\text{bottom: } \underline{\psi} = S e^{-sz} e^{i(kx - \omega t)} \quad (z \geq 0) \quad (\text{Eq. 7b})$$

$$\text{with } k = \frac{\omega}{c}$$

to fulfil the wave equations (Eq. 4), the vertical wave numbers describing the transverse decay of the field have to be:

$$m = \sqrt{k^2 - k_w^2}, \quad q = \sqrt{k^2 - k_p^2}, \quad s = \sqrt{k^2 - k_s^2} \quad (\text{Eq. 8})$$

The use of the continuity conditions (Eq. 6) leads finally to a set of three equations for the amplitude factors:

$$\begin{pmatrix} 2ikq & (k^2+s^2) & 0 \\ \mu(k^2+s^2) & -2i\mu ks & \delta_w(k^2-m^2) \\ q & -ik & m \end{pmatrix} \begin{pmatrix} Q \\ S \\ M \end{pmatrix} = \begin{pmatrix} 0 \\ 0 \\ 0 \end{pmatrix} \quad (\text{Eq. 9})$$

According to the first and the last equation these amplitude factors are related by:

$$S = -\frac{2ikq}{k^2+s^2}Q \quad Q = \frac{m}{q} \frac{k^2+s^2}{k_s^2}M \quad (\text{Eq. 10})$$

The set of homogeneous, linear equations (Eq. 9) has a non-trivial solution only if the coefficient determinant is vanishing (in the case of more complex systems the same procedure leads to the pertinent dispersion relations from which the characteristic phase and group velocities are calculated.) With the abbreviations:

$$H = \frac{\rho_w}{\rho} \quad N = \left(\frac{c_s}{c_w}\right)^2 \quad (\text{Eq. 11})$$

$$R = \left(\frac{c_s}{c_p}\right)^2 = \frac{1-2\sigma}{2(1-\sigma)} \quad X = \left(\frac{c_s}{c}\right)^2$$

the decay constants (Eq. 8) take the form

$$k = k_s \sqrt{X} \quad (\text{Eq. 12})$$

$$m = k_s \sqrt{X-N}, \quad q = k_s \sqrt{X-R}, \quad s = k_s \sqrt{X-T}$$

and the vanishing determinant leads to the following equation for  $X$  and thus to the phase velocity  $c$  of the Scholte wave

$$4X\sqrt{X-1} \sqrt{X-R} - (2X-1)^2 = H \frac{\sqrt{X-R}}{\sqrt{X-N}} \quad (\text{Eq. 13})$$

For the limiting case  $H = 0$  (i.e.  $\rho_w = 0$ ), the right-hand side disappears and we end up with the well-known Rayleigh wave equation, which has always one positive real root  $c = c_R < c_s$  (see, for example, [6,18,22]).

The latter phase velocity is frequency independent and can be approximated to high accuracy by a simple formula [38]:

$$c_R = \frac{0.87 + 1.12\sigma}{1 + \sigma} c_s . \quad (\text{Eq. 14})$$

For  $H \neq 0$ , Eq. 13 describes a coupled system of two components, each of which contains "one degree of freedom", which is why we have to expect two different roots with physical significance [6,11,15,22]. The first root is always complex and characteristic for the so-called pseudo-Rayleigh wave with the phase velocity  $\underline{c} = c_R + ic_R'$ ; the second is always positive real and belongs to the Scholte wave  $\underline{c} = c_{\text{Sch}}$ . (To find those solutions numerically it makes no sense to square Eq. 13 and to profit from standard subroutines for digital computers, because, as this procedure leads to a polynomial of the eighth degree in  $\underline{X}$ , it may be extremely difficult to separate the two pairs of "physical roots" for the genuine and the pseudo-interface from the other six pairs of extraneous ones.)

If the adjacent fluid has a very low density ( $H \ll 1$ , such as air, for example) and thus represents merely a "slight disturbance" of the solid, only the pseudo-Rayleigh wave will be excited. As the sound speed  $c_0$  in such a gaseous atmosphere is usually smaller than the phase and trace-velocity  $\tilde{c}_R \approx c_R$  of this interface wave, a slight amount of energy is continuously transferred to a dragged sound field (head wave) in the fluid medium. Due to these radiation losses the pseudo-Rayleigh wave shows an additional (non-dissipative) decay of the amplitude in the propagation direction. This decay causes a fast extinction of that wave type in most liquid/solid systems with  $c_0 < \tilde{c}_R$  (such as at a water/rock interface), because the higher density of typical liquids creates a much stronger coupling (better impedance matching) and thus a more intense energy drain. As a consequence of this peculiarity, the pseudo-Rayleigh wave can no longer be excited if the sound speed of the liquid reaches or exceeds the trace velocity, i.e.  $c_0 \geq \tilde{c}_R$  (such as at most water/sediment interfaces). In this connection the reader may think of the famous "air-coupled" Rayleigh wave often generated by earthquakes with shallow epicentres or by big explosions near to the earth's surface. However, this most prominent signal of many seismic records is a coupling phenomenon of two independent wavefronts and occurs merely as a sort of "non-radiating" limit of the pseudo-Rayleigh wave. This coupling of the shock wave in air with a

"speed-synchronized" wavelet of a realistic Rayleigh wave pulse in the bottom is due to the unavoidable dispersion of seismic interface waves (see Sect. 1.4). Thus the wavelet of the "air-coupled" Rayleigh wave separates the pulse's low-frequency head, with pseudo Rayleigh-wave character, from its high-frequency tail, with almost "pure" Rayleigh-wave features.

When the liquid has a lower or a higher sound speed than the Rayleigh velocity of the solid, the Scholte wave becomes the more important, or all-important, propagation mechanism. As a more detailed investigation has shown in [30] the resulting phase velocity  $c_{sch}$  of this wave type is also frequency-independent (non-dispersive propagation), and always slightly smaller than the lowest velocity occurring in both media i.e.,  $c_{sch} < \text{Min}(c_o, c_R)$  (see Table 1). The interested reader may find many normalized solutions  $X^{-\frac{1}{2}}$  or  $(X/N)^{-\frac{1}{2}}$  of Eq. 13 in the paper of Strick and Ginzburg [24], where they are plotted as a function of the velocity ratio  $N^{\pm\frac{1}{2}}$ , with the Poisson-modulus  $\sigma$  and the density ratio  $H$  as parameters. Thus velocity and wavelength of the Scholte wave amount almost to the corresponding entities of a frequency-synchronized water wave, if we deal with an "extremely-hard" sea floor ( $c_s > c_w$ ), such as mother-rock, for example. Normally, with a "relatively hard" or a "soft" ocean bottom ( $c_s < c_w$  or  $c_s \ll c_w$ ), such as sedimentary rocks or marine sediments, these entities are much smaller and may even decrease to a few percent of those of the water wave. With the use of hydrophones or geophones one can detect the omni-directional pressure within the water mass or the vector of particle displacement (or its time derivatives: particle velocity and particle acceleration). For this reason we now determine the real components of the displacement vector and of the stress tensor caused by a plane, monochromatic Scholte wave. With the aid of Eqs. 3, 7 and 12 we find the following displacement components:

$$u_w = \hat{u}_w \sin(kx - \omega t)$$

with

$$\hat{u}_w = -k_s M Y e^{mz} = -k_s Q \frac{\sqrt{X-R}}{\sqrt{X-N}(2X-1)} e^{mz} < 0$$

water:

(Eq. 15a)

$$w_w = \hat{w}_w \cos(kx - \omega t)$$

with

$$\hat{w}_w = k_s M \sqrt{X-N} e^{mz} = k_s Q \frac{\sqrt{X-R}}{2X-1} e^{mz} > 0$$

$$u = \hat{u} \sin(kx - \omega t)$$

with

$$\hat{u} = k_s Q Y \left\{ \frac{2\sqrt{X-R}}{2X-1} e^{-sz} - e^{-qz} \right\} \begin{matrix} < 0 \\ > 0 \end{matrix}$$

bottom:

(Eq. 15b)

$$w = \hat{w} \cos(kx - \omega t)$$

with

$$\hat{w} = k_s Q \sqrt{X-R} \left\{ \frac{2X}{2X-1} e^{-sz} - e^{-qz} \right\} > 0$$

The results are in each case the parametric representation of an ellipse having its main axes parallel to the axes of our coordinate system. With increasing distance from the interface, the displacement amplitudes  $\hat{u}_w$ ,  $\hat{w}_w$  and  $\hat{w}$  decrease exponentially without changing sign. The horizontal amplitude in the bottom,  $\hat{u}$ , shows the same asymptotic behaviour after having changed sign at a depth of the order of one tenth of the pertinent wavelength. Figures 1a and b give qualitative sketches of these particle displacements and their resulting orbits for a typical water/sediment interface. While the "penetration depth" in the solid is always limited to a range of about one wavelength (similar to that of the Rayleigh wave), it is slightly or substantially bigger on the side of the liquid if the solid medium is acting as a "relatively hard" or a "very hard" boundary (relatively-bad or extremely-bad impedance matching). As the sea floor in coastal waters consists mainly of unconsolidated and consolidated sediments we may expect that waterborne infrasound is transmitted as a Scholte wave even in very shallow water areas.

The interesting components of the stress tensor can be derived from Eq. 5 by referring once more to Eqs. 7 and 12:

$$p = \hat{p}_w \cos(kx - \omega t)$$

water:

(Eq. 16a)

with

$$\hat{p}_w = -\delta_w k_w^2 M e^{mz} = -k_s^2 Q \frac{\mu H \sqrt{X-R}}{\sqrt{X-N} (2X-1)} e^{mz}$$

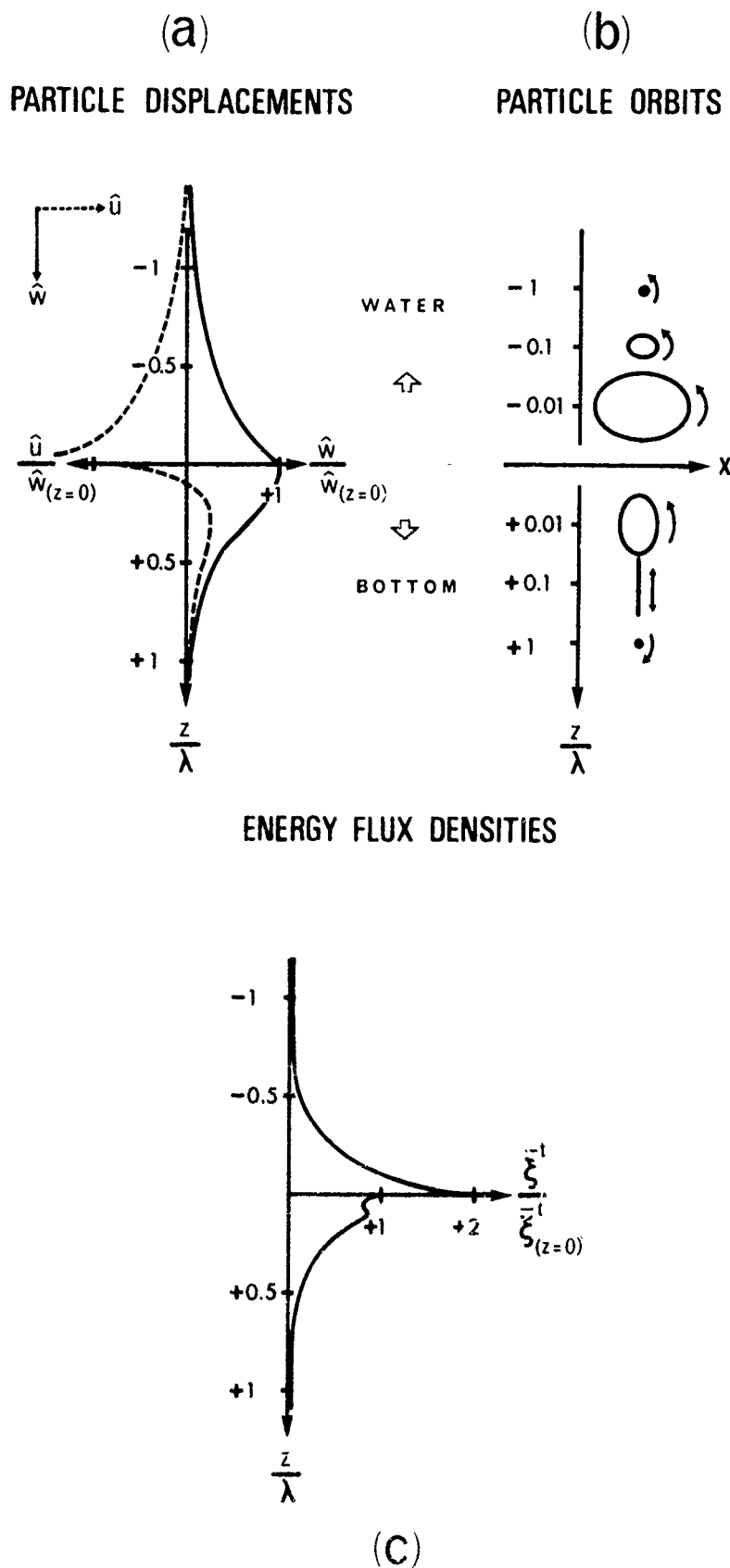


FIG. 1 PARTICLE DISPLACEMENTS, THEIR RESULTING ORBITS, AND ENERGY FLUX DENSITIES, FOR A MONOCHROMATIC SCHOLTE WAVE AT A WATER/SEDIMENT INTERFACE

$$\tau_{xx} = \hat{\tau}_{xx} \cos(kx - \omega t)$$

with

$$\hat{\tau}_{xx} = k_s^2 Q \left\{ \frac{4\mu X \sqrt{X-R} \sqrt{X-1}}{2X-1} e^{-sz} - [\delta R + 2\mu X] e^{-qz} \right\}$$

$$\tau_{xz} = \hat{\tau}_{xz} \sin(kx - \omega t)$$

bottom:

(Eq. 16b)

with

$$\hat{\tau}_{xz} = -2\mu k_s^2 \gamma \sqrt{X-R} Q \{ e^{-sz} - e^{-qz} \}$$

$$\tau_{zz} = \hat{\tau}_{zz} \cos(kx - \omega t)$$

with

$$\tau_{zz} = -k_s^2 Q \left\{ \frac{4\mu X \sqrt{X-R} \sqrt{X-1}}{2X-1} e^{-sz} + [\delta R - 2\mu(X-R)] e^{-qz} \right\}$$

From Eqs. 15 and 16 we can finally calculate the purely real energy flux in the Scholte wave.

The elastic energy-flux density is given by the work done by the stress tensor within a unit time and on a unit area normal to the displacement vector:

$$\vec{E} = (\xi, \zeta, \eta) = -\dot{\mathcal{T}} \vec{s}. \quad (\text{Eq. 17})$$

Accordingly we obtain for its non-vanishing components

$$\xi_w = \rho \dot{u}_w = \hat{e}_x \cos^2(kx - \omega t)$$

with

$$\hat{e}_x = \mu \omega k_s^3 M^2 \gamma H e^{2mz} = \mu \omega k_s^3 Q^2 \gamma \frac{H(X-R)}{(X-N)(2X-1)^2} e^{2mz}$$

water:

(Eq. 18a)

$$\eta_w = \rho \dot{w}_w = \hat{e}_z \sin 2(kx - \omega t)$$

with:

$$\hat{e}_z = \mu \omega k_s^3 M^2 \frac{H \sqrt{X-N}}{2} e^{2mz} = \mu \omega k_s^3 Q^2 \frac{H(X-R)}{2 \sqrt{X-N} (2X-1)^2} e^{2mz}$$



$$\begin{aligned}\xi &= -\tau_{xx}\dot{u} - \tau_{xz}\dot{w} \\ &= \hat{e}_x' \sin^2(kx - \omega t) + \hat{e}_x'' \cos^2(kx - \omega t)\end{aligned}$$

with:

$$\hat{e}_x' = \mu\omega k_s^3 Q^2 Y(X-R) \left\{ \frac{2X}{2X-1} e^{-2sz} + e^{-2qz} - \frac{4X-1}{2X-1} e^{-(s+q)z} \right\}$$

$$\begin{aligned}\hat{e}_x'' &= \mu\omega k_s^3 Q^2 Y \left\{ \frac{8X(X-1)(X-R)}{(2X-1)^2} e^{-2sz} + [1+2(X-R)] e^{-2qz} \right. \\ &\quad \left. - \frac{2\sqrt{X-1}\sqrt{X-R}[1+2(X-R)]}{2X-1} e^{-(s+q)z} \right\}\end{aligned}$$

bottom:

(Eq. 18b)

$$\eta = -\tau_{zx}\dot{u} - \tau_{zz}\dot{w} = \hat{e}_z' \sin 2(kx - \omega t)$$

with:

$$\hat{e}_z' = \mu\omega k_s^3 Q^2 \frac{\sqrt{X-R}}{2(2X-1)^2} \left\{ 4X\sqrt{X-1}\sqrt{X-R} e^{-2sz} - (2X-1)^2 e^{-2qz} \right\}$$

For each point of the interface, the term in the braces { } of the amplitude  $\hat{e}_z'$  corresponds to the left-hand side of the Scholte wave equation (Eq. 13) and therefore guarantees the continuity of the amplitudes  $\hat{e}_z'$  and  $\hat{e}_z''$ . As we could further expect, the amplitude  $\hat{e}_z''$  disappears in the limiting case  $\rho_w = 0$ . By taking the time average of the above results (Eq. 18), the energy flux normal to the interface vanishes and only the component in the propagation direction remains:

$$\text{water: } \bar{\xi}_w^t = \frac{\hat{e}_x}{2} \quad (\text{Eq. 19a})$$

$$\text{bottom: } \bar{\xi}^t = \frac{\hat{e}_x' + \hat{e}_x''}{2} \quad (\text{Eq. 19b})$$

According to the comments given in connection with the displacement components (Eq. 15), these mean energy-flux densities also have their maxima at the interface and show a very rapid frequency-dependent decay with increasing distance from this plane, as is shown in Fig. 1c.

For this reason, both energy flux densities can usually be neglected for distances  $|z| > \lambda$  and our assumption of treating the problem as two half-spaces holds if both the depth of the water and that of the sediment layer

are larger than this limit. Only with an "extremely-hard" crystalline rock bottom may a greater water depth be required to guarantee the existence of such a "pure" or "non-modified" Scholte wave.

To complete our mathematical description we write down the expressions for the total energy flux on both sides of the interface as:

$$\Gamma_W = \int_0^{\infty} \bar{\xi}_W t \, dz = \mu \omega k_S^2 M^2 Y \frac{H}{4\sqrt{X-N}}$$

water:

$$= \mu \omega k_S^2 Q^2 Y \frac{H(X-R)}{4\sqrt{X-N} (X-N)(2X-1)^2} \quad (\text{Eq. 20a})$$

$$\Gamma = \int_0^{\infty} \bar{\xi} t \, dz = \mu \omega k_S^2 Q^2 Y \left\{ \frac{X(X-R)(4X-3)}{\sqrt{X-1} (2X-1)^2} + \frac{1+4(X-R)}{4\sqrt{X-R}} \right.$$

bottom:

(Eq. 20b)

$$- \frac{(X-R)(4X-1) + \sqrt{X-1} \sqrt{X-R} [1+2(X-R)]}{(\sqrt{X-1} + \sqrt{X-R})(2X-1)} \}$$

Under real-world conditions the above-described wave type is strongly modified of course not only by less-pronounced interfaces within the ocean floor but also by changes in parameter profiles, inhomogeneities, and material losses within the resulting layers (see Sects. 1.4 and 2.2).

Because of the frequency-dependent penetration depth it is already obvious that the low-frequency components of a given Scholte-wave pulse are affected more by the bottom layers, and by the sea surface too if the occasion arises, while the high-frequency components are mainly affected by the inhomogeneities and the relative high dissipation of the unconsolidated top layers of the sea floor.

### 1.3 Wave-front Pattern of a Point Source Close to an Interface

Based on Cagniard's rigorous mathematical treatment [11,39,40] (which does not suffer from the usual restrictions required by asymptotic methods) and von Schmidt's famous Schlieren photos [41] (taken from model experiments), many seismic and acoustic papers have described the different contributions to the field of an impulsive point source  $S_0$  located close to a plane interface separating two semi-infinite, homogeneous, and isotropic elastic media. Unfortunately, almost all these treatments are limited or so incomplete that the user who wants to predict or interpret experimental results has to make his way through the theory again and again. In the following we try to describe the facts and compile the consequences in a clearly arranged scheme, so that the type and shape of almost all possible wave fronts can be quickly identified. The experienced reader will soon recognize that our discussion of phenomena makes use of many more partial contributions to the field than those that can be separated clearly by the classical mathematical tools [17,42] or even more modern methods [22,24,28, 43 to 51].

To cover the most relevant cases we assume an impulsive point source  $S_0$  for compressional (P-) waves and denote the two bulk- (or body-) wave velocities of the original medium as  $c_p$  and  $c_s$  and those of the adjacent medium as  $c'_p$  and  $c'_s$ . Besides this "hypocentre"  $S_0$ , our geometrical considerations will be based on the fictitious mirror source,  $S'_0$ , and on the intersection point of the connecting line,  $\overline{S_0 S'_0}$ , and the interface, which is called the "epicentre" E, (nadir of  $S_0$ ). If the expanding spherical P-front impinges on the flat interface, the line of intersection — hereafter called "trace"  $T_p$  — is an enlarging circle. This circle emanates from the epicentre E with an infinitely high radial velocity  $v_p$  that decreases continuously until it approaches the velocity of the incident spherical front:  $v_p \rightarrow c_p$ . By means of this primary trace,  $T_p$ , the incident front implements a sort of "moving perturbation" at the interface, which has to be balanced by an elastic wave field. Without repeating it every time we assume that all outgoing waves of this resulting field fade away with growing distance from the source  $S_0$  ("radiation condition").

To fulfil the transition conditions at the interface — the continuity of all displacement (or velocity) and stress components always requires the

interplay of two compressional and two shear potentials — this relaxation process is performed by at least four different radiated or guided waves, which may be "pure" bulk-waves (body-waves) or more complicated interface phenomena. The selection of the wave types that participate in the transmission of the incoming energy is simply made by the law of causation: each primary trace and all eventually emerging secondary traces can radiate or drag only those fronts whose velocity is less than or equal to the momentary trace velocity. Expressed in other words we can say: the field generated by a source is completely detached by radiation from its origin or is at least moving with it if the characteristic propagation of this field is "too slow" or just "sufficient" to follow the changes in the position of the source".

From these fundamentals we can easily deduce and understand the well-known wave front patterns presented in many papers without exhaustive interpretation: the reflected compressional front, PP, has always a spherical shape — apparently it emanates from the fictitious mirror source  $S'_0$  — while the slower, reflected shear front, PS, is the cap of a hyperbolic enclosed therein. Strictly speaking this latter front is created by "inner refraction" and not by reflection. As long as the trace  $T_p$  is moving faster than the bulk waves of the second medium — at least in the early stage of our propagation process this condition is always fulfilled — the refracted fronts, PP' and PS', are also hyperbolic caps. Thus all radiated wavefronts intersect the interface at the trace  $T_p$ , with acute angles  $\alpha_v$  (corresponding to the angles of incidence) that are determined by Snells' law (see Fig. 2a).

Under the condition  $c_p > c'_p$  this quite simple set of wave fronts remains essentially unchanged for all time. During its propagation, all these angles grow slowly, but only (the real part of)  $\alpha_p$  reaches its maximum  $\pi/2$  in the far-field.

If the source is located not too far from the interface, and additional conditions concerning the elastic parameters are fulfilled, free interface waves form the "tail" of the resulting elastic wave field. As mentioned above, the excitation of these slowest, guided contributions is due to the inhomogeneous character of the incident spherical front, which can be demonstrated by the classical mathematical treatment of boundary-value

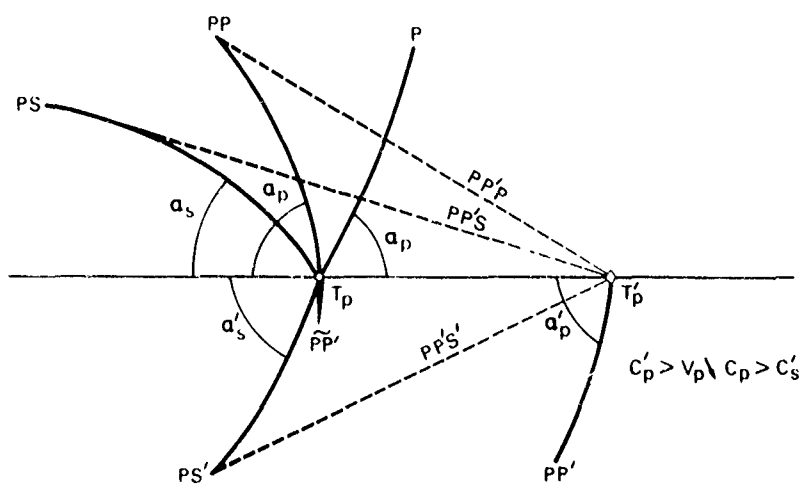
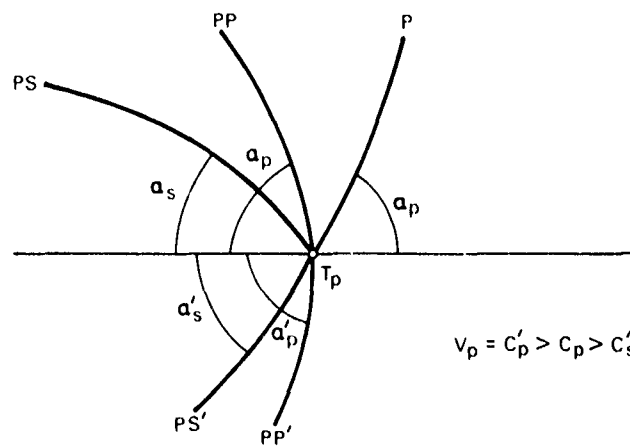
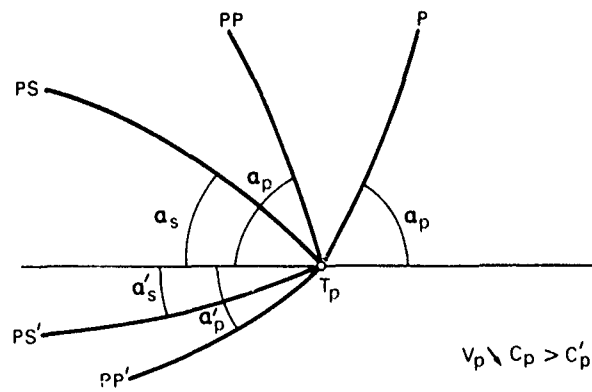


FIG. 2 PRIMARY (T) AND SECONDARY TRACES (T') AS THE RESULTS OR ORIGINS OF DIFFERENT WAVE-FRONT PATTERNS AT THE INTERFACE OF TWO SOLIDS

problems in homogeneous and isotropic media. The first step towards the solution usually consists in adapting the original representation of the wave field to the geometry of the boundary or interface. This modification has to be done in such a way that the resulting separation of variables allows a suitable fulfilment of the transition conditions. In our quite simple case of a flat interface these adapted representations are given by the already-mentioned contour integrals derived by Sommerfeld and Weyl [3 to 9]. These expressions decompose an incoming spherical or cylindrical field into an infinite sum of cylindrical or plane waves with complex wave vectors or complex angles of incidence. The imaginary part of these vectors or angles describes the inhomogeneity of the individual element in relation to its distance from the interface. Because they represent crosswise evanescent waves of a subordinate geometry, these components are provided with features that are similar to the free interface waves to be excited. In our special case the genuine type is characterized by cylindrical phase surfaces orthogonal to the "guiding" interface and plane amplitude surfaces parallel to it and thus by a restricted penetration depth inside both media. Synthesizing the incoming field from those inhomogeneous elements we get integrals that resemble the well-known Fourier or Fourier-Bessel transformation [52,53]. From the subsequent integration along a suitable path on the admissible Riemann sheet, we can work out in general the contributions of one saddle-point (reflected wave), up to four branch-points (refracted bulk waves), and up to two major poles (free interface waves) [11,17,23,42,43, 46 to 51].

The facts so far outlined characterize completely the simplest case A of Table 2, assuming  $c_p > c'_p$ . In this scheme we have classified all outgoing wave fronts as "non-homogenous" because of the complicated amplitude weighting of the reflected and refracted fronts. Their deviation from homogeneity is easy to understand if one bears in mind that the reflection and transmission coefficients depend on the angle of incidence according to the way that the ensemble of these outgoing waves forms the "radiation pattern" of the insonified interface region.

To simplify Table 2 we have characterized all wave fronts by only the last and most significant letter of their usual seismic classification. Under the condition  $c'_p > c_p > c'_s$  of case B in Table 2 there occurs a moment at

HOMOGENEOUS INCIDENT WAVE FRONT	NON-HOMOGENEOUS OUTGOING WAVE FRONTS			TRACES AT THE INTERFACE WITH DESIGNATION OF THE INTERSECTING FRONTS HEAD WAVES FLANK WAVES
	TYPE	CRITERIA	SHAPE	
<p>SPHERICAL P</p> <p>SOURCE <math>S_0</math></p> <p>DISTANCE <math>h</math></p> <p>PLANE INTERFACE</p> <p>Medium <math>M</math> <math>c_p, c_s</math></p>	<p>REFLECTED P</p> <p>REFLECTED S</p> <p>INTERFACE WAVES</p> <p>REFRACTED <math>S'</math></p> <p>REFRACTED <math>P'</math></p>	<p>Case:</p> <p><math>c_p &gt; c_s</math></p> <p><math>c_p &lt; c_s</math></p> <p><math>c_p = c_s</math></p>	<p>SPHERICAL</p> <p>HYPERBOLICAL</p> <p>ANNULAR</p> <p>HYPERBOLICAL</p> <p>HYPERBOLICAL</p>	
			<p>SPHERICAL</p> <p>HYPERBOLICAL</p> <p>ANNULAR</p> <p>HYPERBOLICAL</p> <p>ELLIPTICAL</p>	

TABLE 2 CLASSIFICATION OF DIFFERENT WAVE-FRONT PATTERNS AT THE INTERFACE OF TWO SOLIDS

which the decreasing trace velocity  $v_p$  reaches and passes the value of the compressional velocity  $c_p'$  in the second medium. At this intermediate stage of the resulting field the real part of angle  $\alpha_p'$  of the refracted front  $PP'$  adopts its (real) maximum  $\pi/2$  (see Fig. 2b) and continues with complex values. Thus the refracted front  $PP'$ , having a hyperbolic shape until now, is converted into a half-ellipsoid that ends orthogonally at the interface and expands with its characteristic velocity  $c_p'$ . Accordingly, this modified front  $PP'$  has to be disconnected from the primary trace  $T_p$  (indicated by "o"), which is dropping back continuously. In term of ray theory this moment corresponds to the reaching and exceeding of the critical angle of incidence  $\alpha_{p \text{ crit}}$  with the "disappearance" of the refracted front  $PP'$  and the corresponding intensification of the reflected front  $PP$ . To fulfil the later transition conditions, the field emanating from the relative "slow" trace  $T_p$  has to be "completed" again by the aid of a new compressional component in the second medium. Because it is dragged but not radiated by the (primary) trace  $T_p$ , this attached "near-field" is created by a guided, inhomogeneous wave  $PP'$  belonging to a class of evanescent fields that are frequently called "flank-waves" (see Fig. 2c). In Table 2 these coupled annular flank waves are indicated by downward pointing, dotted arrows. Due to their low energy level they have almost no importance for seismic investigations, but together with the free interface waves they exercise an influence on the fine-structure of totally-reflected beams [57,60], which becomes quite complicated close to the so-called Rayleigh angle [61]. On the other hand, the relative "fast" front  $PP'$  has to create its own (secondary) trace  $T_p'$  (indicated by "o") with at least three additional contributions to the field. For historical reasons those secondary bulk-wave traces, such as  $T_p'$ , are designated somewhat misleadingly as "lateral waves". As it propagates with a higher velocity than all other wave types, trace  $T_p'$  can easily satisfy the transition conditions by radiating residual "pure" bulk waves. Because they are dragged by  $T_p'$  and tangent to the respective fronts of the same type (emanating from  $T_p'$ ) these new wave fronts,  $PP'P$ ,  $PP'S$ , and  $PP'S'$ , have a conical shape (see Fig. 2c). They are the famous "head waves" that were long an unsolved problem in seismology until Cagniard succeeded in explaining them theoretically and von Schmitt proved their existence experimentally. In our scheme they are designated in the last column by upward pointing arrows emanating from the corresponding secondary traces. As these head waves continuously draw



their energy from the pertinent lateral waves (traces), it is obvious that their amplitudes must always be greater in sections previously radiated than in subsequent ones. This fact is indicated schematically in Fig. 2c by the line thickness of the three corresponding fronts. Thus their amplitude/distance characteristic is apparently a rising function with increasing distance from the interface and reaches its maximum at the junction with the respective bulk-wave front. Such a head wave provokes the one-sided radiation loss of the pseudo-interface waves described in the previous Section.

Under the condition  $c_p' > c_s' > c_p$  of case C in Table 2 the refracted shear-front  $PS'$  is also converted into a half-ellipsoid and thus creates its own (secondary) trace  $T_s'$  subsequent to the separation of  $T_p$  and  $T_p'$ . This process corresponds to the reaching and exceeding of a second critical angle of incidence  $\alpha_{s \text{ crit}}$  characterized by the "disappearance" of the ultimate refracted front  $PS'$  and thus, in fact, by the "total" reflection of the incoming front  $P$ . Due to its intermediate velocity this third trace  $T_s'$  drags two head waves,  $PS'P$  and  $PS'S$ , in the first medium but only a compressional flank wave  $\widetilde{PS'P'}$  in the second medium.

After this exhaustive discussion we can easily translate the most complicated case C of our scheme into the corresponding wave-front pattern of Fig. 3, where it is seen to be characterized by the occurrence of five head waves and three flank waves. In general, the interesting free interface waves cannot be incorporated in such a clear illustration with the same surety, because their number (0, 1, or 2) and type has to be investigated for each individual case. The shape of their phase surface is cylindrical if they form the "slowest" contribution to the field (genuine interface waves) otherwise composed from an open cone in the "fast" medium and an almost closed head-wave cone in the adjacent "slow" medium (pseudo-interface waves) [46].

It should be mentioned that the above description of the different wave fronts is restricted to the most important phenomena. Cagniard for instance has shown that all hyperbolic and elliptical fronts are followed by blurred spherical fronts of the same type, which are like a "shadow" of their early stage. These weak "archetypes" create additional obliterated traces at the interface with the corresponding remainders of head and flank waves. Those very weak flank waves are called "surface waves of the second type" by Cagniard, but a much less confusing name for them would simply be



"smeared flank waves". In his study of leaking interface waves, Phinney [32] describes a so-called pseudo-P wave that may appear as an appendage to the front of the P-wave or may become a distinct signal between the arrival of the P and S fronts. Its particular velocity always adopts that value that minimizes the losses by conversion to radiated head waves.

At first glance, the above-described occurrence of several non-homogeneous and inhomogeneous wave fronts with a different shape may remind the reader of apparently similar phenomena in crystal optics, such as double and conical refraction, for example. A cursory examination reveals, however, the complete difference in the underlying physics. With the matter-connected elastic waves this division into several wave fronts is already the consequence of all possible independent oscillations of the microscopic elements relative to the regular lattice or the molecular cluster of the medium and relative to the shaping interfaces of the body. With the matter-independent electromagnetic waves consisting merely of one basic type with transverse field vectors (at least when far from the source) this splitting effect is due to the relative orientation of the radiated field vectors and the anisotropic microstructure of the exposed medium (polarization effects).

#### 1.4 Sound Propagation in a Stratified Oceanic Lithosphere and a Wedge-shaped Water Layer on Top

By discussing the propagation of elastic waves inside unlimited, homogeneous, and isotropic media, and along the plane interfaces that separate them, we have covered the fundamentals of more complicated phenomena occurring in finite bodies composed of different media. If the sound field interacts with more than one of the interfaces that bounds the medium the totality of all internally reflected and refracted components may create other mixed-wave types that are tuned to the corresponding body as a whole and synthesize its natural vibrations or modes. As this tuning is based on constructive interference in the resulting field, the dimensions of the body have to be large enough with respect to the sound frequencies above certain cut-off limits. Thus a free plate represents a wave guide for (relatively high-frequency) Rayleigh waves and an infinite number of normal modes; this is usually given the collective name of Lamb waves [6,17,21, 62 to 65]. It should here be mentioned that Lamb was the first to tackle

successfully the half-space problem in a classical paper [16] that already included a very useful mathematical description of Rayleigh-wave pulses. If these mixed modes in plates provoke symmetrical deformations with respect to the middle plane (due to transverse contraction) they are called, by analogy, "longitudinal" or, more correctly, "dilatational" or "extensional" waves ( $s_v$ ), while their antisymmetric counterparts (being essentially shear phenomena) form the well-known family of "bending" waves ( $a_v$ ).

In general, the numbering of those modes reflects the number of zero-crossings passed through by the amplitude distribution along the cross-section of the wave guide. For both symmetries the zeroth-order mode occupies a special position: it adopts finite values of phase velocity in the low-frequency range (no cut-off) and the high-frequency limit of its dispersion curve is determined by the speed of the Rayleigh wave, as we have plotted qualitatively in Fig. 4.

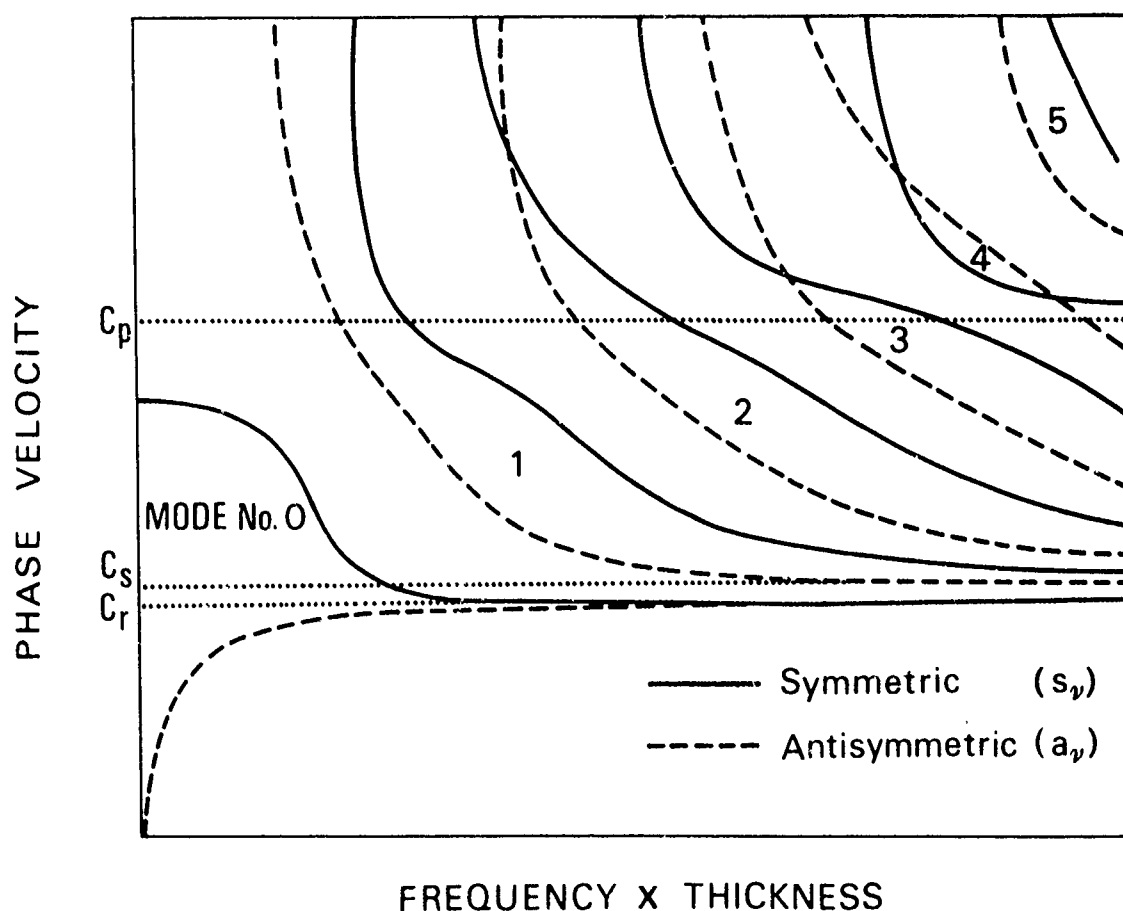


FIG. 4 DISPERSION CURVES FOR THE SYMMETRICAL ( $s_v$ ) AND ANTISYMMETRICAL ( $a_v$ ) PROPAGATION MODES IN A FREE PLATE

Because it represents a sort of elastic counterpart of the electromagnetic skin effect, the latter feature has lead to many applications in ultra-sonics using the Rayleigh wave as a tool for non-destructive testing (see e.g. [66,67]) and signal processing (see e.g. [68,69]). By increasing the frequency (or the plate thickness) the dispersion curves of all higher-order modes start with an infinite phase velocity at the corresponding cut-off frequency and drop to the shear speed of the plate medium.

A liquid layer on a solid sub-stratum can support only a family of pure compressional modes that behave similarly to the extensional waves of the plate, but cause, in general, asymmetric deflections of the layer [5,70]. The zeroth mode, also, has no cut-off frequency and its phase velocity is identical with the Rayleigh speed in the range of extreme low frequencies (or for very thin layers) and approaches the Scholte speed for extreme high frequencies (or very thick layers) [71]. Under the quite rare condition that the sound speed of the liquid exceeds both the bulk-wave velocities of the solid substratum, no other modes of higher order can be propagated through the liquid layer. Usually the sound speed of the liquid is smaller than one or both bulk velocities of the underlaying solid, so that an infinite number of higher-order modes can be excited, as indicated qualitatively in Fig. 5. Going up the frequency scale (or increasing the layer thickness) the dispersion curves of all these higher-order modes

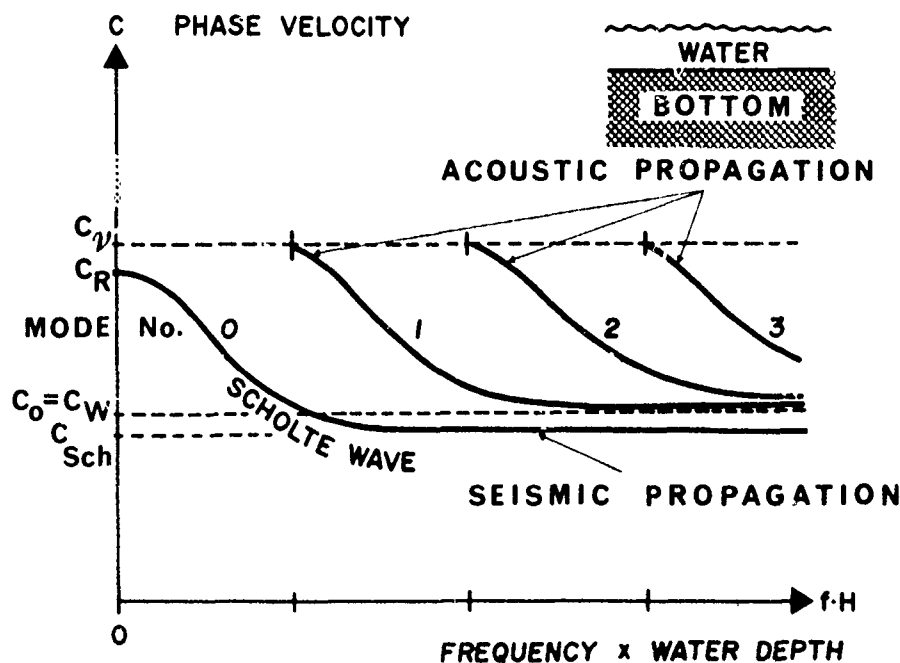


FIG. 5 PHASE-VELOCITIES OF THE LOWEST MODES IN SHALLOW WATER OVER A LIQUID-LINE OR ROCK-LIKE BOTTOM

start with the bulk-velocity  $c_v$  of the solid (at the corresponding cut-off frequencies  $f_\mu$ ) and drop to the sound speed  $c_0$  of the liquid. The bulk velocity  $c_v$  is identical with the compressional speed  $c_p$  under the condition (A):  $c_p > c_w \gg c_s$  (such as shallow water overlying a "very soft" sedimentary sea floor), or identical with the shear speed  $c_s$  under the condition (B):  $c_p > c_s > c_w$  (such as shallow water overlying "very hard" rock-bottom). These two possibilities can be easily understood in terms of mode synthesis by constructive interference.

In Fig. 6 we have therefore plotted qualitatively the absolute value of the reflection coefficient for both conditions A and B against the grazing angle  $\beta_w = \frac{\pi}{2} - \alpha_w$ , i.e. the complement of the angle of incidence  $\alpha_w$  [5,72]. The smooth dotted curve takes into account material losses and therefore approaches the familiar experimental results. While condition A offers the possibility of constructive interference for all angles  $\beta_w$  remaining below  $\beta_{p,crit}$ , condition B can do this only below the usually smaller angle  $\beta_{s,crit}$  and, in principle, for a small region around  $\beta_{p,crit}$ . The narrow width of the peak at  $\beta_{p,crit}$  and its suppression under realistic conditions indicates that this interval is of no importance in practice. Thus the upper velocity limit of the higher-order modes is determined by  $c_p$  for condition A and by  $c_s$  for condition B.

So far, the "mode picture" has served as a very familiar and convenient scheme to explain and to illustrate the consequences of our shift to the low-frequency regime. At this point, however, we should draw the reader's attention to the fundamentals of the normal-mode theory. Only condition B deals with a real eigenvalue problem and thus justifies our reasoning for those discrete modes and well-defined cut-off conditions. Condition A already belongs to the more general complex eigenvalue problems that do not permit strict mode assignments except for the interesting Scholte wave, which always represents a discrete propagation mode, as we have shown in Sect. 1.2 (zeroth mode with respect to the above-mentioned classification of the water wave). With our limitation to "very soft" sediments ( $c_w \gg c_s$ ) we presumed tacitly a quasi-discrete eigenvalue problem corresponding to an almost liquid-like bottom. As usual, the most common and realistic environmental conditions lie between ( $c_w \gg c_s$ ; "normal" bottom-types, such as "relatively hard" sediments or "relatively soft" sedimentary rocks) and therefore create a more complicated and much less transparent field

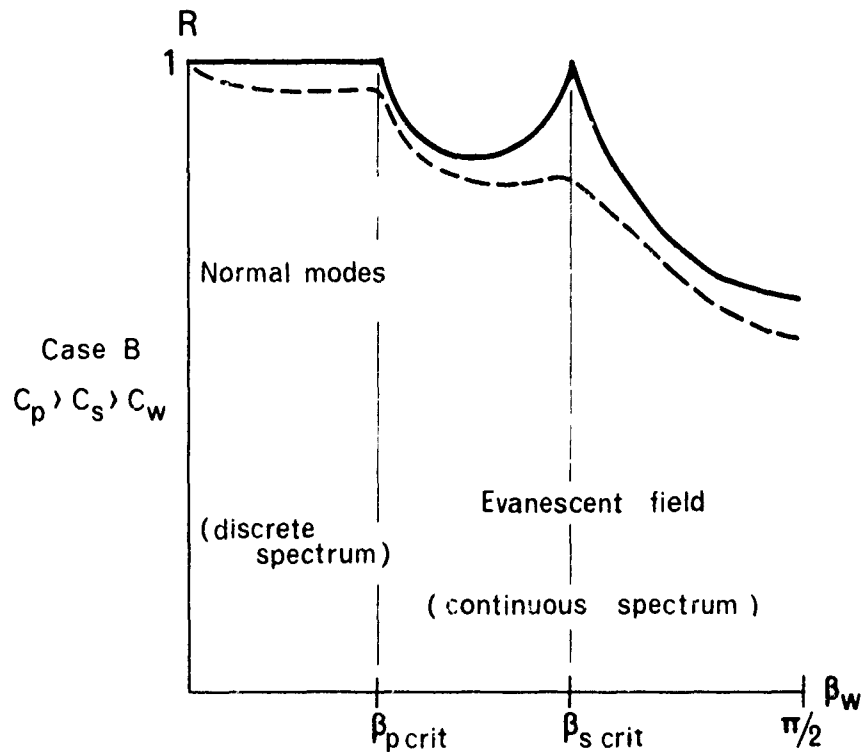
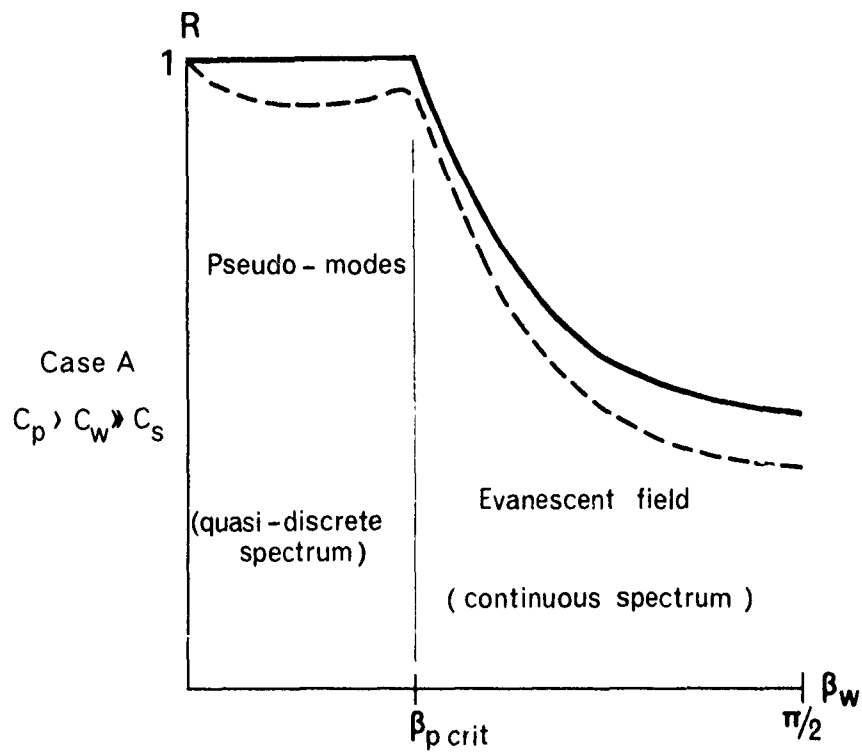


FIG. 6 TYPICAL REFLECTION COEFFICIENTS AT A VERY SOFT SEDIMENTARY SEA FLOOR (A) AND AT A VERY HARD ROCK-BOTTOM (B)

composition. In Fig. 7 the dotted curves are intended to demonstrate that the pertinent blurred interference patterns still behave like a non-systematic and less pronounced mode structure. We will therefore continue to use the vivid mode picture and use arguments based on those discrete phenomena to describe qualitatively the underlying physics.

The two simple examples above should be the starting point from which to obtain at least some impression of the quite complicated wave propagation in the earth's crust. The ocean-floor environment that is of particular interest to us in this report is an irregularly-layered structure of inhomogeneous, anisotropic, and dissipative media with pronounced parameter profiles. For example, densities and bulk wave velocities increase with depth and losses decrease simultaneously (see Sect. 2.2). All internal interfaces impose additional transition conditions on the elastic field and they may support different types of interface waves (see Sect. 1.1 and [73]). Furthermore, some of the layers may be distinct wave guides for certain trapped modes [74,75], such as Love waves in sedimentary layers [5,76,77].

While the general influence of bottom stratification on the reflection coefficient was carefully explored by underwater acousticians and geophysicists in the past (see e.g. [78 to 82]), it was only a short time ago that Hawker [83,84] demonstrated how the specific influence of interface waves resulted in a pronounced minimum of this coefficient occurring next to grazing incidence, i.e. for small angles  $\beta_w$ . Due to the greater variety of seismic-wave types, the dispersion curve of the "zeroth mode" of the system may be split into different branches forming several "sub-modes" characterized by the pronounced interfaces. The high-frequency limit of each of these separated branches should be strongly related to the velocity of a Scholte or Stoneley wave at the upper margin of a pronounced top layer, while the corresponding low-frequency limit should be linked to a somewhat higher velocity characterizing a sort of "modified Rayleigh wave" of the underlying stratified half-space. Generalizing this dynamic elasticity of simple structures, the phase velocities of higher-order modes should vary between the most significant bulk-wave velocities of the stack. Thus we can expect that their upper limit at the low-frequency cut-off is determined by the sub-bottom, while their lower limit in the high-frequency range is a sort of "mean value" that refers to the top layers. Obviously the excitation of those resulting modes that insonify the complete



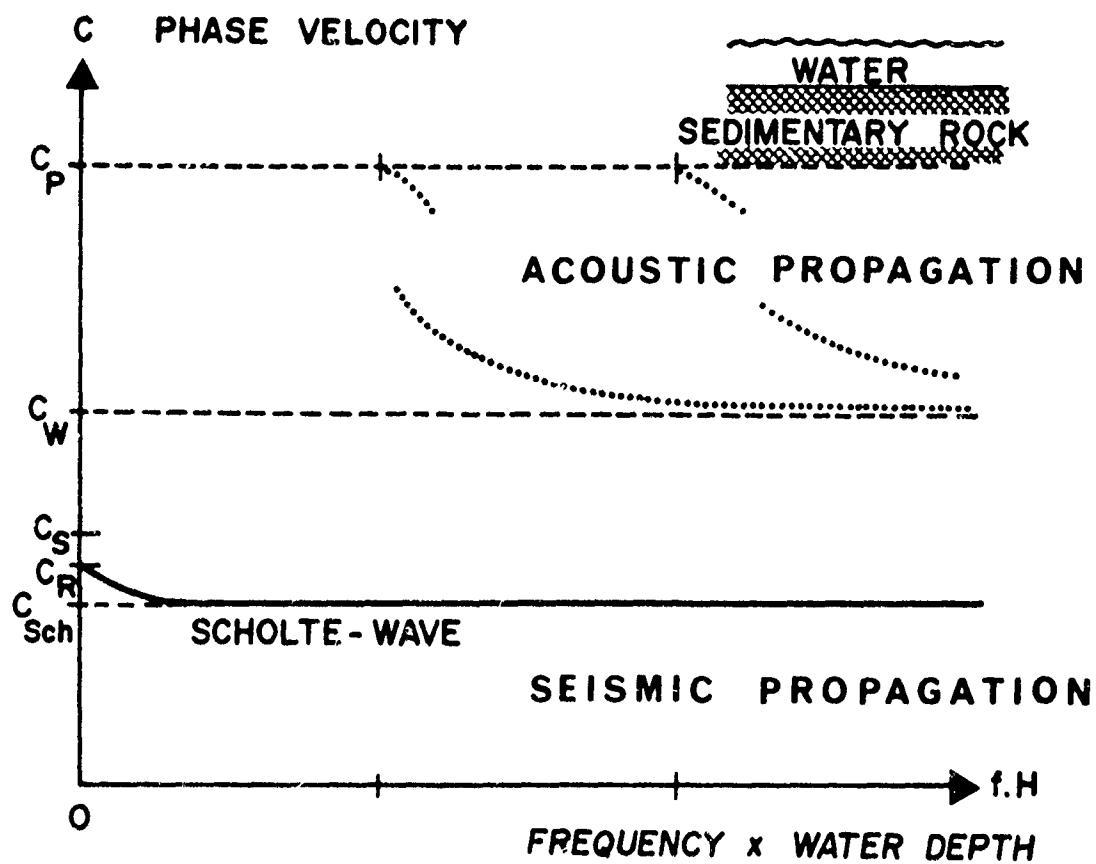


FIG. 7 PHASE-VELOCITIES OF THE LOWEST MODES IN SHALLOW WATER OVER A RELATIVE "SOFT" ROCK-BOTTOM

structure and of those trapped modes that are restricted to certain layers or interfaces depends on the given frequency scale and last, but not least, on the type and position of the source. The successful application of the normal-mode model for many sonar purposes [5, 85 to 90] shows that very simple bottom models may already be sufficient to make allowance for the influence of the sea floor on water-borne sound in the medium- and high-frequency regime. However, in the range of low and very low frequencies we have to proceed to seismic models of the earth's crust, because the water depth and the thickness of many bottom layers may be comparable to, or even smaller than, one wavelength of the transmitted sound field. A reasonable model for such infrasonic propagation problems is already given by a horizontally-stratified half-space composed of homogeneous and isotropic layers characterized by constant parameters. A progressive refinement of the idealized layering provides us moreover with the possibility of approximately shaping the typical parameter profiles if needed (see Sect. 1.3).

Other very common features of sound propagation in shallow water are the coupling or conversion effects of different modes belonging to the same wave type or even to quite dissimilar propagation phenomena. Those interactions may already happen in regularly-layered systems with range-dependent parameter profiles (see e.g. [26,70]), but they are typical for structures with varying layer thicknesses (see e.g. [91 to 93]) and/or range-dependent parameter profiles (see e.g. [94]).

To end this discussion of the influence of layering on wave propagation we would therefore like to drop a hint on the effects of a sloping bottom. As they propagate towards the apex of the wedge-shaped liquid layer, the higher-order modes of the "water wave" are "stripped" one after another. On each occasion the energy is partly transferred to the next lower-order mode (mode conversion), partly reflected back into deeper water, and partly refracted into the substratum in the form of a well-defined beam consisting mainly of radiated P-waves ("soft" bottom) or SV-waves ("hard" bottom). While these coupling effects (conversion from multi-mode to single-mode propagation) and radiation characteristics of tapered wave guides have already been studied carefully in connection with guided micro-waves and light waves (see e.g. [95-97]), their counterparts in underwater acoustics have attracted little attention in the past. With the growing interest in

seismic sensing the latter problems can now be expected to experience a revival. Based on the results with the less-complicated electromagnetic fields, Coppens and Sanders [98] and Odom et al [99] started to model theoretically and experimentally the shallow-water edge with different, quite-small, taper — or "beach" — angles. In accordance both with simplified theories and model experiments, they demonstrated that the acoustic energy is rapidly dumped into the bottom before the first mode reaches the pertinent cut-off depth. The refracted compressional or shear wave in the substratum always formed a well-defined beam (narrower with decreasing slope or taper angle) but their predicted depression angle (about  $15^\circ$  for most realistic parameter combinations) always exceeded the measured result (below  $10^\circ$ ). Modelling this problem with a more sophisticated mathematical tool (Parabolic Equation) Jensen and Kuperman [100] reached better agreements with those experimental data (for a liquid-like bottom) and also showed the corresponding refraction phenomena for some of the higher-order modes.

The top layers of the ocean bed mostly consist of unconsolidated sediments (condition A), which is why the primary conversion or bottom coupling of the suppressed modes usually creates a P-wave in the sea-floor. The pertinent beam then suffers repeated and more complicated reflection- and refraction-splittings due to deeper interfaces, and simultaneously undergoes a strong broadening as a consequence of the different upward-refracting parameter profiles and inhomogeneities within the layers (see Sect. 2.2). This latter comment on the stripping of all higher-order modes underlines again the special position of the Scholte wave or its modifications (see Sect. 3.2): that they are not only free from those radiation losses but may even profit from them (see e.g. 83,84).

### 1.5 Some Analytic Approaches and Model Experiments Regarding Annular Scholte-Wave Pulses

As mentioned in Sect. 1.1, in the 1930s Cagniard [11] solved the problem of an impulsive point source located close to a plane, solid/solid or liquid/solid interface. His famous "method" of deriving the closed-form solutions for all ranges (see also [39,40]) is essentially based on Lamb's work [17] and was developed independently and almost simultaneously by

Smirnow and Sobolev [101,102]. However, due to the sophistication of the mathematics involved, these results never became a practical tool to solve geophysical or acoustical problems.

Thus after World-War II a few physicists tried to find more practicable approaches and, especially in the years 1960-65, some efforts were devoted to the derivation of much simpler mathematical descriptions and to their "testing" with the aid of model experiments in the laboratory (e.g. [103]). It is obvious that the results of those small-scale experiments can merely reflect some very pronounced features of real-world data but they may provide at least a very helpful cross-check on the theoretical set-up and give some confidence in applying it under more realistic conditions.

Before discussing some of these efforts in detail we would like to review the pertinent mathematics in general. The wave propagation of interest along an interface is characterized by up to four branch points of the pertinent integrands, corresponding to a maximum of four "undisturbed" bulk waves. To restore the uniqueness of the complex plane of integration we have therefore to choose up to four branch lines or "cuts" that divide the ambiguous Riemann surface of the integrals into a maximum of five "sheets" or "leaves". Due to the different ways of making these cuts, and to the resulting definition of those sheets, one has often several possibilities for calculating the different contributions to the integrals. The final choice is usually determined by the requirement for a fast convergence and by a need to facilitate the evaluation. For a fixed source/receiver configuration those joined sheets can be interpreted quite plausibly as the subsequent "time windows" of the synthetic seismogram (being separated by the arrivals of the bulk waves) and thus their contributions can be interpreted as the pertinent sections of the calculated signal. The only sheet without any contribution and thus "without physical meaning" is usually classified as the "lowest" one corresponding to the period between the onset of the source and the first arrival at the receiver position.

The genuine interface waves of interest are characterized by poles on the "top sheet" that contribute to the "tail" of the signal, while the pseudo-interface waves result from poles on "lower sheets" between the mentioned extremes.

Despite the fact that the integration has to be performed on the top sheet, those lower sheet poles may have an influence on the synthetic seismograms by their proximity to the cuts. With respect to the more practicable approaches that reveal this correlation between the mathematical and the physical aspects, the three-part paper by Roever, Vining and Strick [24] and the publication by Phinney [32] may be called milestones in the field of elastic interface waves.

To simplify the mathematics, Strick reduced the problem to two dimensions, assuming a delta-function-excited, horizontal, line source instead of a similar point source. As the resulting field terms of these sources differ at large ranges by essentially an amplitude factor and a half-order differentiation, such a line source may be regarded as a point source with an excitation between a delta- and a step-function. The chosen line source is therefore a good simulation of a detonating chemical charge or of an electrical-spark discharge, which are the commonest source devices for field studies and laboratory tests. The only substantial adulteration results from the characteristic "tail-effect" of a line source, which can be easily understood from Huyghen's principle. (The source cannot be blanketed off and thus cannot be weighted by an amplitude assignment.) Assuming two adjacent half-spaces, Strick calculated the pressure response and the particle velocities at a water/solid interface corresponding to a "relatively soft" (condition I:  $c_s < c_w$ ) and an "extremely hard" (condition II:  $c_s > c_w$ ) sea floor. In both cases he proved the excitation of a relatively strong Scholte-wave pulse, and demonstrated impressively that the already-mentioned suppression of the pseudo-Rayleigh wave at a soft ocean bottom (for the physical interpretation see Sect. 1.2) is due to the off-axis position of the pertinent pole. In addition, Strick has demonstrated that the real part of this pseudo-Rayleigh pole is practically identical with the true, real-Rayleigh pole and thus with the zero-crossings of the pertinent signals propagating with the same velocity.

Figure 8 compares two examples from Strick's theoretical results with the pressure records of a transient point source (spark gap) made by Roever and Vining. The agreement is indeed outstanding, and as was to be expected (from our theoretical findings in Sects. 1.1 and 1.2) the Scholte-wave pulse is more compressed under "very hard" bottom conditions but also more difficult to separate from the direct P-wave arrival in the water column.

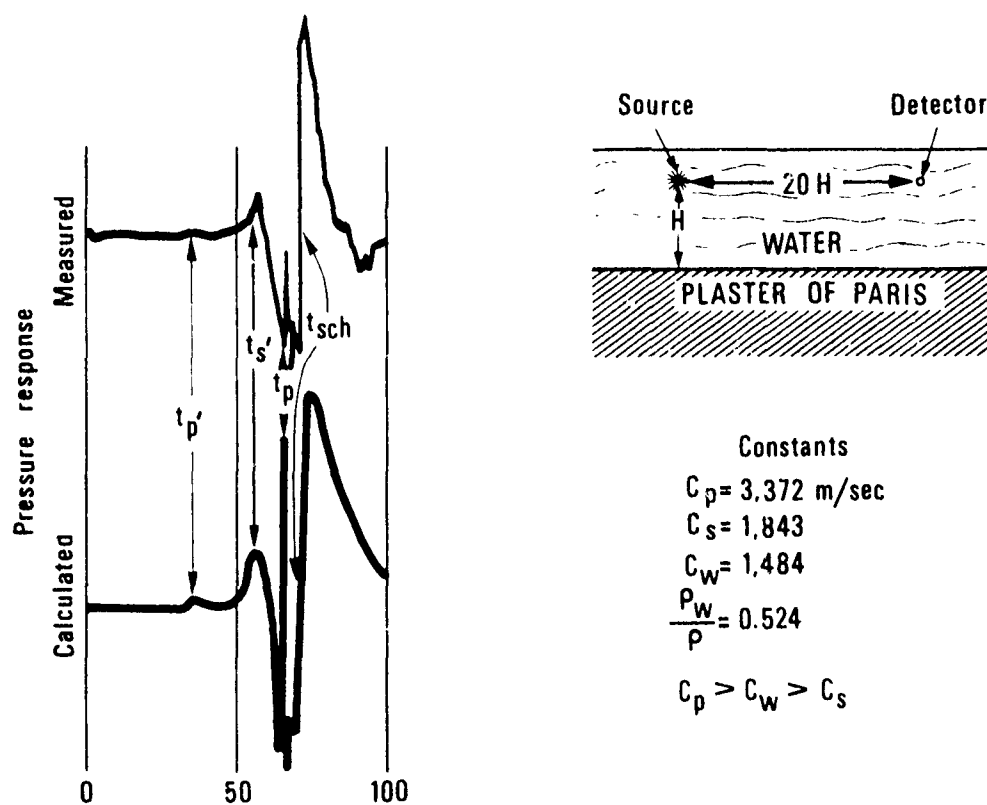
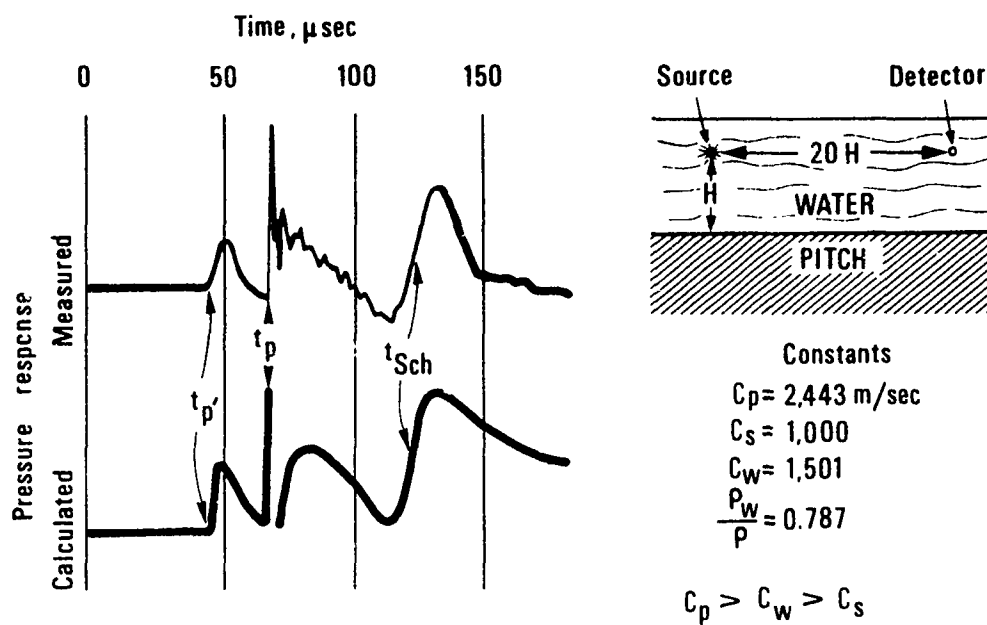


FIG. 8 COMPARISON OF STRICK'S MODELLING RESULTS WITH THE LABORATORY MEASUREMENTS BY ROEVER AND VINING [23]

Strick's mathematical treatment of a given source/interface/receiver constellation already demonstrates the decisive role of the so-called "period-function"  $F$  and "response-function"  $G$ , which are given by:

$$F = \sqrt{X-N} (S_R - S_L) \quad (\text{Eq. 21a})$$

$$G = \sqrt{X-N} (S_R + S_L), \quad (\text{Eq. 21b})$$

with:  $X, N$  defined by Eq. 11.

$S_R, S_L$  right-and left-hand side of Eq. 13.

For an exponentially-decaying source pulse (pressure  $p$  or displacement  $u, w$ ), such as:

$$\chi_0 = B_0 e^{-\frac{t}{T_0}}; \quad (\text{Eq. 22})$$

with  $B_0, T_0 = \text{constant real factors.}$

Phinney has shown that for  $T_0 \rightarrow 0$  and  $B_0 \rightarrow \infty$  (i.e.  $\chi_0 \rightarrow \delta(t)$ ) the excited wavelets of the genuine or pseudo-interface waves can be described by:

$$\chi_{n,m} \Big|_{z=0} \approx A_{n,m} \frac{B_1 B_2(\omega) B_3(r,t)}{\sqrt{r}} \cos \Omega_n(\omega, r, t) \quad (\text{Eq. 23})$$

with

$$\chi_{n,m} = \begin{Bmatrix} P \\ u \\ w \end{Bmatrix} \quad \text{for } n = \begin{Bmatrix} 0 \\ 1 \\ 1 \end{Bmatrix} \quad \text{and } m = \begin{Bmatrix} 0 \\ 1 \\ 2 \end{Bmatrix}$$

$A_{n,m} = \text{complex amplitude factor}$

$$B_1 = \lim_{\substack{T_0 \rightarrow 0 \\ B_0 \rightarrow \infty}} (B_0 T_0) \quad \text{constant source parameter}$$

$$C(F, G) = \frac{1}{k} \left( \frac{iG}{\partial F / \partial \omega} \right) \Big|_{\omega=kc} = B_2(\omega) e^{i\psi(\omega)}$$

system's "excitation function".

$$D(r, t) = (r - c_w \sqrt{\frac{N}{X}} t) - i h \sqrt{1 - \frac{N}{X}} = B_3(r, t) e^{i\phi(r, t)}$$

signal's "pulse-envelope".

$$\Omega_n(\omega, r, t) = [\psi(\omega) + n \frac{\pi}{2}] - \frac{5}{2} \phi(r, t)$$

signal's "phase angle".

The most prominent features of the general expression of Eq. 23 are determined by the expected term for cylindrical spreading, by a characteristic weighting function  $C$  of the system (having the well-known features of a reflection or transmission coefficient), and by a sort of "carrier" having the variable frequency  $\Omega_n$  and being shaped by the "amplitude-modulation"  $D$ . As the results for  $u$  and  $w$  are very similar but without any point of symmetry (which occurs in such two-dimensional problems as the above-discussed approach by Strick) and are phase-shifted against each other, the resulting particle orbit, and thus the hodographs of particle velocity and acceleration, are generalized lemniscates (see also [11]).

In agreement with our monochromatic findings in Sect. 1.2, the broadband results of Strick and Phinney demonstrate that the effect of removing source or receiver from the interface is to suppress the higher frequencies of the excited interface wave. If the radiated pulse shape and the receiver depth are well known, the spectrum of the detected signal reflects the distance of the source from the interface.

Under real-world conditions this feature is certainly of secondary importance because of the effects of dispersion (see Sect. 1.4) and absorption (see Sect. 2.2).

Between 1963 and 1965, Spitznogle, McLeroy, and co-workers extended Strick's theoretical work and the experimental studies by Roever and Vining to a two-layered, solid half-space covered by a homogeneous liquid counterpart [104-108] or by a liquid layer with an adjacent gaseous half-space [109-110]. To compose the theoretical seismograms, their calculations took into account up to two subsequent interactions of the primarily radiated P-wave front with the crucial liquid/solid interface. Using four, different, small-scale models and a spark gap they recorded numerous pressure responses at the liquid/solid interface. In almost all cases the



measured signals again showed very good agreement with the synthesized pressure/time curves. Usually the Scholte-wave pulse turns out to be the most prominent portion of the signal after the above-mentioned direct arrival in the liquid.

The extension by McLeroy and other underwater acousticians of these successful laboratory tests to the more complicated and contradictory field experiments in shallow water will be described in Sect. 2.4.

## 2 EXPERIMENTAL ASPECTS OF SEISMIC SENSING AT THE OCEAN BOTTOM

### 2.1 Geophones as Standard Transducers for the Detection of Seismic Signals

The classical mass-spring geophone is a relatively simple electromechanical transducer. Its mechanical system consists of a mass that is suspended by a system of springs within a frame or a container. For different technical reasons the motion of the mass has to be restricted by an axial guidance, which is why the geophone acts always as an unidirectional sensor. The amplitudes of this axial motion have also, of course, to be limited by damping stops. Usually the superimposed electromagnetic system consists of permanent magnets that are attached to the housing and a coil of wire that is wound around the moving mass. The magnets are fitted to the frame in such a way that they create optimal field conditions around the moving coil. As the moving components of the geophone are coupled to the container both by the springs and by a damping dashpot, its response curve is characterized by a flat branch for all higher frequencies and by a mechanical resonance for a relatively low frequency. This resonance is usually suppressed partially or totally by a suitable electrical load but nevertheless it determines the low-frequency cut-off of the instrument. The response curve of the sensor decreases for all frequencies falling below this cut-off, usually at the relatively high rate of 18 to 20 dB/octave.

Roughly speaking this resonance frequency or "natural frequency" is between 0.05 and 1 Hz if a stationary geophone is used for earthquake monitoring, and between 1 and 30 Hz if the transducer is employed for seismic prospecting or surveillance. By putting such a geophone or seismometer on or in the earth we try to create a rigid connection between the housing and the moving environment. Owing to its inertia, the suspended mass of the sensor represents the "fixed point in space" relative to which we want to determine the earth's motion. Due to the above-mentioned coupling of mass and container, such a fixed point can be established only approximately. The electrical signal at the output of the

coil is proportional to the rate of relative motion of magnet and coil — thus the classical geophone is primarily a velocity detector. Sometimes this output signal is immediately differentiated or integrated by incorporated electronic circuits to tune the sensor to acceleration, or displacement measurements. The interested reader may find the pertinent mathematics in such books on applied geophysics as [111,112], special papers [113], or technical publications of the seismic industry [114].

As seen, the geophone acts as a unidirectional motion detector sensing only the velocity component parallel to its axis. The resulting sensitivity pattern is therefore proportional to the cosine of the angle measured from the axis. Thus it has a dumbbell-like shape with no gain in any direction but with increasing attenuation towards the off-axis directions. For an omnidirectional background of ambient noise and an on-axis signal field, the signal-to-noise ratio has been calculated to be approximately 5 dB higher than for such omnidirectional sensors as most of the commonly-used hydrophones [115]. In practice, however, this signal-to-noise ratio will always be smaller, because the sensitivity pattern of real geophones never disappears completely in the off-axis directions. This imperfection is simply a consequence of a slight cross-axis coupling due to the suspension and axial guidance of the moving mass by a mechanical spring system.

This two-fold function of the springs is responsible for other typical features of the classical geophone: the greater delicacy required in its handling and the care that has to be taken in adjusting its horizontal sensors. Even with relatively large masses, the vertical geophones are quite rugged and operational even for alignments between  $\pm 5^\circ$  and  $\pm 20^\circ$  from the vertical. On the other hand their horizontal counterparts have to be handled more carefully, be positioned correctly, and adjusted within a few degrees.

The tilt sensitivity of all traditional sensor models decreases if the resonant frequency is increased by reducing the moving mass and/or stiffening the springs. As this improves the general ruggedness, we can easily understand the success of short-period phones with high natural frequencies (above about 5 Hz) in the field of seismic prospecting. It is equally obvious why the use of high-performance 1 Hz seismometers has been restricted more or less to scientific purposes.

In 1977 Teledyne-Geotech marketed a 1-Hz geophone (model S-500) that can be transported carefully without mass-locking and can be operated in any wanted direction. In the past such favourable characteristics have been offered only by the much less sensitive piezoelectric acceleration sensors. With these new, high-performance, 1-Hz geophones it is now possible to reach intrinsic sensitivities of the order of  $10^3$  V/m/s by using closer winding and integrated electronics.

By using these sensors together with a few low-noise amplifier stages, the seismic-noise background in the infrasonic frequency band can easily be recorded on magnetic tape even at very "quiet" sites on land or on the deep ocean floor (see Sect. 2.3) where the vertical deflection (p-p) lies between approximately 1  $\mu$ m at 1 Hz and 0.01  $\mu$ m at 30 Hz.

Other very important experimental aspects of ocean-bottom seismometers are their suitable mechanical design (no infrasonic system resonances), their proper coupling to the sea bed, and their protection against spurious motion effects from the overlying water mass [112,115-119]. The ideal condition would be approached by using very small embedded sensors that have a density equal to the average of the surrounding bottom. Thus the impedance matching should be optimized by a proper choice of weight and shape (especially footpad size) of the receiver-station, and it should be as well sheltered as possible from currents and pressure variations in the water column (e.g. by covering with acoustically-insulating material).

By using several of these sensor stations on or just below the sea floor one can install different types of arrays or distributed systems and thus profit from the more sophisticated signal-processing methods (such as beamforming) developed for those more elaborate receiver configurations (see e.g. [115,118,]).

## 2.2 Some Essential Features of Sea-Floor Acoustics

For many years there has been intense research on sound propagation in the ocean bottom and the literature is rich with reports of the great many theoretical studies, modelling, and field experiments performed. We recommend newcomers to the field to the summary papers by Nafe et al

[120,121] or Hampton [122], and the more modern reviews by Hamilton [123,124] or Hampton [125] as starting points. However, because of the large variety of marine sediments, and the unavoidable deterioration of model experiments (such as scaling problems) and of sample tests in the laboratory (using piston-cores or grab-samples), together with the technical difficulties of in-situ measurements, there still remains a substantial lack of knowledge about the subject, particularly within the infrasonic frequency range that is of interest in the present context.

We therefore do not want to encumber the reader with a detailed discussion of the numerous theoretical models (such as [124,126,127,128]) and experimental techniques or with a presentation of extensive data sets (such as [129,130]). Thus the following comments are intended merely to give a general overview of the main features and some specific hints. Speaking generally, the sea floor consists of a series of "soft" sediment strata overlying a "hard" rock sub-bottom. Under real-world conditions this scale of hardness is of course very smooth and the transition zones may be described as "relatively-hard" sediments or "quite-soft" rocks. In order of increasing depth, the lithosphere below the ocean may be classified roughly as follows:

- A. water-saturated, unconsolidated sediment layer(s) (e.g. mud, silt, sand, clay).
- B. water-saturated, consolidated sediment layer(s) (e.g. silt, sand, clay).
- C. sedimentary rock layer(s) (e.g. sand or limestone).
- D. crystalline rock basement (e.g. basalt or granite).

The thicknesses of the layers in A and B may vary from some centimetres to some hundred metres (see e.g. [131]) while the primitive rock basement D can be regarded as an almost homogeneous half-space. The sedimentary-rock strata of group C lie between these extremes. The consistency of these layer materials ranges from the quasi-liquid character of suspensions ("very soft") to the extreme hardness of crystals ("extremely hard"). For the layers in A, B and C this increasing consolidation is mainly caused by the weight of the overburden but is also partly due to chemical processes. With increasing pressure, the packing density of their mineral components

(with many different grain sizes and mixture ratios) becomes greater and consequently the contact between the particles becomes more rigid. Thus the resulting or mean mass-density  $\rho$  of the layers grows from about  $1.0 \text{ g/cm}^3$  (water) up to about  $3.0 \text{ g/cm}^3$  (crystalline rocks), the porosity (percentage of porous space) dropping from almost 100% (at the water/bottom interface) to 0% (in sedimentary rocks), and the loose contact of the particles changes into a quite regular solid frame or internal skeleton. From this it is evident that all elastic moduli, and thus the sound speeds  $c_p$ ,  $c_s$ , must have a positive gradient with growing depth, while the damping losses (mainly due to internal friction) must show the opposite trend.

These very general considerations of the acoustic features indicate that the ocean floor always represents a "very hard" solid if we penetrate sufficiently deeply and may be composed of "quite soft" or even liquid-like media near the water/bottom interface. If we disregard the influence of pronounced interfaces and inhomogeneities, these general features explain clearly the steady upward refraction of seismic waves and the often unexpectedly good conditions for long-range transmission via deep refracted paths. Our knowledge of the acoustic properties of the deep layers involved originates mainly from the well-known techniques of reflection and refraction shooting [132 to 136].

As here we are mainly interested in the propagation of infrasound at or just below the water/bottom interface we will concentrate our attention on the acoustics of the upper sea-floor strata. The exploration of these top layers is carried out by means of the already-mentioned remote techniques (see also [137-140]), by *in-situ* implantation of probes ([141-145]), by laboratory tests of grab or core-samples (see e.g. [138,140]), or by combined methods [146,147].

At this point we would like to offer a rough idea of the parameter values that govern the propagation of P- and S-waves in the sea-floor. To simplify matters, we assume a normalized sound speed,  $c_w = 1500 \text{ m/s}$  at the bottom of the water column, and relate the compressional and shear velocity of the bottom layers to it by two constants  $n_p$  and  $n_s$ :

$$c_p = n_p c_w \quad ; \quad c_s = n_s c_w \quad . \quad (\text{Eq. 24})$$

For the same reason, we generalize the well-known high-frequency behaviour of many materials by assuming that the attenuation coefficients  $\bar{\alpha}_p$  and  $\bar{\alpha}_s$  (dB/m) always increase linearly with frequency,  $f$  (kHz), according to:

$$\bar{\alpha}_p = K_p f \quad ; \quad \bar{\alpha}_s = K_s f. \quad (\text{Eq. 25})$$

Above 1 kHz this simple relation is generally valid for most sedimentary bottom strata, as the numerous data-points of Fig. 9 [127] demonstrate. In this way we have two frequency-independent attenuation factors  $K_p$  and  $K_s$  (dB/km/Hz) by which to characterize the different media. Table 3 summarizes the ranges of  $n_p$ ,  $K_p$ ,  $n_s$ ,  $K_s$  and  $\rho$  within the general A-D classification previously described.

	$\rho$	$n_p$	$K_p$	$n_s$	$K_s$
A	1.0	0.97	0.35	0.04	17
B	1.5	1.2	0.15	0.5	5.0
C	1.5	1.5-4.0	0.005-0.3	0.6-2.5	0.005-0.3
D	3.0	2.5-5.0		1.7-3.0	

**TABLE 3** DENSITIES  $\rho$ , VELOCITY RATIOS  $n$ , AND ATTENUATION FACTORS  $K$ , FOR TYPICAL BOTTOM LAYERS

Compared with the quite steady and moderate increase of density with depth [148], the values of the other parameters increase much less regularly and cover greater ranges, sometimes even of orders of magnitude. Because of the great diversity of bottom materials the limits of the intervals indicated in Table 3 can vary widely, so the figures given should therefore be regarded as indicative.

The mean value of the compressional velocity gradient has been determined to about  $1(\text{s}^{-1})$  in the sedimentary layers A-B-(C) (to a depth of about 1 to 2 km) and becomes much smaller in the rock basement (C)-D (see e.g. [149, 150]). Thus the depth profile of  $c_p$  is much steeper than that

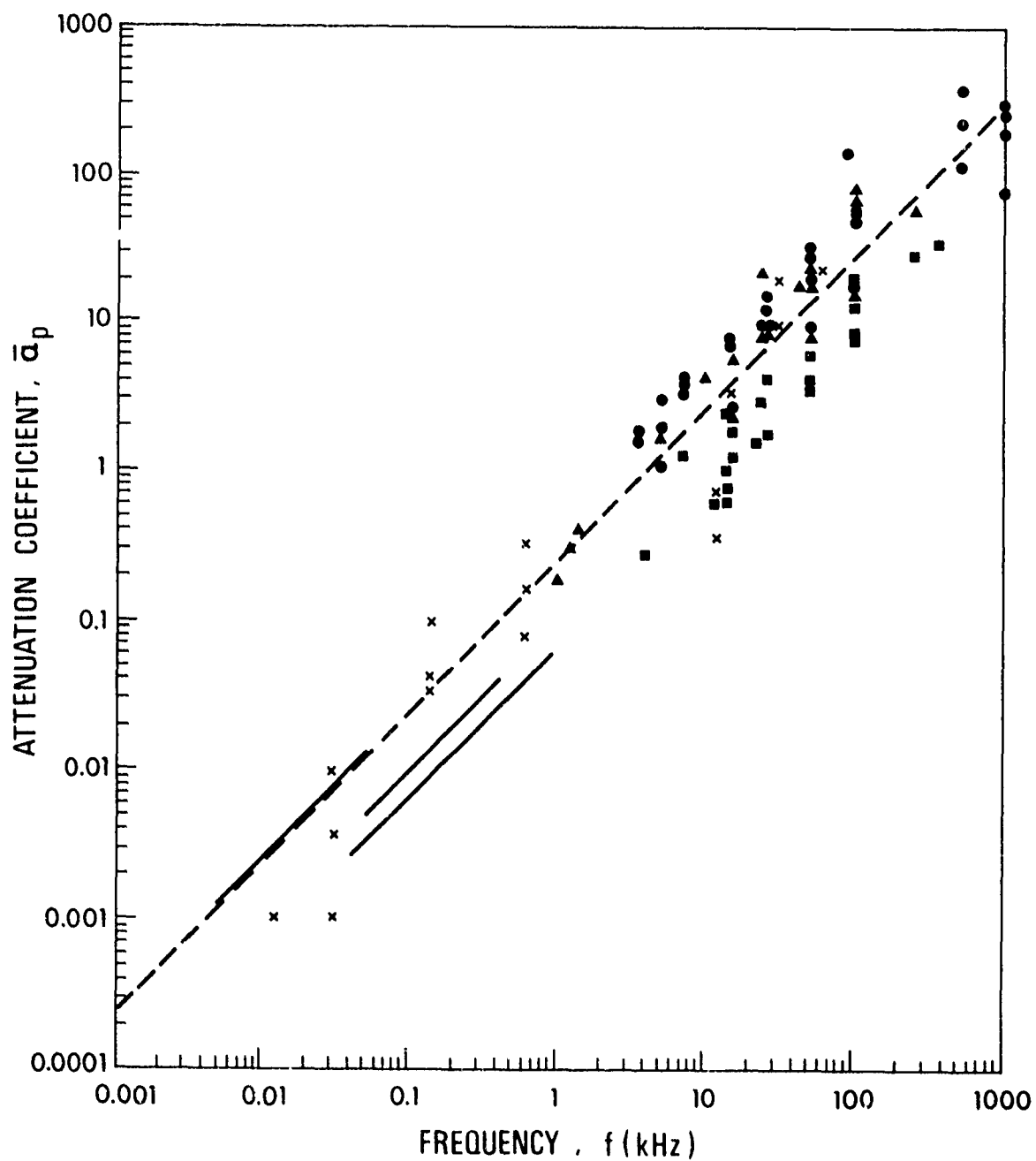


FIG. 9 FREQUENCY DEPENDENCE OF THE ATTENUATION COEFFICIENT  $\alpha_p$  FOR COMPRESSIONAL WAVES IN SEDIMENTS (data compiled from literature)



of the overlying water column and explains the often-observed strong upward refraction of P-waves, which may sometimes even create apparent low, or even negative, bottom-reflection losses (see e.g. [151-153]). The low starting value of 0.97 for  $n_p$  demonstrates a well-known suspension feature: that the "disorder" of the dispersed, "fast", solid particles in a "slow" liquid may even decrease the original sound speed of the dispersing agent.

The dashed line in Fig. 9 shows a mean value of  $K_p \approx 0.25$  dB/km/Hz for the attenuation of P waves in sediments. With growing depth the attenuation factor  $K_p$  usually decreases quite rapidly, as shown in Fig. 10, and then reaches the characteristic value for rocks,  $K_p \approx 0.034$  dB/km/Hz, at a depth of approximately 1.5 to 2 km [154]. This behaviour is a consequence of the fact that the total loss mechanism is more or less reduced to the basic material losses (internal friction and scattering effects) because those due to the friction of the grains in a sort of "low-frequency skeleton" ("external" friction) and viscosity are eliminated stepwise by compaction. Table 3 gives only one  $K_p$  interval for all rock types, because it may sometimes happen that intermediate sedimentary rock layers are even less lossy than their crystalline basement. More modern studies [128] call in question the validity of Eq. 25 for the infrasonic frequency regime and thus assume much smaller  $K_p$  values in the "soft" top-layers due to the above mentioned "low-frequency skeleton" which is thought to be a macroscopic counterpart to the microseismic lattice structure of crystals.

The  $n_s$ -values in Table 3 indicate that the shear velocity in unconsolidated sediments may be very low (down to about 5% of the sound speed in the overlying water), but even the extremely small amount of data concerning the depth dependence suggests the already expected high velocity gradient of about  $10(s^{-1})$  for the first 10 m and of about  $3(s^{-1})$  for the following 100 m [155,156]. The often neglected existence of S-waves in those very "soft" top-layer sediments is usually explained with help of a sort of macroscopic shear rigidity assigned to the "low-frequency skeleton".

However, the pertinent attenuation is very high, as Table 3 and the few published data sets [157] show, and a mean value given by  $K_s \approx 11$  dB/km/Hz may be quite reasonable in this case. With growing depth, the attenuation factor  $K_s$  is also expected to decrease extremely fast, because we know

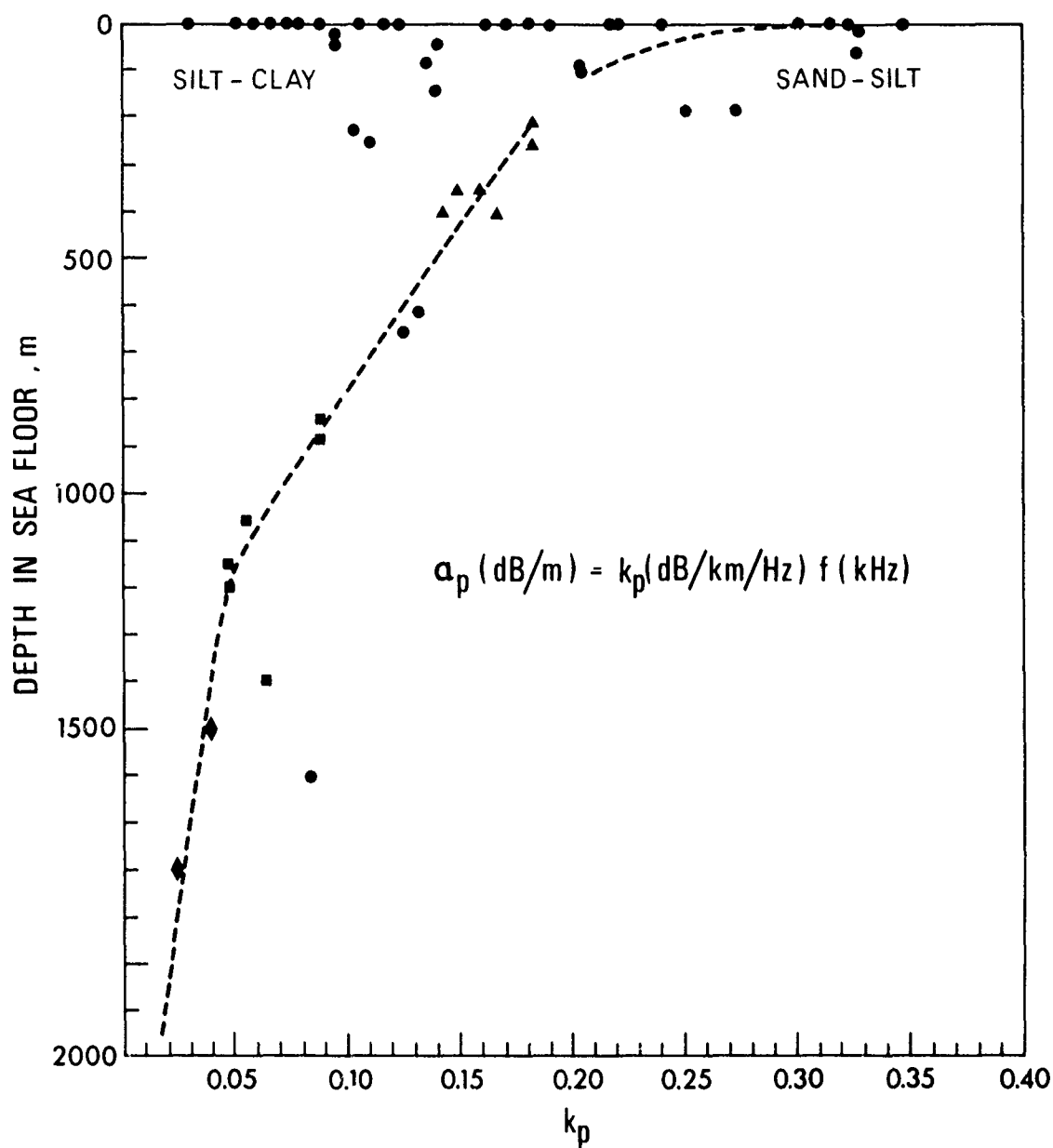


FIG. 10 DEPTH DEPENDENCE OF THE ATTENUATION FACTOR  $k_p$  FOR COMPRESSIONAL WAVES IN SEDIMENTS (data compiled from literature)

(e.g. from cores taken during the Deep Sea Drilling Project) that in the underlying rock materials  $K_s$  adopts values of the same order as  $K_p$ .

As the top layers of the sea floor usually belong to the stratifications A, B and C, the velocities of the infrasonic interface waves ("pure" or modified Scholte waves; see Table 1) may range from about  $c_{sch} \approx 60$  m/s in case of relatively thick (at least more than one wavelength) and "very-soft" sediment covers ( $c_s \ll c_w$ ), to that of the sound speed in water  $c_{sch} \approx 1500$  m/s in case of "quite hard" sedimentary rocks ( $c_s > c_w$ ).

Because they result from a combined action of compression and shear, these interface waves are governed by the usually quite high shear attenuation. Thus we cannot expect long-range or even medium-range propagation of this wave type in areas where the basement is covered by very thick and "extremely soft", unconsolidated sediment strata [147].

In case of a "hard" rocky sea floor that may even have a thin and very lossy sediment cover ("coating"), the propagation conditions are certainly much better and may allow the successful use of those guided waves as a tool for the seismic sensing of waterborne infrasound. (see Sect. 3.2).

Unfortunately these more promising aspects of a rock-like bottom are merely based on the material parameters and do not account for the macroscopic structure and shape. Under real-world conditions such a hard sea floor is not only restricted to relatively small areas (e.g. banks and reefs) but is mostly made up of inclined and sometimes irregular layers and therefore presents a surface full of features. These latter features are particularly obstructive to the excitation and propagation of all guided seismic waves. Thus the optimal conditions for a successful excitation and propagation of interface waves may be found in those wide-spread areas where the marginal zone of the sea floor is composed of a quite regular sediment layering providing a smooth surface and a rapid consolidation with growing depth.

### 2.3 Acoustic and Seismic Ambient Noise Data from Shallow-Water Areas

In sensing acoustic or seismic signals we must always operate against a certain noise background that is of many origins (sources), qualities (spectra), and quantities (levels). As with sea-floor acoustics, the study of ambient-noise characteristics on land and at sea is a large field and we must restrict ourselves to some highlights and to referring the reader to the pertinent literature.

Since World War II underwater acousticians have devoted much effort to the registration and interpretation of waterborne or acoustic noise, and seismologists have acted likewise with regard to earth movements. As summary papers on the first subject we recommend the book by Ross [158], the article by Arase [159] and the classical paper by Wenz [160]. A good insight into the nature of seismic noise spectra is given by the publications of Frantti et al [161,162] and Brune et al [163]. Both the spatial division of these research domains and the interest in different frequency bands caused quite poor overlapping of the data within the range between 1 Hz and 100 Hz. With a growing interest of the sonar community in the low-frequency regime and the development of more versatile seismic sensor stations (OBS's) this gap started to be filled in the early 1960s. While the underwater acousticians extended their noise measurements into coastal waters [164-166] the seismologists have been mainly concerned with data collections in the deep ocean floor [167-171].

Consequently our knowledge of infrasonic seismic noise in shallow water is still quite poor and based on a few field trials. Another shortcoming of the existing seismic data is given by the fact that most of them have been recorded merely with vertical geophones (see Sect. 2.1).

We will now reproduce a few representative curves and discuss their most prominent features. Figure 11, taken from [166], recapitulates the well-known pressure spectrum levels of the infrasonic and low-frequency noise in shallow water and indicates the main noise sources.

With increasing frequency the acoustic noise level generally drops at a rate of -8 to -10 dB/oct. Below 10 Hz the wind-generated pressure

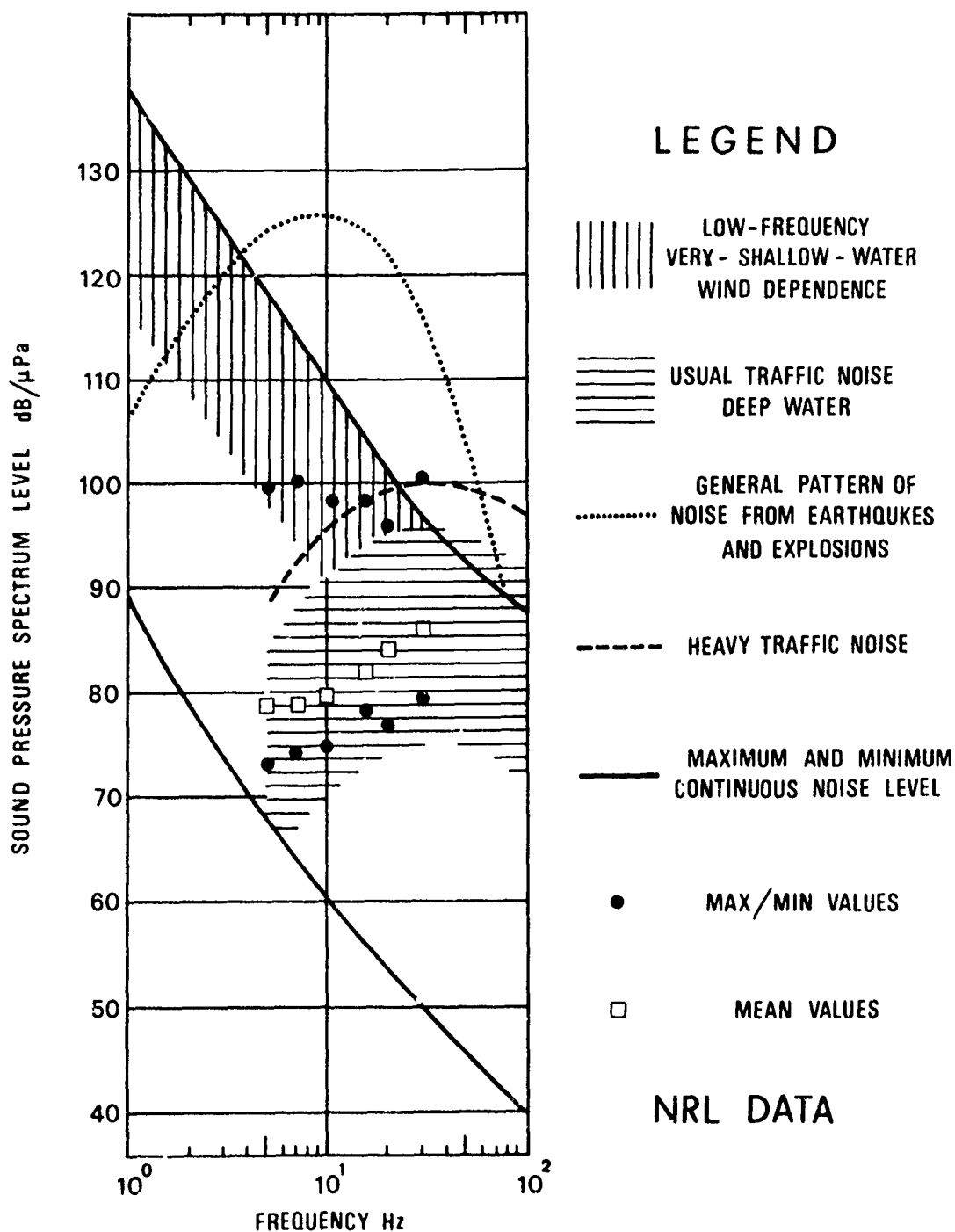


FIG. 11 SOUND-PRESSURE SPECTRUM LEVELS FOR DIFFERENT NOISE SOURCES IN THE SEA

fluctuations (surface waves and turbulences) form the dominant source mechanism, while above 10 Hz the traffic noise becomes increasingly important. As a seismic counterpart, we have plotted in Fig. 12 two pairs of curves  $S_1$  and  $S_2$  based on measurements by McLeroy [172] at two different shallow-water locations. The smooth, dashed curves give the averaged velocity spectrum levels of the vertical sensor while the undulating, solid curves represent (two of the few examples for) the averaged horizontal levels. The magnitude of the horizontal components exceeds that of the vertical ones by approximately 10 dB, which is also typical for propagation studies (see Sect. 2.4) and may be a consequence of trapped shear waves in sediments [173]. However, the "snapshot" character of these curves does not permit far-reaching conclusions. With increasing frequency these seismic noise levels indicate a fall-off that amounts to only about -6 dB/oct and thus seems to be less than in the acoustic case. Figure 13 presents another simplified plot [172] that compares the average  $\bar{S}$  of the dashed curves in Fig. 12 with different deep sea results  $D_i$ , and with average,  $\bar{L}$ , and minimum values,  $L_0$ , on land. Curve  $D_1$  is based on data from [171],  $D_2$  from [169],  $D_3$  from [168],  $D_4$  and  $D_4'$  from [167], and  $\bar{L}$  and  $L_0$  from [163]. As the most important noise sources that concern the deep ocean bottom are formed by microseisms (mainly due to moving water masses), by biological activity, and by distant shipping, the levels there are not very different from those on land, merely that the fall-off with increasing frequency is much steeper (approximately -10 to -20 dB/oct) than it is for land sites (about -8 dB/oct). This latter discrepancy did not occur in connection with the Black Sea data published by Rykunov et al [170] for the band from 2 to 15 Hz.

Bradner [174] has shown that the feed-back from these microseisms creates the often-observed increase in the acoustic noise-level towards the water/bottom interface (positive gradient of the depth profile) due to the microseismic Scholte waves.

The spectrum levels of seismic noise in coastal waters are expected to be higher than those measured at the deep ocean floor. The shallow bottom regions are much closer to the moving sea surface, to the routes of heavy ship-traffic, to offshore platforms, and to the shore line with its natural unrest (e.g. breaking waves) and its man-made noise sources (industrial and

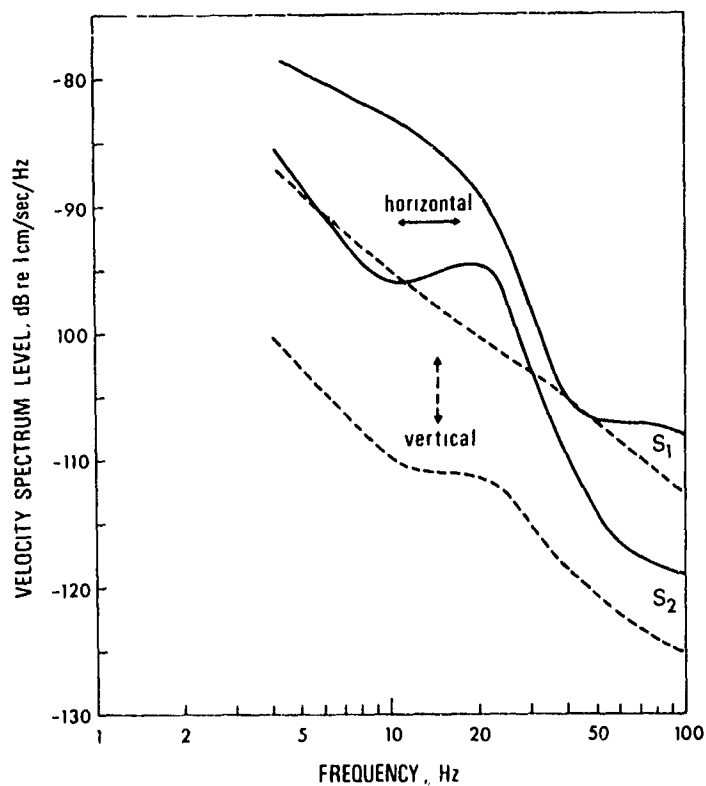


FIG. 12 AVERAGED VERTICAL AND HORIZONTAL VELOCITY SPECTRUM LEVELS ON THE SEA FLOOR IN SHALLOW WATER [172]

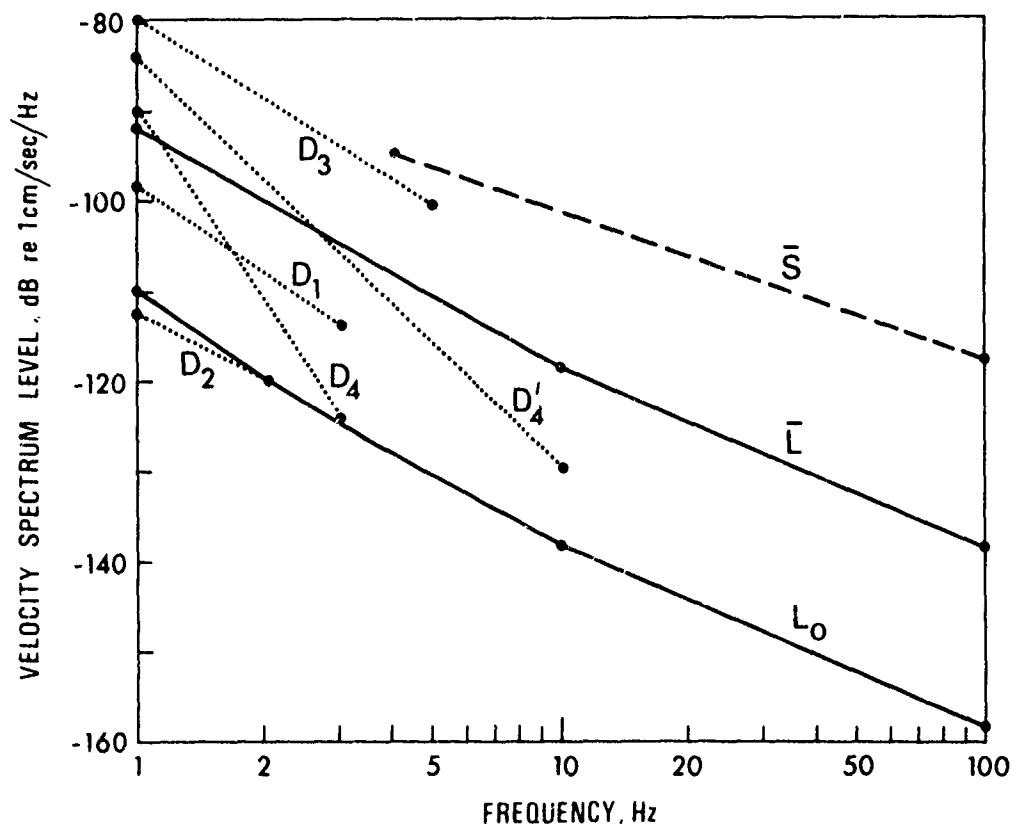


FIG. 13 AVERAGED VERTICAL VELOCITY SPECTRUM LEVELS FOR DIFFERENT SITES ON LAND AND ON THE SEA FLOOR IN SHALLOW AND DEEP WATER [172]

cultural activities). This trend was also confirmed by two more shallow sensor installations (at 500 and 300 m water depth) during the above-mentioned Black Sea experiment (the levels were about 20 dB above the deep-bottom results). More actual deep-ocean data published by Asada et al [175] confirm the steep decay of the spectrum level in the range from 1 to 10 Hz (about -25 dB/oct) but their magnitudes are almost 30 dB higher and thus exceed even the shallow-water records presented above. In addition, their curve passes a pronounced minimum at about 15 Hz and then again shows a modest increase towards higher frequencies. Some preliminary results from noise measurements with a prototype of SACLANTCEN's ocean-bottom seismometer in Italian coastal waters (at about 20 m depth off Viareggio) seem to confirm the existence of such a minimum in the seismic noise level between 10 Hz and 20 Hz.

The acoustic counterpart of this noise minimum has been found both at higher (at about 25 Hz in [164]) and at lower frequencies (at about 6 Hz in [165]).

Besides the favourable aspects of seismic paths for infrasound propagation (see Sect. 3.2) this "low-noise window" (just in the middle of the frequency band of interest) may play a decisive role in the successful application of seismic sensing to detection purposes.

#### 2.4 Field Experiments Concerning Seismic Detection of Waterborne Infrasound

The results of some of the classical shallow-water studies [70,74,85] and developments in the detection of microseisms (see Sect. 2.3) and nuclear blasts [176] stimulated a few underwater acousticians to make various small tests and to perform some quite extensive experiments under real-world conditions to explore low-frequency transmission in shallow water. Unfortunately, in its early days this field work had quite different objectives from the present subject, often put no efforts on the collection of environmental data, and partially suffered from inadequate equipment. The latter technical shortcoming refers especially to the horizontal geophones, which frequently had to be excluded because of the need for delicate handling (see Sect. 2.1).



During the years 1943/44 Worzel and Ewing [177] installed a sensor station with two hydrophones and one vertical geophone on the ocean bottom in different shallow-water areas. At water depths between 15 m and 180 m they sensed the pressure and displacement signals from explosive charges dropped at distances of between 0.5 and 50 km. Their main interest was devoted to the so-called "ground-wave" [85], which is composed of the shallow-refracted arrivals having dominant frequencies in the 10 to 30 Hz band.

About 1958 Worley and Walker [178] performed a similar study with a more versatile receiver package but unfortunately their horizontal geophone failed. Nevertheless they were able to show that the signals from the hydrophone and the vertical geophone have the same range-dependent fall-off in the 15 to 70 Hz frequency regime.

Approximately at the same time, Blaik and Clay [179] tried to sense waterborne sound on land. They towed powerful low-frequency transducers in shallow water and installed vertical geophones in a well on shore at depths between about 100 and 600 m. Profiting from the refracted field at shallow and medium depth they succeeded in detecting CW signals (10, 24, 88 and 148 Hz) over ranges up to about 9 km.

From 1960 to 1963 Shorthouse [180] developed and successfully applied a seismic system to observe P-head waves from velocity discontinuities in the oceanic crust and layering in the sediment overburden. Using a geophone and several hydrophones on the deep sea floor he recorded the signals from 5 lb (2.3 kg) charges exploded on the ocean bottom at different distances. As a by-product, long, late-arriving wave trains were observed up to ranges of 2.5 km; these showed a substantial dispersion and quite strong amplitude decay proportional to  $r^{-1.4}$ . Analyzing the pertinent data, Davies [181] clearly identified these "tails" of the records as Scholte waves with phase velocities between 130 and 60 m/s in the frequency interval from 2 to 10 Hz.

Since 1958 McLeroy and co-workers have carried out different theoretical studies, model experiments (see Sect. 1.5), and quite extensive field tests on use of seismic paths for detection and communication in coastal waters. Using a shallow, buried, triaxial OBS station and a nearby hydrophone they recorded the signals from high-power broadband CW-sources and explosives. Despite the fact that their model studies successfully synthesized the

different contributions to the sound field at an interface, they were often unable to ascribe the complex real-world data to these well-defined wave types. In general, they were therefore merely able to distinguish between the ensembles of the "ground-wave" and the "water wave". However, they noticed that at all frequencies there was a much higher signal-to-noise ratio on the horizontal geophones (up to 20 dB) than on the two other sensors. During one of these field experiments they observed a distinct interface wave that they interpreted as a Scholte wave despite some deviations from the expected characteristics [182]. The pertinent wavelets occurred at frequencies between 6 and 7 Hz and at short distances (up to 600 m) their propagation loss was slightly smaller (about 3 dB) than that of the sound energy being trapped in the water column. This latter feature is in contradiction to some other sea-floor studies that used the interface wave as a probe and has disclosed very high losses even for the infrasonic frequency regime (see Sect. 2.2).

In 1968 Urick [183,184] tried to track small craft (controlled runs) and large freighters (uncontrolled runs) with a similar sensor package on the sea floor (at about 18 m depth) in an area with a rapidly sloping bottom. For all frequencies below 100 Hz the signal-to-noise ratio of the vertical geophone was less than that of the hydrophone and showed a very rapid fall-off with range, while that of horizontal sensors was always greater and decreased more slowly with range. None of the results so far mentioned has given an indication of strong interface waves and all appear bewildered by the unexpectedly high levels of the cross-deflection (up to 50% of the radial displacement [183]). The latter phenomenon was generally explained by a relatively high energy transfer to Love waves caused by inhomogeneities and a non-regular layering (see Sect. 1.4).

Approximately at the same time O. Hastrup and T. Akal of SACLANTCEN had already made a systematic test in the Gulf of La Spezia to investigate the existence of an explosion-generated Scholte wave at the water-bottom interface. Unfortunately their efforts failed because of the shortcomings of the equipment, which consisted of quite insensitive vertical sensors (prospecting geophones) in conjunction with very modest display and recording facilities (oscilloscopes and photographic recorders).

Despite our devaluation of the application of vertical geophones, it must be noted that Bucker [185] has recently demonstrated that such bottom-mounted sensors are well suited to detect the infrasonic lines of passing ships in shallow water.

In 1976 McLeroy and his co-workers [186] again performed a very extensive real-world experiment in the Gulf of Mexico. Using a receiving array of nine triaxial OBS stations and six bottom-mounted hydrophones, they conducted numerous acoustical runs in shallow water with towed, powerful CW sources (operated at distances up to about 50 km) and some 200 explosive charges at 20 m depth and/or 1 m above the sea-floor (detonated at distances of up to about 16 km). This time the environmental background was very carefully checked by taking many samples of bathymetry, sound-speed profile, wind speed, wave height, currents, bottom layering, and sub-bottom structure (see Sect. 2. 2).

Until the end of 1978 only a few of these data had been analyzed but the preliminary results already indicated a much better signal-to-noise ratio for the radial and the vertical geophone than for the transverse sensor and the nearby hydrophone. This contradiction to the outcome of all former field tests has to be confirmed by the remaining data and investigated in detail. On the other hand, this surprising result is typical of the complexity of seismic sensing and of the associated experimental difficulties.

In 1976/77 a simple triaxial OBS prototype was developed by SACLANTCEN's Environmental Acoustics Group using three highly-sensitive 1-Hz geophones of the Geospace HS-10/1B type and one nearby hydrophone. During some shallow-water trials in 1977 and 1978 analogue data of background and ship noise as well as signals from small explosive charges were transferred via cable or radio link to a receiving ship [187]. Owing to many problems with the very delicate sensors, the mechanical design of the station, and the electronics, our initial experimental results have not been satisfactory (see Sect. 2.3).\*

---

\* Since writing this text, these problems have been overcome and successful field work was performed in 1979 (see Appendix A for details).

In most of the above-mentioned field trials the OBS station was fitted with a hydrophone to provide a better understanding of the propagation phenomena (clear distinction between the different wave types, which in most instances has not yet been achieved) and/or to get a true standard of comparison between the detection methods (direct comparison between the acoustic and seismic signal-to-noise ratios).

This procedure proved successful in the famous Vela Uniform Program (of the Advanced Research Projects Agency) for the monitoring of large underground explosions (see also [188]), and it may be extremely helpful as a means of eliminating or profiting from the influence of converted or trapped shear waves (see Sects. 2.2 and 2.3).

### 3 MODELLING OF SEISMIC WAVE PROPAGATION IN THE SEA-FLOOR

#### 3.1 Characteristics of the Thomson-Haskell Matrix Method

In Ch. 1, Sects. 1.1, 1.3 and 1.5 attempted to describe the very complex seismic field as a whole and Sects. 1.2 and 1.4 concentrated on interface waves. For a more realistic evaluation of the role of different wave types and more reliable predictions for field experiments, we have to fit all available environmental data into a theoretical model. Such a model should be as comprehensive as possible and, at the same time, well suited for computer application.

Section 1.3 suggested that the separation of the different contributions to the sound field by means of classical mathematics would often be very elaborate, sometimes extremely difficult, and, moreover, quite inexact in most cases.

If we treat the earth's crust as a horizontally-stratified half space consisting of homogeneous liquid and solid layers with constant parameters (density  $\rho$ , sound speeds  $c_p$  and  $c_s$ , attenuation coefficients  $\bar{\alpha}_p$  and  $\bar{\alpha}_s$ ), all these requirements are met by the well-known Thompson-Haskell matrix method [7, 189, 190]. Here we will give merely a short outline of its basic principles.

Under simple geometrical conditions (plane waves incident from infinity, or else cylindrical or spherical waves radiated by a horizontal or vertical line source or by a point source) the solutions to the wave equations in homogeneous, source-free layers are well known [3 to 8, 22]. The classical way to solve those range ( $x$  or  $r$ ), depth ( $z$ ), and time ( $t$ )-dependent propagation problems is the application of a Fourier transform [52-53] for the range and a Laplace transform [54-56] for the time in the case of impulsive sources. Thus the original partial differential equations are converted to algebraic equations with respect to the complex wave number ( $k$ ) space and the complex object space of the Laplace transform. There the resulting

ordinary differential equations concerning  $z$  can be solved easily with regard to the similarly transformed boundary conditions due to the separation of the original variables. Most of the mathematical difficulties usually arise from the reverse transform of the solution back to the physical space/time domain, and therefore classical approaches [7], computer-aided numerical methods [191], or unusual concepts [11] have to be used.

As the harmonic time-dependence of incident waves can be separated and thereby excluded immediately, Thomson [189] and Haskell [190] have demonstrated by means of monochromatic plane waves that the resulting sound field within the  $m$ -th layer can be represented by a four-vector  $\underline{\mathcal{L}}_m$  in the  $k$ -space. Because it arises from the interference of obliquely-downward and upward-travelling waves, this vector may be related to the  $z$ -dependent amplitudes of the basic potentials (displacement or velocity potential of P- and S- waves) or to such intermediate terms as the  $z$ -dependent amplitudes of the two particle velocities  $\dot{u}$ ,  $\dot{w}$  and the two stresses  $\tau_{zz} = p$ ,  $\tau_{xz} = \tau$  according to:

$$\hat{\underline{\mathcal{L}}}_m = \begin{pmatrix} \hat{u}_m \\ \hat{w}_m \\ \hat{p}_m \\ \hat{\tau}_m \end{pmatrix} \quad (\text{Eq. 26})$$

This latter form of the layer vector  $\underline{\mathcal{L}}_m$  is obvious: the most convenient one because it already contains those terms that have to be continuous at the interfaces. Being composed exclusively from the solutions to a system of two wave equations, the vertical "propagation" through the pertinent homogeneous layer with constant parameters is also well defined. Thomson and Haskell have shown that this correlation implies relatively simple and favourable mathematical consequences. The vector at the bottom,  $\underline{\mathcal{L}}_{\underline{m}}$ , of the layer,  $m$ , can be calculated from its counterpart at the top,  $\underline{\mathcal{L}}_{\overline{m}}$ , or viceversa by a simple matrix multiplication (linear operation):

$$\hat{\underline{\mathcal{L}}}_{\underline{m}} = \underline{\mathcal{A}}_m \hat{\underline{\mathcal{L}}}_{\overline{m}}; \hat{\underline{\mathcal{L}}}_{\overline{m}} = \underline{\mathcal{A}}_m' \hat{\underline{\mathcal{L}}}_{\underline{m}} \quad (\text{Eq. 27})$$

The  $4 \times 4$  layer matrix  $\underline{\mathcal{A}}_m$  is a function of the medium parameters, the layer thickness  $H_m$ , the complex wave number  $\underline{k}$ , and the resulting phase

velocity  $\underline{c}$ , and thus includes the effects of damping and dispersion. The interested reader may find the explicit form of the layer-matrix elements  $a_{\mu\nu}$  in the repeatedly-cited original papers, in the book by Bath [7], and in a report by Kutschale [192]. As the boundary – or transition – conditions at the top and the bottom of layer  $m$  require the fulfilment of the relations:

$$\hat{\mathcal{L}}_{\underline{m-1}} = \hat{\mathcal{L}}_{\underline{m}} \quad \hat{\mathcal{L}}_{\underline{m}} = \hat{\mathcal{L}}_{\underline{m+1}} \quad (\text{Eq. 28})$$

and Eq. 27 is valid for all three adjacent layers, we can also link the vector  $\hat{\mathcal{L}}_{\underline{m+1}}$  to its more remote counterpart  $\hat{\mathcal{L}}_{\underline{m-1}}$  by matrix multiplication:

$$\begin{aligned} \hat{\mathcal{L}}_{\underline{m+1}} &= \mathcal{A}_{\underline{m+1}} \mathcal{A}_{\underline{m}} \mathcal{A}_{\underline{m-1}} \hat{\mathcal{L}}_{\underline{m-1}} = \mathcal{A}_{\text{syst}} \hat{\mathcal{L}}_{\underline{m-1}} \\ \hat{\mathcal{L}}_{\underline{m-1}} &= \mathcal{A}_{\text{syst}}^{-1} \hat{\mathcal{L}}_{\underline{m+1}} \end{aligned} \quad (\text{Eq. 29})$$

Thus the resulting matrix  $\mathcal{A}_{\text{syst}}$  of a stack of layers (each of them with constant parameters) is simply the product of all section matrices, and we can finally link the radiation condition (allowing only outgoing waves) of the deepest layer (forming the sub-bottom half-space) to the pressure-release surface of the top layer (earth or sea surface) or viceversa:

$$\hat{\mathcal{L}}_{\underline{n}} = \mathcal{A}_{\text{syst}} \hat{\mathcal{L}}_{\underline{T}} \quad (\text{Eq. 30a})$$

$$\hat{\mathcal{L}}_{\underline{T}} = \mathcal{A}_{\text{syst}}^{-1} \hat{\mathcal{L}}_{\underline{n}} \quad (\text{Eq. 30b})$$

Proceeding in this way, all solution elements are compatible with all transition conditions and we thus obtain a mathematical description (in the complex  $\underline{k}$ -space) of the complete wave field.

The above-mentioned fact that each layer-matrix  $\mathcal{A}_{\underline{m}}$ , and accordingly the resulting stack-matrix  $\mathcal{A}_{\text{syst}}$ , is making allowance for dispersion may be easily checked by considering its version for extremely-low and extremely-high frequencies, [7, 190]. In the low-frequency limit the resulting field is identical with a Rayleigh-type wave at the surface of a layered half-space [193] and in the high-frequency limit it splits into the typical interface waves at the various interfaces.

Because of the exclusion of range dependence, the above-defined field vectors and layer matrices can be used in connection with all two-dimensional wave-propagation problems. In practical operation these mathematical tools have to be applied in the following way: the surface-vector  $\hat{\mathcal{L}}_{\top}$  has to be calculated from the deepest sub-bottom vector  $\hat{\mathcal{L}}_{\bar{n}}$  according to Eq. 30b by "carrying" the field vector  $\hat{\mathcal{L}}_{\bar{m}}$  across all layers and interfaces. The field vector then has to be "shifted" down again to the depth at which the seismic signal is of interest by using a reduced system matrix in Eq. 30a. Thus it is obvious that the receiver depth must coincide with the coordinate of an actually existing interface or of an artificially inserted auxiliary boundary without physical meaning. Similar arguments are valid for the positioning of the source that is of most practical interest: the point source  $S_0$  that radiates spherical P-waves. In the range-independent object space such a source provokes a well-defined discontinuity of the vertical particle velocity  $\dot{w}$ . This discontinuity can be incorporated in our formalism by inserting another extra interface that divides the original source-layer  $s$  into two sub-layers  $s'$  and  $s''$ , and by defining a pertinent "source vector"  $\mathcal{P}_0$  to be added to the field-vector  $\hat{\mathcal{L}}_{\bar{s}''}$

$$\hat{\mathcal{L}}_{\bar{s}'} = \hat{\mathcal{L}}_{\bar{s}''} + \mathcal{P}_0 \quad (\text{Eq. 31})$$

during the composition of the total field by means of Eq. 30b. In the case of a harmonic point source this source vector  $\mathcal{P}_0$  is of the simple form [86]:

$$\mathcal{P}_0 = \begin{pmatrix} 0 \\ 2k \\ 0 \\ 0 \end{pmatrix}. \quad (\text{Eq. 32})$$

Finally, to establish the encoded range dependence of the resulting wave field (which is independent of the bearing), and thus to describe the seismic signal with respect to a remote receiver position, we have to perform an inverse Fourier transform, which can be carried out using modern computer techniques [191,192].



### 3.2 Some Preliminary Results from the Fast-Field-Program

In Sects. 1.4 and 2.2 we have already mentioned that realistic bottom conditions usually create a complex eigenvalue problem (with regards to sound propagation in the shallow-water channel) that can not be solved by the classical normal-mode technique. The interesting Scholte wave (zeroth mode) always corresponds to a real eigenvalue but neither can it be handled in a proper way because of basic limitations in the underlying theory. Fortunately this and other seismic problems can be tackled with the help of the above-described Thompson-Haskell matrix method. Harkrider's solution technique of the wave equation [194] and Dorman's matrix notation [193] simplified the application of this many-membered method but its successful breakthrough did not become possible until the introduction of the Fast-Field-Program technique by Marsh and Elam [195] and by Di Napoli [196].

At this point we would like to demonstrate the capabilities of such an FFP, made available to SACLANTCEN by Kutschale [192] from Lamont-Doherty Geological Observatory. The version implemented on SACLANTCEN's UNIVAC 1106 computer [197] is able to calculate the complete monochromatic wave field in a stack of isovelocity liquid and solid layers using optional depths of source and receiver.

To work out some of the essential features and trends of the interesting seismic contribution to long-range transmission we have chosen a very simple but realistic type of sea bed in which a sand layer ( $\rho = 2.0 \text{ g/cm}^3$ ;  $c_p = 1800 \text{ m/s}$ ;  $c_s = 700 \text{ m/s}$ ) with high absorption ( $\bar{\alpha}_p = 0.75 \text{ dB}/\lambda$ ;  $\bar{\alpha}_s = 1.5 \text{ dB}/\lambda$ ) and constant thickness  $H_2 = L$  rests on top of a sedimentary rock ( $\rho = 2.2 \text{ g/cm}^3$ ;  $c_p = 3000 \text{ m/s}$ ;  $c_s = 1400 \text{ m/s}$ ;  $\bar{\alpha}_p = 0.1 \text{ dB}/\lambda$ ;  $\bar{\alpha}_s = 0.05 \text{ dB}/\lambda$ ;  $H_3 = \infty$ ). We assume a 10 Hz sound source,  $S_0$ , in the middle or at the bottom of a water-column ( $\rho = 1.0 \text{ g/cm}^3$ ,  $c_w = 1500 \text{ m/s}$ ;  $\bar{\alpha}_w = 1.8 \times 10^{-6} \text{ dB}/\lambda$ ) of mostly  $H_1 = W = 60 \text{ m}$  depth, with the receiver always placed on the ocean floor.

For extreme simplification, all wave types propagating faster than the speed of sound in water are included in the "acoustic portion" of the field while all slower types are counted as the "seismic portion". Such a drastic splitting of the total elastic wave field can be justified by means

of Fig. 7 where the phase velocities of the blurred modes in the water are seen to be well separated from those of the interface wave. The present example is more complex of course, and such a combination obscures the fine structure of the field as it disregards the overlapping and interaction of certain wave types. However, with respect to the energy input, we can easily tolerate these adulterations. To demonstrate the influence of the sediment layer we keep the source position fixed in the middle of a 60 m water column and decrease the layer thickness stepwise. In Fig. 14 we have plotted the transmission loss against range in the acoustic (dashed curves) and the seismic (solid curves) fields for the cases of two enormous sand layers of 120 m and 60 m thickness. In both cases the acoustic propagation is quite bad and the seismic one even worse, but we realize at once that a decrease in the layer thickness slightly improves the conditions for seismic sensing and worsens those for acoustic detection. A more detailed analysis reveals that the acoustic field comprises merely one mode-like structure, while there are different weak contributions to the seismic field. Among the latter, the Scholte wave at the water/sand interface ( $c_{sch} \approx 600$  m/s) can be identified clearly, but due to the high absorption in the sediment it is of no importance.

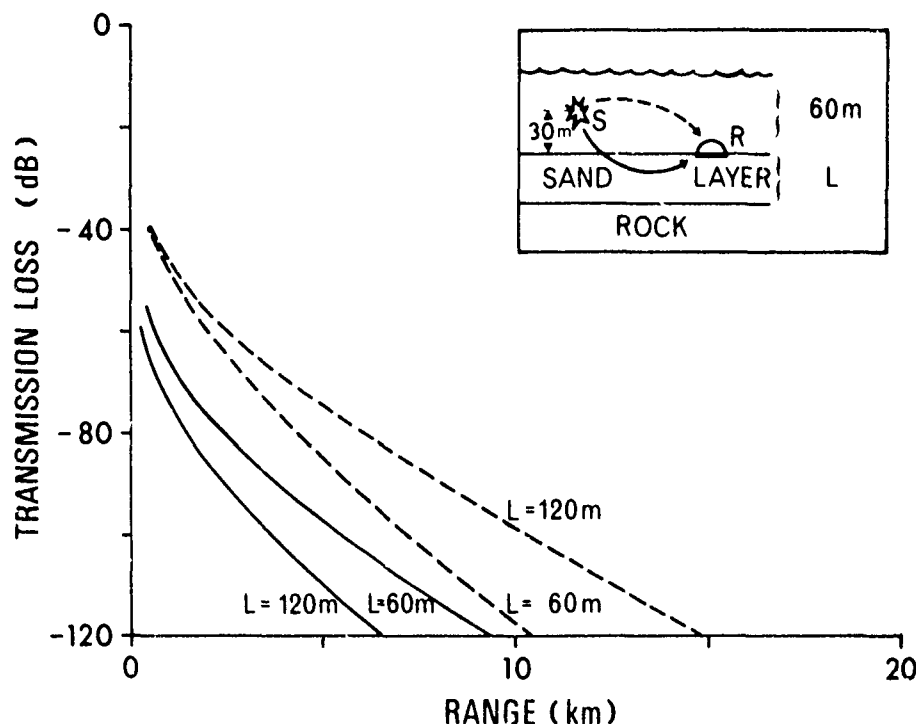


FIG. 14 RANGE DEPENDENCE OF THE ACOUSTIC (DASHED) AND SEISMIC (SOLID) TRANSMISSION LOSS FOR A 10 HZ SOURCE OVER DIFFERENT THICK SAND LAYERS

Omitting some intermediate steps, which confirm the above-mentioned trend, we pass immediately to three relatively-thin sand layers of 10 m, 5 m, and 0.5 m thicknesses. The pertinent curves in Fig. 15 demonstrate impressively that seismic sensing can offer not only an alternative but, on the contrary, may represent a superior detection method. The remarkable ranges achieved by seismic propagation are solely a consequence of a modified or generalized Scholte wave that is guided along the "sand-coated" water/rock interface ( $c_{sch} \approx 1150$  m/s).

It should be mentioned that there is no direct contribution to the seismic field from the side of the sand/rock interface, because our choice of parameters excludes the existence of a "pure" Stoneley wave at this boundary (see Sect. 1.1).

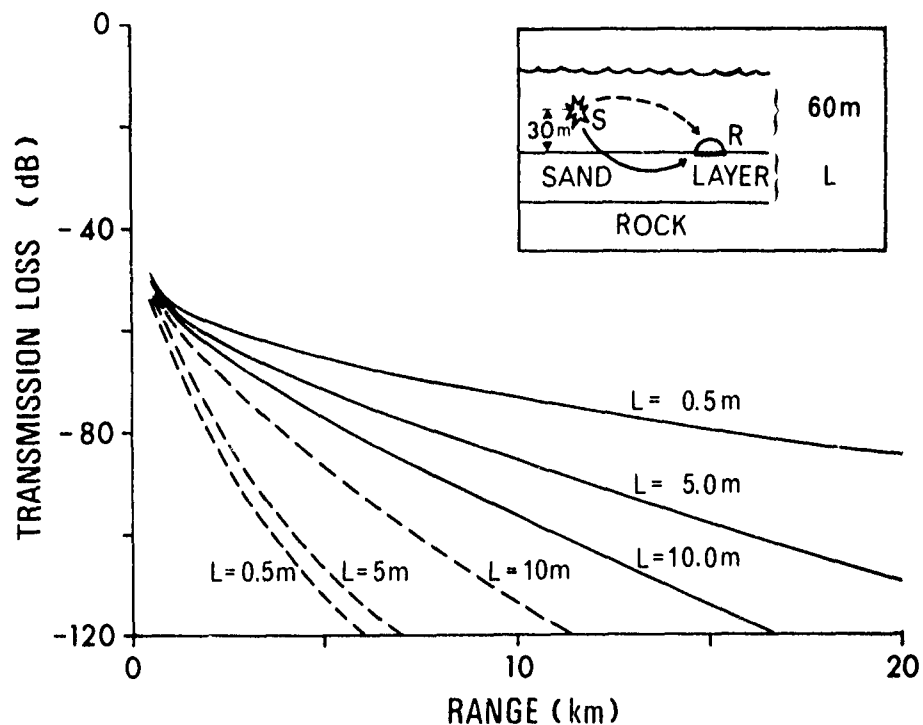


FIG. 15 RANGE DEPENDENCE OF THE ACOUSTIC (DASHED) AND SEISMIC (SOLID) TRANSMISSION LOSS FOR A 10 HZ SOURCE OVER DIFFERENT THIN SAND LAYERS

The excitation of the modified Scholte wave, and thus the good seismic propagation, would be improved if the source position were shifted towards the ocean floor. For that reason Fig. 16 compares the seismic transmission loss of the preceding plot with the corresponding curves calculated for a bottom-mounted transmitter  $S_0$  of the same source level. In all three cases a decrease of the loss by about 10 dB confirms the expected better coupling of source and sea bed.

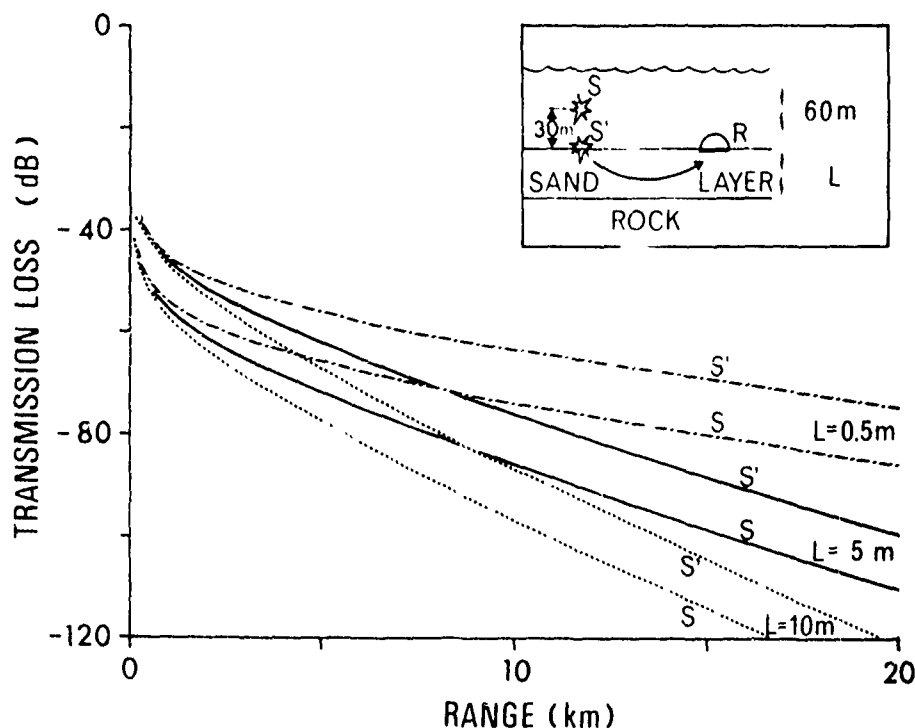


FIG. 16 RANGE DEPENDENCE OF THE SEISMIC TRANSMISSION LOSS FOR A 10 HZ SOURCE OVER AND ON A THIN SAND LAYER

Finally, to show that the selected water depth  $H_1$  of merely 60 m does not imply a serious limitation to our conclusions, we returned to the intermediate example of Fig. 15 (source,  $S_0$ , 30 m above a 5 m sand layer) and calculated the transmission loss for water columns of 80 m, 100 m, and 120 m. From the resulting curves of Fig. 17 we see that the poor acoustic propagation improves only slightly with increasing water depth, while the relatively good seismic propagation is not affected.

To give an estimation of the optimum frequency range for seismic detection on top of such a "sand-coated" rock bottom (intermediate case of Fig. 17) the frequency was varied instead of the range (receiver distance 10 km).

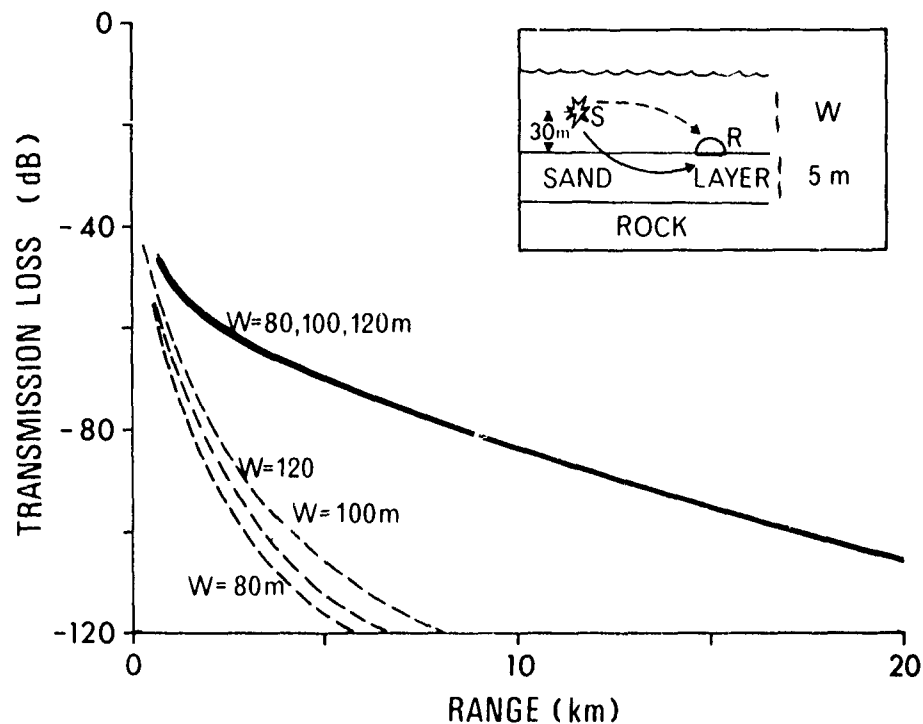


FIG. 17 RANGE DEPENDENCE OF THE ACOUSTIC (DASHED) AND SEISMIC (SOLID) TRANSMISSION LOSS FOR A 10 HZ SOURCE IN DIFFERENT WATER COLUMNS OVER A THIN SAND LAYER

Figure 18, which stems from another study [100], shows the pertinent spectrum levels of the acoustic and the seismic transmission losses. If the frequency is decreased below 30 Hz the acoustic propagation loss increases drastically by about 40 dB, with a relatively broad maximum between 20 and 10 Hz. At about 5 kHz the acoustic propagation again reaches its former "high-frequency" quality in the form of a relatively sharp loss-minimum, but then it is more or less completely extinguished below 3 Hz. This narrow-band improvement around 5 Hz is due to the incorporation of the sand layer into the acoustic duct.

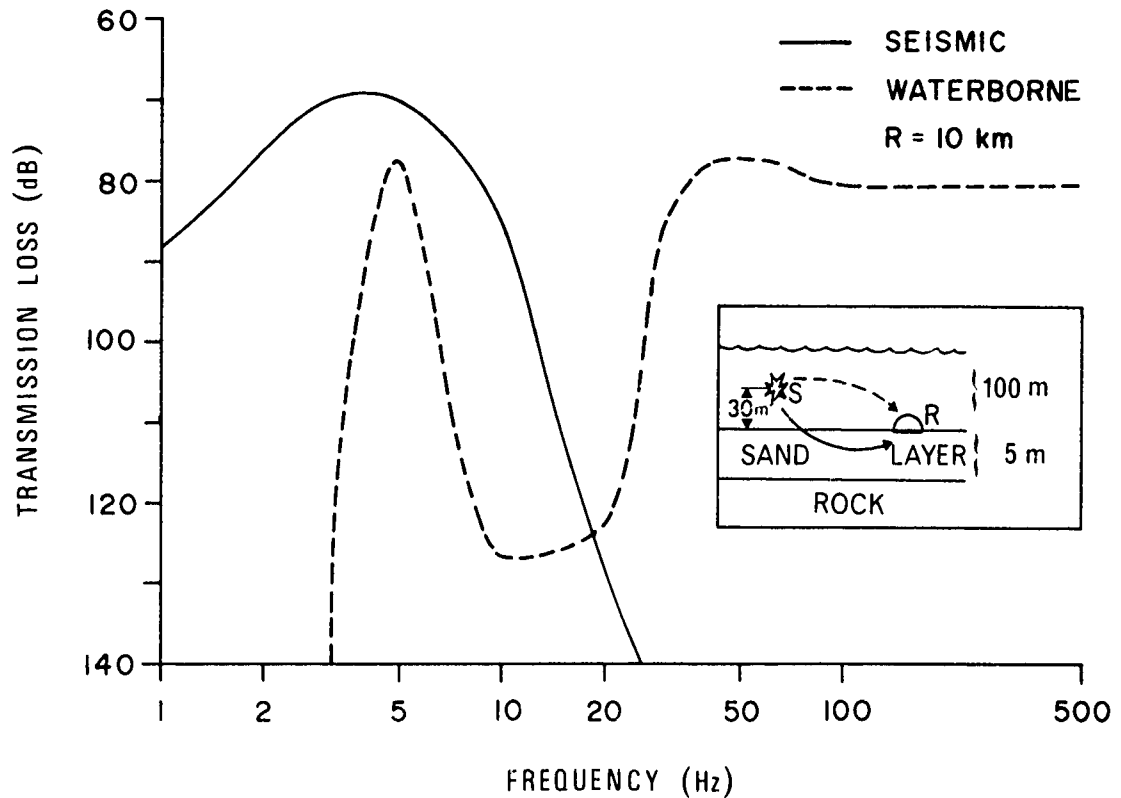


FIG. 18 FREQUENCY DEPENDENCE OF THE ACOUSTIC (DASHED) AND SEISMIC (SOLID) TRANSMISSION LOSS AT A FIXED RANGE OF 10 km FOR A 10 Hz SOURCE OVER A THIN SAND LAYER

On the other hand, the initially very high seismic propagation loss falls below its acoustic counterpart at about 20 Hz, then drops for another 50 dB, and finally passes a relative flat minimum between 7 and 2 Hz. Thus for each tonal below 20 Hz the seismic propagation is much better than its acoustic counterpart.

An additional support for the better seismic sensing (better signal-to-noise ratio) may result from a typical minimum of the ambient noise spectrum levels in the 10 to 20 Hz band (see Sect. 2.3).

## CONCLUSIONS AND PROPOSALS FOR FUTURE RESEARCH PROGRAMMES

A substantial part of the world's oceans can be classified as shallow water (e.g. water depth of 200 m or less), and, what is more important, many of these areas (the continental shelves and most of the straits) are strategically important. It is in just these areas that the approved and highly-developed sonar techniques for long- and medium-range detection lose their accuracy or even fail.

When propagating in shallow water, or from deep to shallow water over a sloping bottom, the acoustic energy of "water-waves" becomes rapidly attenuated through repeated interactions with surface and bottom, similarly the coherence of the pertinent sound field is also lost. On top of that, all very shallow regions, and thus areas close to shore, are impenetrable for infrasonic energy (approximately the 1 to 30 Hz frequency band) due to the existence of an absolute low-frequency cut-off for the water wave (meaning the one for the first or lowest propagation mode of this field).

Thus the conventional acoustic surveillance techniques suffer from shortcomings (on the part of both hardware and software) and ask for alternatives. Besides different non-acoustic methods (based on optical, magnetic, or chemical phenomena) a closely-related alternative may be offered by that fraction of the acoustic energy that becomes coupled with the bottom and is thus transmitted in the form of seismic waves along and in the sea floor. Although seismology has been an extensive field of research for many years this coupling mechanism is still poorly understood (especially with respect to interface waves), not to mention the very confusing variety and interaction of different propagation modes. That is why we tried to give a comprehensive qualitative description of the underlying physics in Ch. 1. Despite the use of directional sensors and highly-sophisticated signal-processing techniques in seismology, the related and very crucial problems of signal strength and coherence have been largely neglected due to the fact that the questions of energetics are of minor interest in prospecting and earthquake monitoring. Nevertheless

we are now able to extract numerical results under strongly simplified conditions with the help of modern computer programs, as has been shown in Ch. 3.

Unfortunately these latter possibilities are not only restricted by the natural limitations of the existing models but also, and even more, by our lack of knowledge concerning the environmental input data.

The large amount of published data on the lithosphere below the oceans can merely indicate the limits and trends for modelling work and predictions. That is to say, the seismic parameters involved are not only more numerous but are also affected by much stronger variations with depth and range due to (non-regular) layering and inhomogeneities. Especially with respect to reliable data on shear phenomena in sediments, we are still largely groping in the dark. Concerning the seismic ambient-noise levels in shallow water, the starting conditions are even worse. The very few existing measurements with vertical geophones differ considerably and do not permit us to draw any conclusions with regard to the more interesting horizontal unrest of the sea floor (including the questions of directionality). Thus the only information on favourable signal-to-noise ratios of bottom-mounted horizontal geophones (exceeding those of nearby mounted hydrophones by about 5 to 20 dB) stems from a few non-coordinated field trials in the past (see e.g. [182-184]).

Likewise, the coherence characteristics of the wave types in the marginal portion of the seismic field at or just below the sea floor (mainly interface and trapped shear waves) are widely unknown but it has to be expected that they are strongly deteriorated by lateral inhomogeneities [198].

In Ch. 2 we tried to shed some light on the historical and technical reasons for all these short-comings and contradictory results in former studies. As a result, we can define the outline of future research activities by listing the necessary experimental and theoretical tasks in order of importance.



More careful and systematic measurements should be performed with OBS-stations in shallow water to identify and explore:

- a. The excitation and propagation mechanisms of the different interface phenomena (pertinent levels, phase and group velocities, losses, and directionality).
- b. The levels and directional characteristics of acoustic and seismic ambient noise in the infrasonic frequency range (about 1 to 30 Hz).
- c. The achievable improvements of the signal-to-noise ratio by using horizontal geophones instead of or together with omnidirectional hydrophones.
- d. The bottom characteristics of the top layers in general and the shear damping in particular.
- e. The deterioration of signal coherence by lateral inhomogeneities.

These experimental studies should be accompanied by a lot of interacting modelling work to facilitate the interpretation of field data and to support the selection of suitable test areas.

# REFERENCES

1. URICK, R.J. Sound transmission from deep to shallow water, NOLTR 72-1. White Oak, Md., U.S. Naval Ordnance Laboratory, 1971.
2. U.S. DEPARTMENT OF THE NAVY, OFFICE OF NAVAL RESEARCH. Proceedings, Workshop on seismic propagation in shallow water, 6-7 July, 1978. Arlington, Va, U.S. Office of Naval Research, 1978.
3. SOMMERFELD, A. Partial Differential Equations in Physics. New York, Academic Press, 1967.
4. SOMMERFELD, A. Über die Ausbreitung der Wellen in der drahtlosen Telegraphie. Annalen der Physik, 28, 1909: 665-736.
5. EWING, W.M., JARDETZKY, W.S. and PRESS, F. Elastic Waves in Layered Media. New York, McGraw-Hill, 1957.
6. SCHOCH, A. Schallreflexion, Schallbrechung und Schallbeugung. Ergebnisse der exakten Naturwissenschaften, 23, 1950: 127-234.
7. BATH, M. Mathematical Aspects of Seismology. Amsterdam, Elsevier, 1968.
8. GRANT, F.S. and WEST, G.F. Interpretation Theory in Applied Geophysics. New York, McGraw-Hill, 1965.
9. WEYL, H. Ausbreitung elektromagnetischer Wellen über einem ebenen Leiter. Annalen der Physik, 60, 1918: 481-507.
10. BANOS, Jr., A. Dipole Radiation in the Presence of a Conducting Half-Space. Oxford, Pergamon Press, 1966.
11. CAGNIARD, L. Reflection and Refraction of Progressive Seismic Waves. New York, N.Y., McGraw-Hill, 1962.
12. RAYLEIGH, J.W.S. On waves propagated along the plane surface of an elastic solid. Proceedings of the London Mathematical Society, 17, 1885: 4.
13. SCHOLTE, J.G. The range of existence of Rayleigh and Stoneley waves. Monthly Notices, Royal Astronomical Society, 1947: 120-126.
14. SCHOLTE, J.G. On the large displacements commonly regarded as caused by Love waves and similar dispersive surface waves. Proceedings, Koninklijke Nederlandse Akademie van Wetenschappen, 51, 1948: 533-543, 642-649, 828-835, 969-976.
15. SCHOLTE, J.G. On true and pseudo Rayleigh waves. Proceedings, Koninklijke Nederlandse Akademie van Wetenschappen, 1949: 652-653.
16. STONELEY, R. Elastic waves at the surface of separation of two solids. Proceedings of the Royal Society, 106A, 1924: 416-428.

17. LAMB, H. On the propagation of tremors over the surface of an elastic solid. Philosophical Transactions of the Royal Society, 203A, 1904: 1-42.
18. VIKTOROV, I.A. Rayleigh and Lamb Waves. New York, N.Y., Plenum Press, 1967.
19. FARNELL, G.W. Properties of elastic surface waves. In: MASON, W.P. and THURSTON, R.N., eds. Physical Acoustics: Principles and Methods, Vol. VI. New York, N.Y., Academic Press, 1970: 109-166.
20. FARNELL, G.W. Types and properties of surface waves. In: OLINER, A.A., ed. Acoustic Surface Waves. Berlin, Springer, 1978.
21. UBERALL, H. Surface waves in acoustics. In: MASON, W.P. and THURSTON, R.N., eds. Physical Acoustics; Principles and Methods, Vol. X. New York, N.Y., Academic Press, 1973: 1-60.
22. BREKHOVSKIKH, L.M. Waves in Layered Media. New York, N.Y., Academic Press, 1960.
23. ROEVER, W.L., VINING, T.F. and STRICK, E. Propagation of elastic wave motion from an impulsive source along a fluid/solid interface. Philosophical Transactions of the Royal Society, 251A, 1959: 467-523.
24. STRICK, E. and GINZBARG, A.S. Stoneley-wave velocities for a fluid-solid interface. Bulletin, Seismological Society of America, 46, 1956: 281.
25. GILBERT, F. and LASTER, S.L. Excitation and propagation of pulses on an interface. Bulletin, Seismological Society of America, 52, 1961: 299-319.
26. BIOT, M.A. The interaction of Rayleigh and Stoneley waves in the ocean bottom. Bulletin, Seismological Society of America, 42, 1952: 81-83.
27. KUPRADZE, V.D. and SOBOLEN, S.L. The propagation of elastic waves on an interface between two media with different elastic properties. Trudy Seismologicheskaya Instituta Akademii Nauk SSSR, (10), 1930.
28. SEZEWA, K., KANAI, K. The range of possible existence of Stoneley waves and some related problems. Bulletin, Earthquake Research Institut, Tokyo University, 17, 1939: 1-8.
29. GOGOLADZE, V.G. On Rayleigh waves on the confines of two solid elastic media. Doklady Akademii Nauk, SSSR, 33, 1947: 15-17.
30. KOPPE, H. Über Rayleigh-Wellen an der Grenzfläche zweier Medien. Zeitschrift für Angewandte Mathematik und Mechanik, 28, 1948: 355-360.
31. GINZBARG, A.S. and STRICK, E. Stoneley-wave velocities for a solid-solid interface. Bulletin, Seismological Society of America, 48, 1958: 51.

32. PHINNEY, R.A. Propagation of leaking interface waves. Bulletin, Seismological Society of America, 51, 1961: 527-555.
33. LOVE, A.E.H. Some Problems of Geodynamics, 2nd ed. London, Cambridge University Press, 1926.
34. STATO, Y. Study on surface waves XI. Definition and classification of surface waves. Bulletin, Earthquake Research Institute, Tokyo University, 32, 1954: 161-167.
35. YAMANOUCHI, K., IWAHASHI, K., and SHIBAYAMA, K. Piezoelectric acoustic boundary waves propagating along the interface between  $\text{SiO}_2$  and  $\text{LiTaO}_3$ . IEEE Transactions on Sonics and Ultrasonics, 25, 1978: 384-389.
36. MOROCHA, A.K. and OVSYANNIKOVA, O.B. Existence of a transverse acoustic wave propagating along an interface between two solid media. Soviet Physics Acoustics, 24, 1978: 321-322.
37. MARADUDIN, A.A., WALLIS, R.F., IPATOVA, I.P., and KLOCHIKHIN, A.A. Surface spin waves. In: Localized Excitations in Solids. Proceedings of a conference held in Milan, 1966.
38. BERGMANN, L. Der Ultraschall und seine Anwendung in Wissenschaft und Technik. Stuttgart, Hirzel, 1954: p.563.
39. DIX, C.H. The method of Cagniard in seismic pulse problems. Geophysics, 19, 1954: 722-738.
40. DE HOOP, A.T. A modification of Cagniard's method for solving seismic pulse problems. Applied Scientific Research, 8B, 1960: 349-356.
41. SCHMIDT, O. von. Über Knallwellenausbreitung in Flüssigkeiten und festen Körpern. Zeitschrift der Technischen Physik, 19, 1938: 554-560. (Some Schlieren photos are also published in: Physikalische Zeitschrift, 39, 1938: 868, and SCHARDIN, H. Ergebnisse der exakten Naturwissenschaften, 20, 1942.)
42. RUDNICK, I. The propagation of an acoustic wave along a boundary. Journal of the Acoustical Society of America, 19, 1947: 348-356.
43. BREKHOVSKIĬ, L.M. The reflection and refraction of spherical waves. Uspekhi Fizika Nauk, 38, 1949: 1.
44. ZVOLINSKIĬ, N.V. Reflected and head waves arising at a plane interface between two elastic media. Bulletin, Academy of Sciences, USSR, Geophysical Series, (10), 1957: 1-21.
45. HEELAN, P.A. On the theory of head waves. Geophysics, 18, 1953: 871-893.
46. DIACHOK, O.I. and MAYER, W.G. Conical reflection of ultrasound from a liquid-solid interface. Journal of the Acoustical Society of America, 47, 1970: 155-157.

47. IVANOV, I.D. Reflection of a spherical pulse from a liquid-solid interface. Soviet Physics Acoustics, 21, 1975: 259-261.
48. STICKLER, D.C. Reflected and lateral waves for the Sommerfeld-model. Journal of the Acoustical Society of America, 60, 1976: 1061-1070.
49. DONATO, R.J. Propagation of a spherical wave near a plane boundary with a complex impedance. Journal of the Acoustical Society of America, 60, 1976: 34-39.
50. DONATO, R.J. Spherical-Wave reflection from a boundary of reactive impedance using a modification of Cagniard's method. Journal of the Acoustical Society of America, 60, 1976: 999-1002.
51. TSANG, L. Time-harmonic solution of the elastic head wave problem incorporating the influence of Rayleigh poles. Journal of the Acoustical Society of America, 63, 1978: 1302-1309.
52. BRACEWELL, R.M. The Fourier Transform and its Application. New York, N.Y., McGraw Hill, 1965.
53. ASELTINE, J.A. Transform Method in Linear System Analysis. New York, N.Y., McGraw Hill, 1958.
54. JOETSCH, G. Handbuch der Laplace-Transformation. Basel, Birkhäuser, 1950.
55. DOETSCH, G. Anleitung zum praktischen Gebrauch der Laplace-Transformation. Oldenbourg, Thieme, 1961.
56. SPIEGEL, M.R. Laplace-Transforms. New York, N.Y., McGraw Hill, 1965.
57. GOOS, F. and HANCHEN, H. Ein neuer fundamentaler Versuch zur Totalreflexion. Annalen der Physik, 1, 1947: 333
58. GOOS, F. and LINDBERG-HANCHEN, H. Neumessung des Strahlversetzungseffektes bei Totalreflexion. Annalen der Physik, 5, 1949: 251.
59. SCHOCH, A. Seitliche Versetzung eines total reflektierten Strahles bei Ultraschallwellen. Acustica, 2, 1952.
60. GAUNAURD, G.C., and ÜBERALL, H. Acoustics of finite beams. Journal of the Acoustical Society America, 63, 1978: 5-16.
61. BERTONI, H.L. and TAMIR, T. Unified theory of Rayleigh-Angle phenomena for acoustic beams at liquid-solid interfaces. Journal of Applied Physics, 2, 1973: 157-172.
62. LAMB, H. On waves in an elastic plate. Proceedings of the Royal Society, 93A, 1917: 114.
63. MEEKER, T.R. and MEITZLER, A.H. Guided wave propagation in elongated cylinders and plates. In: MASON, W.P., ed. Physical Acoustics; Principles and Methods, Vol. 1A. New York, N.Y., Academic Press, 1964: 112-116.

64. KOLSKY, H. Stress Waves in Solids, 2nd edn. New York, N.Y., Dover Publications, 1963.
65. TAMM, K. and WEIS, O. Wellenausbreitung in unbegrenzten Scheiben und in Scheibenstreifen. Acustica, 11, 1961: 8-17.
66. KRAUTKRÄMER, J. and KRAUTKRÄMER, H. Werkstoffprüfung mit Ultraschall. Berlin, Springer, 1961.
67. Nondestructive evaluation. IEEE Transactions on Sonics and Ultrasonics, 23, (5), 1976: 283-378.
68. ATZENI, C. and MASOTTI, L. Surface acoustic-wave devices. In: SETTE, D. ed. New Directions in Physical Acoustics. Proceedings of the International School of Physics "Enrico Fermi" Course LXIII, Varenna. Amsterdam, North Holland, 1974.
69. OLINER, A.A. ed. Acoustic Surface Waves. Berlin, Springer, 1978.
70. TOLSTOY, I. Guided waves in a fluid with continuously variable velocity overlying an elastic solid: theory and experiment. Journal of the Acoustical Society America, 32, 1960: 81-87.
71. VIKTOROV, I.A. Calculation of the phase velocities of surface waves on the boundary of a solid half-space with a liquid layer. Soviet Physics Acoustics, 23, 1977: 541-542.
72. WHITE, J.E. Seismic Waves: Radiation, Transmission, and Attenuation. New York, McGraw Hill, 1965.
73. SAVIN, V.G. and SHUL'GA, N.A. Rayleigh waves in a regular isotropic layered medium. Soviet Physics Acoustics, 21, 1975: 276-277.
74. ROSENBAUM, J.H. The long-time response of a layered elastic medium to explosive sound. Journal of Geophysical Research, 65, 1960: 1577-1613.
75. PHINNEY, R.A. Leaking modes in the crustal waveguide, Part I: The oceanic PL wave. Journal of Geophysical Research, 66, 1961: 1445-1469.
76. SATO, Y. Study on surface waves - VI: Generation of Love and other types of SH-waves. Bulletin, Earthquake Research Institute, Tokyo University, 30, 1952: 101-120.
77. HARKRIDER, D.G. Surface waves in multi-layered elastic media - 1: Rayleigh and Love waves from buried sources in a multilayered elastic half-space. Bulletin, Seismological Society of America, 54, 1964: 627-680.
78. STANGERUP, P. A detailed study of sound reflections from a layered ocean bottom, SACLANTCEN TR-42. La Spezia, Italy, SACLANT ASW Research Centre, 1965. [AD 466 138]

79. HASTRUP, O.F. Reflection of plane waves from a solid multilayered damping bottom, SACLANTCEN TR-50. La Spezia, Italy, SACLANT ASW Research Centre, 1966. [AD 479 437]
80. HASTRUP, O.F. A detailed analysis of acoustic reflectivity in the Tyrrhenian Abyssal Plain, SACLANTCEN TR-145. La Spezia, Italy, SACLANT ASW Research Centre, 1969. [AD 854 842]
81. HASTRUP, O.F. The effect of periodic bottom layering on acoustic reflectivity, SACLANTCEN TR-149. La Spezia, Italy, SACLANT ASW Research Centre, 1969. [AD 856 029]
82. FRYER, G.J. Reflectivity of the ocean bottom at low frequency. Journal of the Acoustical Society of America, 63, 1978: 35-42.
83. HAWKER, K.E. Influence of Stoneley waves on plane-wave reflection coefficients: characteristics of bottom reflection loss. Journal of the Acoustical Society of America, 64, 1978: 548-555.
84. HAWKER, K.E. Identification of the Stoneley wave mechanism, TP-77-45. Austin, University of Texas, Applied Research Laboratory, 1977.
85. PEKERIS, C.L. Theory of propagation of explosive sound in shallow water. In: Propagation of Sound in the Ocean. Memoir, Geological Society of America, (27), 1948.
86. OFFICER, C.B. Introduction to the Theory of Sound Transmission with Application to the Ocean. New York, N.Y., McGraw Hill, 1958: pp. 127-128.
87. TOLSTOY, I. and CLAY, C.S. Ocean Acoustics; Theory and Experiment in Underwater Sound. New York, N.Y., McGraw Hill, 1966.
88. CLAY, C.S. and MEDWIN, H. Acoustical Oceanography; Principles and Applications. New York, N.Y., Wiley, 1977.
89. INGENITO, F., FERRIS, R.H., KUPERMAN, W.A. and WOLF, S.N. Shallow water acoustics, (Summary Report: First Phase), NRL Rept. 8179. Washington, D.C., U.S. Naval Research Laboratory, 1978.
90. JENSEN, F.B. and FERLA, M.C. SNAP: The SACLANTCEN normal-mode acoustic propagation model, SACLANTCEN SM-121. La Spezia, Italy, SACLANT ASW Research Centre, 1979. [AD A 067 256]
91. BRADLEY, D. and HUDIMAC, A.A. The propagation of sound in a wedge shaped shallow water duct, NOLTR 70-235. White Oak, Md., U.S. Naval Ordnance Laboratory, 1970. [AD 716 744]
92. GRAVES, R.D., NAGL, A., ÜBERALL, H., HAUG, A.J. and ZARUR, G.L. Range-dependent normal modes in underwater sound propagation. In: BACHMANN, W. and WILLIAMS, R.B., eds. Oceanic acoustic modelling. Proceedings of a conference held at SACLANTCEN on 8-11 September 1975, SACLANTCEN CP-17: Part 7: Field calculations. La Spezia, Italy, SACLANT ASW Research Centre, 1975: pp. 35/1-35/9.

93. GRAVES, R.D., NAGL, A., ÜBERALL, H. and ZARUR, G.L. Range-dependent normal modes in underwater sound propagation: application to the wedge-shaped ocean. Journal of the Acoustical Society of America, 58, 1975: 1171-1177.
94. CHWIEROTH, F.S., NAGL, A., ÜBERALL, H., GRAVES, R.D. and ZARUR, G.L. Mode coupling in a sound-channel with range-dependent parabolic velocity profile. Journal of the Acoustical Society of America, 64, 1978: 1105-1112.
95. MARCUSE, D. Radiation losses of tapered dielectric slab waveguides. Bell System Technical Journal, 49, 1970: 273-290.
96. TIEN, P.K. and MARTIN, R.J. Experiments on light-waves in a thin tapered film and a new light-wave coupler. Applied Physics Letters, 18, 1971: 398-401.
97. WINN, R.K. and HARRIS, J.H. Coupling from multimode to single mode linear waveguides using horn-shaped structures. IEEE Transactions on Microwave Theory and Techniques, 23, 1975: 92-97.
- 98a COPPENS, A. The model: transmission of sound into a fast fluid bottom from an overlying fluid wedge. In: U.S. DEPARTMENT OF THE NAVY, OFFICE OF NAVAL RESEARCH. Proceedings, workshop on seismic propagation in shallow water, 6-7 July, 1978. Arlington, Va, U.S. Office of Naval Research, 1978: pp. 11/1-11/8.
- 98b SANDERS, J. The experiment: transmission of acoustic waves into a fast fluid bottom from a converging fluid wedge. In: U.S. DEPARTMENT OF THE NAVY, OFFICE OF NAVAL RESEARCH. Proceedings, workshop on seismic propagation in shallow water, 6-7 July, 1978. Arlington, Va, U.S. Office of Naval Research, 1978: pp. 12/1-12/10.
99. ODOM, R.J., Jr., SIEGELMANN, R.A., MITCHELL, G. and REYNOLDS, D.K. Ocean-earth acoustic coupling, TR-209. San Diego, Cal., U.S. Naval Ocean Systems Center, 1978.
100. JENSEN, F.B. and KUPERMAN, W.A. Environmental acoustic modelling at SACLANTCEN, SACLANTCEN SR-34. La Spezia, Italy, SACLANT ASW Research Centre, 1979. [AD A 081 853]
101. SMIRNOV, V. and SOBOLEV, S. On a new method in the problem of elastic vibrations. Trudy Seismologicheskaya Instituta Akademiyi Nauk SSSR, (20), 1932.
102. SMIRNOV, V. and SOBOLEV, S. On the application of a new method of investigation of the elastic vibrations in space with axial symmetry. Trudy Seismologicheskaya Instituta Akademiyi Nauk SSSR, (29), 1933.
103. GILBERT, F., LASTER, S.J., BARKUS, M.M. and SCHELL, R. Observation of pulses on an interface. Bulletin, Seismological Society of America, 52, 1962: 847-868.
104. SPITZNOGLE, F.R. The propagation at short ranges of elastic waves from an impulsive source at a liquid-solid interface: The fluid - two-layer-solid system, Rep. No. 206. Panama City, Fla, U.S. Navy Mine Defense Laboratory, 1963.



105. SPITZNOGLE, F.R. and McLEROY, R.G. Propagation at short ranges of elastic waves from an impulsive source near a fluid-two-layer-solid interface. Journal of the Acoustical Society of America, 35, 1963: 1808-1815.
106. SPITZNOGLE, F.R., NELSON, V.C., McLEROY, E.G. Theoretical and experimental propagation of elastic waves in a fluid-solid-solid layered system, Rep. No. 1-49. Panama City, Fla, U.S. Navy Mine Defense Laboratory, 1963.
107. SPITZNOGLE, F.R. and McLEROY, E.G. Computed pressure-time waveforms for an impulsive source near a fluid-two-layer-solid interface. Journal of the Acoustical Society of America, 36, 1964: 972-973.
108. NELSON, V.C., SPITZNOGLE, F.R. and McLEROY, E.G. Attenuation of Rayleigh-shear and Stoneley waves, and geometric scaling laws in fluid-solid models, Interim Report i-67. Panama City, Fla, U.S. Navy Mine Defense Laboratory, 1964.
109. VICTOR, A.S. and McLEROY, E.G. Theoretical and experimental propagation of elastic waves in an air-fluid-solid and in an air-fluid-solid system, Rep. No. i-68. Panama City, Fla, U.S. Navy Mine Defense Laboratory, 1964.
110. VICTOR, A.S., SPITZNOGLE, F.R. and McLEROY, E.G. Propagation at short ranges of elastic waves from an impulsive source in a shallow fluid overlying a layered elastic solid. Journal of the Acoustical Society of America, 37, 1965: 894-898.
111. JAKOSKY, J.S. Exploration Geophysics, 2nd edn. Newport Beach, Cal., Trija Publ. Co., 1960: pp. 779-796.
112. EVENDEN, B.S., STONE, G.R. Seismic Prospecting Instruments: Vol. 2: Instrument Performance and Testing. Berlin, Borntraeger, 1971.
113. SCHERBATSKOY, S.A. and NEUFELD, J. Fundamental relations in seismometry. Geophysics, 2, 1937: 188-213.
114. GEOSPACE CORPORATION. Geophone response equations and their application, Technical Information Note 100-6. Houston, Texas, Geospace Corporation.
115. HECHT, R.J. Background of the problems associated with seismic detection of signal sources in the ocean. In: U.S. DEPARTMENT OF THE NAVY, OFFICE OF NAVAL RESEARCH. Proceedings, Workshop on seismic propagation in shallow water, 6-7 July, 1978. Arlington, Va, U.S. Office of Naval Research, 1978: pp. 1/1-1/23.
116. ARNETT, R.A. and NEWHOUSE, T.W. Ocean-bottom seismograph. Proceedings of the IEEE, 53, 1965: 1899-1905.
117. SUTTON, G.H., McDONALD, W.G., PRENTISS, D.D. and THANOS, S.N. Ocean-bottom seismic observatories. Proceedings of the IEEE, 53, 1965: 1909-1921.

118. HECHT, R.J. Investigation of the potentialities of using seismic sensors for the detection of ships and other naval platforms. Washington, D.C. U.S. Office of Naval Research, 1978. [AD A 063 218].
119. LATHAM, G.V. Seismic measurements on the sea floor. In: U.S. DEPARTMENT OF THE NAVY, OFFICE OF NAVAL RESEARCH. Proceedings, workshop on seismic propagation in shallow water, 6-7 July, 1978. Arlington, Va, U.S. Office of Naval Research, 1978: pp. 9/1-9/32.
120. NAFE, J.E. and DRAKE, C.L. Physical properties of marine sediments. In: HILL, M.N., ed. The Sea; Ideas and Observations on Progress in the Study of the Seas, Vol. 3: The Earth Beneath the Sea. New York, N.Y., Wiley, 1963: 794-815.
121. EWING, J.I., and NAFE, J.E. The unconsolidated sediments. In: HILL, M.N., ed. The Sea; Ideas and Observations on Progress in the Study of the Seas, Vol. 3: The Earth Beneath the Sea. New York, N.Y., Wiley, 1963: 73-84.
122. HAMPTON, L.D. Acoustic properties of sediments. Journal of the Acoustical Society of America, 42, 1967: 882-890.
123. HAMILTON, E.L. Elastic properties of marine sediments. Journal of Geophysical Research, 76, 1971: 579-604.
124. HAMILTON, E.L. Acoustic properties of the sea floor. In: BACHMANN, W. and WILLIAMS, R.B., eds. Oceanic acoustic modelling. Proceedings of a conference held at SACLANTCEN on 8-11 September 1975, SACLANTCEN CP-17: Part 4: Sea Bottom. La Spezia, Italy, SACLANT ASW Research Centre, 1975: pp. 18/1-18/96. [AD A 020 936]
125. HAMPTON, L., ed. Physics of Sound in Marine Sediments. New York, N.Y., Plenum, 1974.
126. STOLL, R.D. Acoustic waves in saturated sediments. In: HAMPTON, L., ed. Physics of Sound in Marine Sediments. New York, N.Y., Plenum, 1974: 19-39.
127. HAMILTON, E.L. Geoacoustic models of the sea floor. In: HAMPTON, L., ed. Physics of Sound in Marine Sediments. New York, N.Y., Plenum, 1974: 181-221.
128. STOLL, R.D. Acoustic waves in ocean sediments. Geophysics, 42, 1977: 715-725.
129. HAMILTON, E.L., SHYMWAY, G., MENARD, H.W. and SHIPEK, C.J. Acoustic and other physical properties of shallow-water sediments off San Diego. Journal of the Acoustical Society of America, 28, 1956: 1-15.
130. HAMILTON, E.L. Sound velocity and related properties of marine sediments, North Pacific. Journal of the Acoustical Society of America, 75, 1970: 4423-4426.
131. HAMILTON, E.L. Thickness and consolidation of deep-sea sediments. Bulletin, Geological Society of America, 70, 1959: 1399-1424.

132. ANSTEY, N.A. Seismic Prospecting Instruments; Vol. 1: Signal Characteristics and Instrument Specifications. Berlin, Borntraeger, 1971.
133. MUSKAT, M. The theory of refraction shooting. Physics, 4, 1933: 14-38.
134. EWING, J.I. Elementary theory of seismic refraction and reflection measurements. In: HILL, M.N., ed. The Sea; Ideas and Observations on Progress in the Study of the Seas, Vol. 3: The Earth Beneath the Sea. New York, N.Y., Wiley, 1963: 3-19.
135. SHOR, G.G. Jr. Refraction and reflection techniques and procedure. In: HILL, M.N., ed. The Sea; Ideas and Observations on Progress in the Study of the Seas, Vol. 3: The Earth Beneath the Sea. New York, N.Y., Wiley, 1963: 20-38.
136. MUSGRAVE, A.W. Seismic Refraction Prospecting. Tulsa, Okla, Society of Exploration Geophysicists, 1967.
137. BELL, D.L. and PORTER, W.J. Remote sediment classification potential of reflected acoustic signals. In: HAMPTON, L., ed. Physics of Sound in Marine Sediments. New York, N.Y., Plenum, 1974: 319-335.
138. AKAL, T. Acoustical characteristics of the sea floor: experimental techniques and some examples from the Mediterranean sea. In: HAMPTON, L., ed. Physics of Sound in Marine Sediments. New York, N.Y., Plenum, 1974: 447-480.
139. HAMILTON, E.L., BACHMAN, R.T., CURRAY, J.R. and MOORE, D.G. Sediment velocities from sonobuoys: Bengal Fan, Sunda Trench, Andaman Basin and Nicobar Fan. Journal of Geophysical Research, 82, 1977: 3003-3012.
140. AKAL, T. The relationship between the physical properties of underwater sediments that affect bottom reflection. Marine Geology, 13, 1972: 251-266.
141. HAMILTON, E.L. Sediment sound velocity measurements made in situ from the bathyscaph TRIESTE. Journal of Geophysical Research, 68, 1963: 5991-5998.
142. HAMILTON, E.L., BUCKER, H.P., KEIR, D.L. and WHITNEY, J.A. Velocities of compressional and shear waves in marine sediments determined in situ from a research submersible. Journal of Geophysical Research, 75, 1970: 4039-4049.
143. ANDERSON, A.L. and HAMPTON, L.D. A method for measuring in situ acoustic properties during sediment coring. In: HAMPTON, L., ed. Physics of Sound in Marine Sediments. New York, N.Y., Plenum, 1974: 357-371.
144. SHIRLEY, D.J. and ANDERSON, A.L. In situ measurement of marine sediment acoustical properties during coring in deep water. IEEE Transactions on Geoscience Electronics, 13, 1975: 163-169.

145. SHIRLEY, D.J. Determination of the acoustic properties of deep ocean sediments from in situ profiles, TR. Austin, Texas, University of Texas, Applied Research Laboratories, 1976.
146. BRADNER, H. Probing sea-bottom sediments with microseismic noise. Journal of Geophysical Research, 68, 1963: 1788-1791.
147. BUCKER, H.P., WHITNEY, J.A. and KEIR, D.L. Use of Stoneley waves to determine the shear velocity in ocean sediments. Journal of the Acoustical Society of America, 36, 1964: 1595-1596.
148. HAMILTON, E.L. Variations of density and porosity with depth in deep-sea sediments. Journal of Sedimentary Petrology, 46, 1976: 280-300.
149. HAMILTON, E.L. Low sound velocities in high-porosity sediments. Journal of the Acoustical Society of America, 28, 1956: 16-19.
150. HAMILTON, E.L. Sound velocity-density relations in sea-floor sediments and rocks. Journal of the Acoustical Society of America, 63, 1978: 366-377.
151. HAMILTON, E.L. Sound channels in surficial marine sediments. Journal of the Acoustical Society of America, 48, 1970: 1296-1298.
152. CHRISTENSEN, R.E. and GEDDES, W.H. Refraction of sound in the sea floor. In: BACHMANN, W. and WILLIAMS, R.B., eds. Oceanic acoustic modelling. Proceedings of a conference held at SACLANTCEN on 8-11 September 1975, SACLANTCEN CP-17: Part 4: Sea Bottom. La Spezia, Italy, SACLANT ASW Research Centre, 1975: pp. 16/1-16/17. [AD R 020 936]
153. CHRISTENSEN, R.E., FRANK, J.A., and GEDDES, W.H. Low-frequency propagation via shallow refracted paths through deep ocean unconsolidated sediments. Journal of the Acoustical Society of America, 57, 1975: 1421-1426.
154. HAMILTON, E.L. Sound attenuation as a function of depth in the sea floor. Journal of the Acoustical Society of America, 59, 1976: 528-535.
155. HAMILTON, E.L. Shear-wave velocity versus depth in marine sediments: a review. Geophysics, 41, 1976: 985-996.
156. SHIRLEY, D.J. and ANDERSON, A.L. Shear waves in unconsolidated sediments, TR. Austin, Texas, University of Texas, Applied Research Laboratories, 1976.
157. HAMILTON, E.L. Attenuation of shear waves in marine sediments. Journal of the Acoustical Society of America, 60, 1976: 334-338.
158. ROSS, D. Mechanics of Underwater Noise. New York, N.Y., Pergamon Press, 1976.
159. ARASE, E.M. and ARASE, T. Underwater ambient noise. In: STEPHENS, R. and LEVENTHALL, H., eds. Acoustics and Vibration Progress. London, Chapman and Hall, 1974.

175. ASADA, T. and SHINAMURA, H. Observation of earthquakes and explosions at the bottom of the western Pacific: structure of the lithosphere revealed by LONG SHOT experiment. Geophysical Monograph, American Geophysical Union, 19, 1976: 135-153.
176. Nuclear test detection issue. Proceedings of the IEEE, 53, 1965: 1813-2108.
177. WORZEL, J.L. and EWING, M. Explosion sounds in shallow water. In: Propagation of Sound in the Ocean. Memoir, Geological Society of America, 27, 1948.
178. WORLEY, R.D. and WALKER, R.A. Low frequency measurements in the Gulf of Maine. Journal of Underwater Acoustics, 9, 1959: 435.
179. BLAIK, M. and CLAY, C.S. Detection in the ground of sound from a source in shallow water, TR-76. Dobbs Ferry, N.Y., Columbia University, Hudson Labs., 1959.
180. SHORTHOUSE, J.M. Seismic measurements on the deep sea bed. Ph.D. Thesis, Department of Geodesy and Geophysics, University of Cambridge, U.K.
181. DAVIES, D. Dispersed Stoneley waves on the ocean bottom. Bulletin, Seismological Society of America, 55, 1965: 903-918.
182. McLEROY, E.G. and DELOACH, A. Measurements of sea bottom elastic waves from underwater explosions, Rep. No. U2727. Panama City, Fla, U.S. Navy Mine Defense Laboratory, 1968.
183. URICK, R.J. and COLVIN, G.M. Detection of underwater sounds by a geophone planted in the bottom, TR 68-102. White Oak, Md, U.S. Naval Ordnance Laboratory, 1968.
184. URICK, R.J. Underwater sound transmission through the ocean floor. In: HAMPTON, L., ed. Physics of Sound in Marine Sediments. New York, N.Y., Plenum, 1974: 161-180.
185. BUCKER, H.P. U.S. Naval Ocean Systems Center, San Diego, Cal., 92152, Private communication, 1977.
186. McLEROY, G. The NCSC shallow water seismic propagation study. In: U.S. DEPARTMENT OF THE NAVY, OFFICE OF NAVAL RESEARCH. Proceedings, workshop on seismic propagation in shallow water, 6-7 July, 1978. Arlington, Va, U.S. Office of Naval Research, 1978: pp. 4/1-4/28.
187. RAUCH, D. Comparison of low-frequency acoustic and seismic propagation in shallow water; some preliminary modelling results, NATO UNCLASSIFIED. In: Papers presented to the 33rd Meeting of the SACLANTCEN Scientific Committee of National Representatives, 17-19 October, 1978, SACLANTCEN CP-23, NATO CONFIDENTIAL. La Spezia, Italy, SACLANT ASW Research Centre, 1978: 7/1-7/7. [AD C 017 366]
188. WEINSTEIN, M.S. Spectra of acoustic and seismic signals generated by underwater explosions during chase experiment. Journal of Geophysical Research, 73, 1968: 5473-5476.

189. THOMSON, W.T. Transmission of elastic waves through a stratified solid medium. Journal of Applied Physics, 21, 1950: 89-93.
190. HASKELL, N.A. The dispersion of surface waves on multilayered media. Bulletin, Seismological Society of America, 43, 1953: 17-34.
191. BRIGHAM, E.O. The Fast Fourier-Transform. Englewood Cliffs, N.J., Prentice-Hall, 1974.
192. KUTSCHALE, H.W. Rapid computation by wave theory of propagation loss in the Arctic ocean, Tech. Rep. CU-8-73. Palisades, N.Y., Lamont-Doherty-Geological Observatory of Columbia, 1973.
193. DORMAN, J. Period equation for waves of Rayleigh type on a layered liquid-solid half-space. Bulletin, Seismological Society of America, 52, 1962: 389-397.
194. HARKRIDER, D.G. Surface waves in multilayered elastic media: I. Rayleigh and Love waves from buried sources in a multilayered elastic half-space. Bulletin, Seismological Society of America, 54, 1964: 627-679.
195. MARSH, H.W. and ELAM, S.R. Internal Document. New London, Conn, Raytheon Company, Marine Research Laboratory, 1967.
196. DINAPOLI, F.R. Fast field program for multilayered media, Rep. No. 4103. Newport, R.I., U.S. Naval Underwater Systems Center, 1971.
197. KUPERMAN, W.A. SACLANT ASW Research Centre. La Spezia, Italy. Private communication, 1979.
198. BRADNER, H., DODDS, J. and FOULKES, R. Coherence measurements with time sampling ocean-bottom seismometers. Proceedings of the IEEE, 53, 1965: 1906-1908.

A P P E N D I X

## APPENDIX A

## POST-1978 WORK AT SACLANTCEN

## INTRODUCTION

The main text was drafted in late 1978 but other priorities delayed its publication until the end of 1980. Thus its references are to the open literature published before 1979 and the comments made in Sect. 2.4 about SACLANTCEN's unsuccessful field work are valid only for the early stages of SACLANTCEN's project on bottom interface waves.

In late 1978 SACLANTCEN's tri-axial sensor-package and its radio-buoy were completely re-designed and the first version of a new system was built in early 1979. The following pages briefly describe these more advanced tools and present a few typical results from our 1979 sea trials.

A.1 New Equipment

Besides a change to an all-digital technique the main break-through was obtained by using a new type of active and lightweight 1 Hz geophones (Teledyne Geotech S-500). These sensors do not need blocking for transportation and, because they can be applied in any orientation, do not have to be precisely levelled for proper operation. The seismic sensor set is completed by a variable-depth hydrophone mounted outside the container of the ocean-bottom seismometer (OBS) or floating above it. Figure A1 shows how this sensor package is installed in shallow water together with its radio buoy.

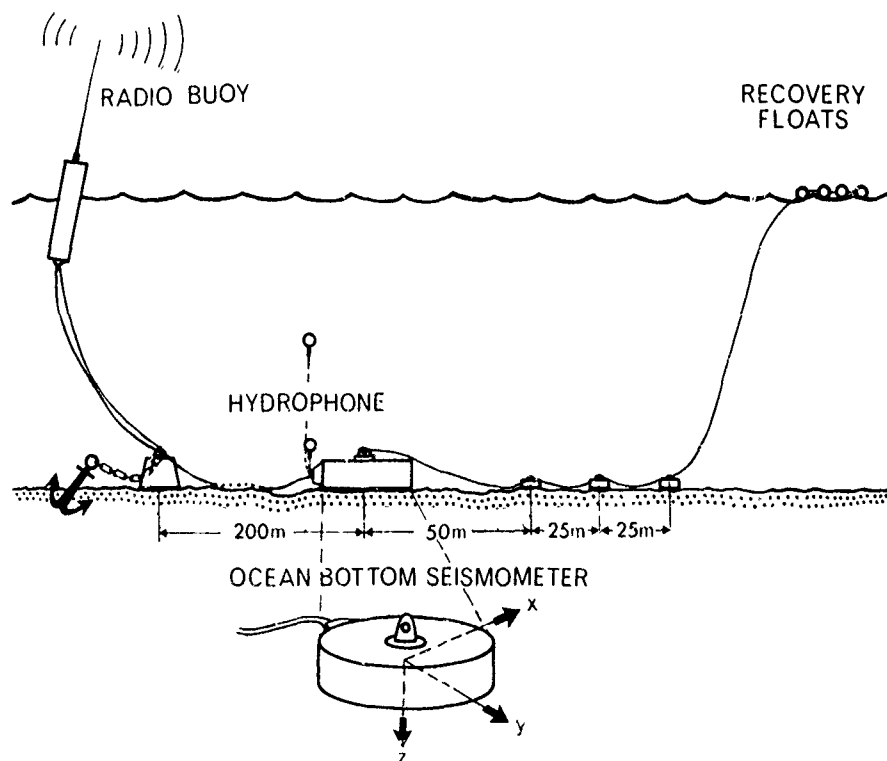


FIG. A1 INSTALLATION OF THE SENSOR PACKAGE ON THE SEA FLOOR AND MOORING OF ITS RADIO BUOY IN SHALLOW WATER



Figure A2(a) presents a simplified block-diagram of the pertinent electronics, which are similar to those described by Blackinton and Odegard <A.1>.

The output of each of the four basic sensors is preamplified, low-pass filtered (100 Hz), and fed direct and via three additional amplifier-stages of 18 dB each into a  $4 \times 4$  channel multiplexer. Each of the four signal levels is scanned with a sampling frequency of 600 Hz, and the optimally-amplified signal is transmitted to a fast 12-bit A/D converter. The resulting 12-bit mantissa is then combined with the pertinent 2-bit exponent, with a parity bit, and with another independent bit to a basic data word of 16 bits. After three scanning cycles of the basic sensors we thus have available twelve additional bits for the transmission of important parameters and control data. Eleven of those are used to form a secondary data word, which is cyclically assigned to one of the four auxiliary sensors (compass, tilt X, tilt Y and temperature) and one of the four electronic checkpoints. Thus, every 24 basic scanning cycles we can not only monitor the actual position of the OBS, the nearby water temperature, and the power supply of four important networks, but also have at our disposal an additional set of eight bits to use for the OBS station's identification code. These digital data-sequences are transferred to the surface buoy via a coaxial cable and from there to the receiving ship by a FM-modulated radio-transmitter (170 MHz, max 15 W) in the surface buoy. This buoy also houses the rechargeable batteries that power the complete system and a radio receiver for the ON-OFF commands sent from the receiving platform. Every time the OBS is switched on, a calibration signal is automatically applied to each geophone calibration coil for about one to two minutes. One of the most prominent features of this digital OBS is given by the very high dynamic range of 120 dB (66 dB from the 12-bit mantissa and 54 dB from the 2-bit exponent), which enables us to cope simultaneously with a low-level seismic background and high-level deterministic signals from nearby CW-sources or explosions.

Figure A2(b) shows the corresponding block-diagram of the data-acquisition and pre-processing facilities on board. Here we are using a Hewlett-Packard 21 MX computer with disc unit, which gives us the possibility of getting a printout or a plot of all essential data channels a few seconds after recording an event.

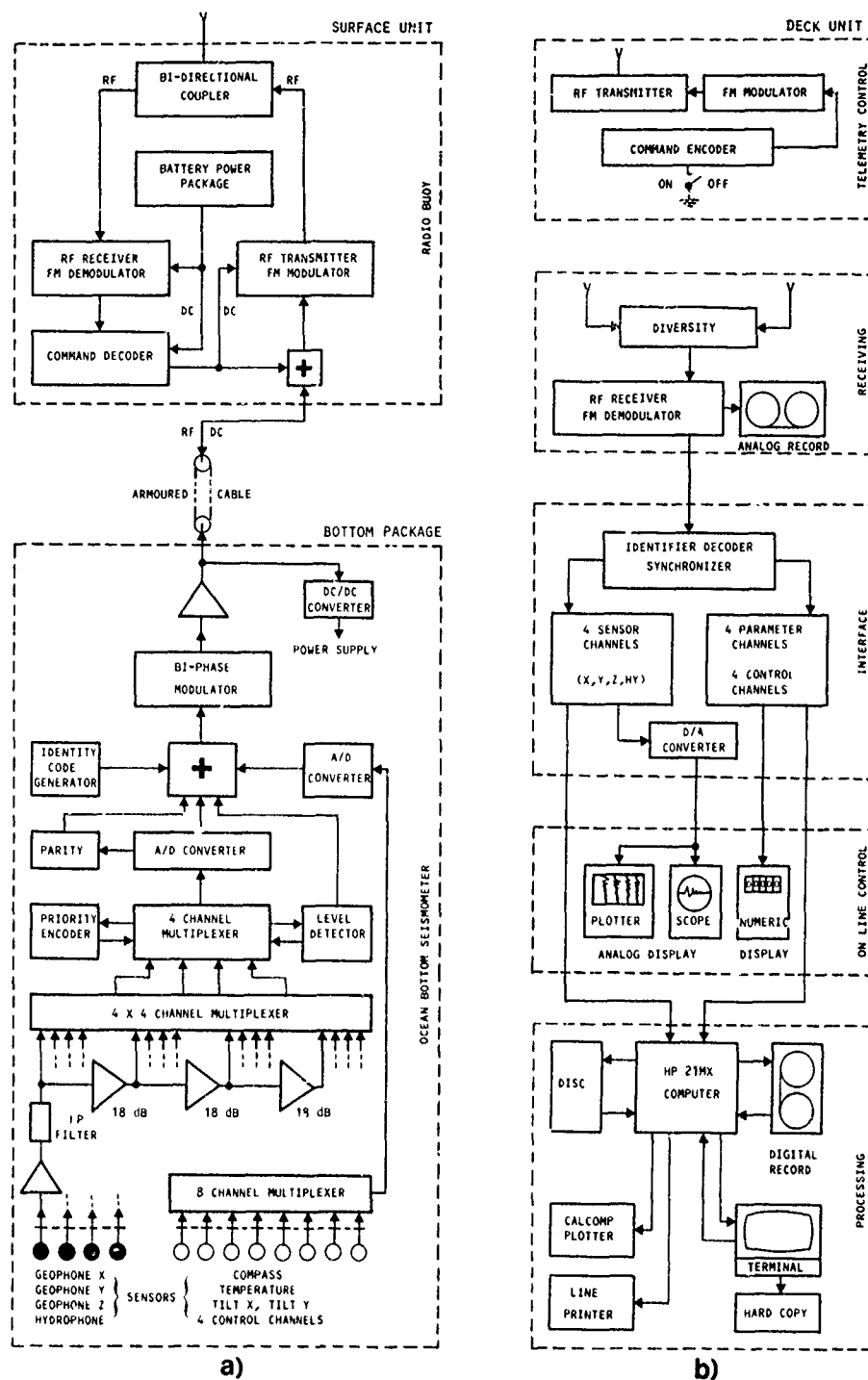


FIG. A2 ELECTRONIC BLOCK-DIAGRAM FOR:  
 (a) the OBS and its radio-buoy,  
 (b) the onboard receiving, recording, controlling and pre-processing systems

## A.2 Experimental Results

Figure A3 indicates two positions off the Italian coast where the instruments were deployed during a cruise in 1979. The sensor station was always oriented in such a way that the directions of the planned acoustic runs (at constant water depth or a sloping sea floor) coincided with the axis of one of the two horizontal geophones. As sound sources we used small TNT charges, which were usually placed on the sea floor and fired electrically.

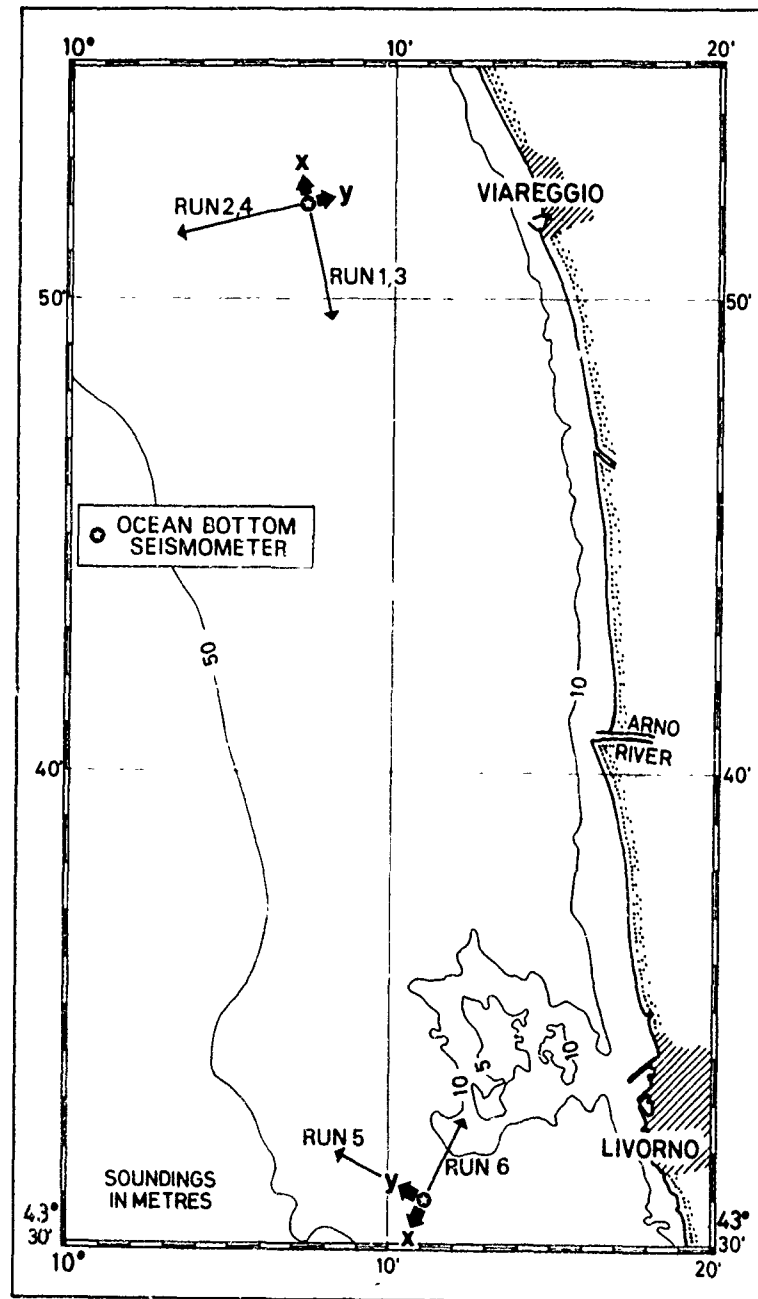


FIG. A3 THE OPERATIONAL AREA OFF THE VERSILIAN COAST (ITALY)  
WITH THE TWO CHOSEN OBS-POSITIONS

To discuss some of the typical features of the interface waves, we will look first at an event from Run 3 along the 20 m depth profile off Viareggio, where the hydrophone was floating in the middle of the water column. Figure A4 presents a lineprinter plot of the four time-series generated by a charge of 180 g TNT at a distance of about 1.3 km. The lower three traces display the measured particle velocities,  $u$ ,  $v$  and  $w$ , while the upper trace shows the pressure history recorded by the hydrophone. The latter channel was always subject to an additional pre-amplification of 30 dB. Due to this scaling factor we usually had to clip the first arrival, which was formed by the unavoidable, high-frequency water wave. On this and all following plots the time-series were passed through a 10 Hz low-pass filter to stay below the cut-off frequency of the water duct.

The interface wave we are looking for arrives somewhat later than the water wave. As expected from our geometrical consideration, this interface wave is detected only by the vertical geophone GeoZ and the radial one GeoX, which is horizontal and oriented parallel to the direction of propagation. The ripples on the output of the transverse sensor GeoY are probably due to imperfections of the wave guide and lateral inhomogeneities.

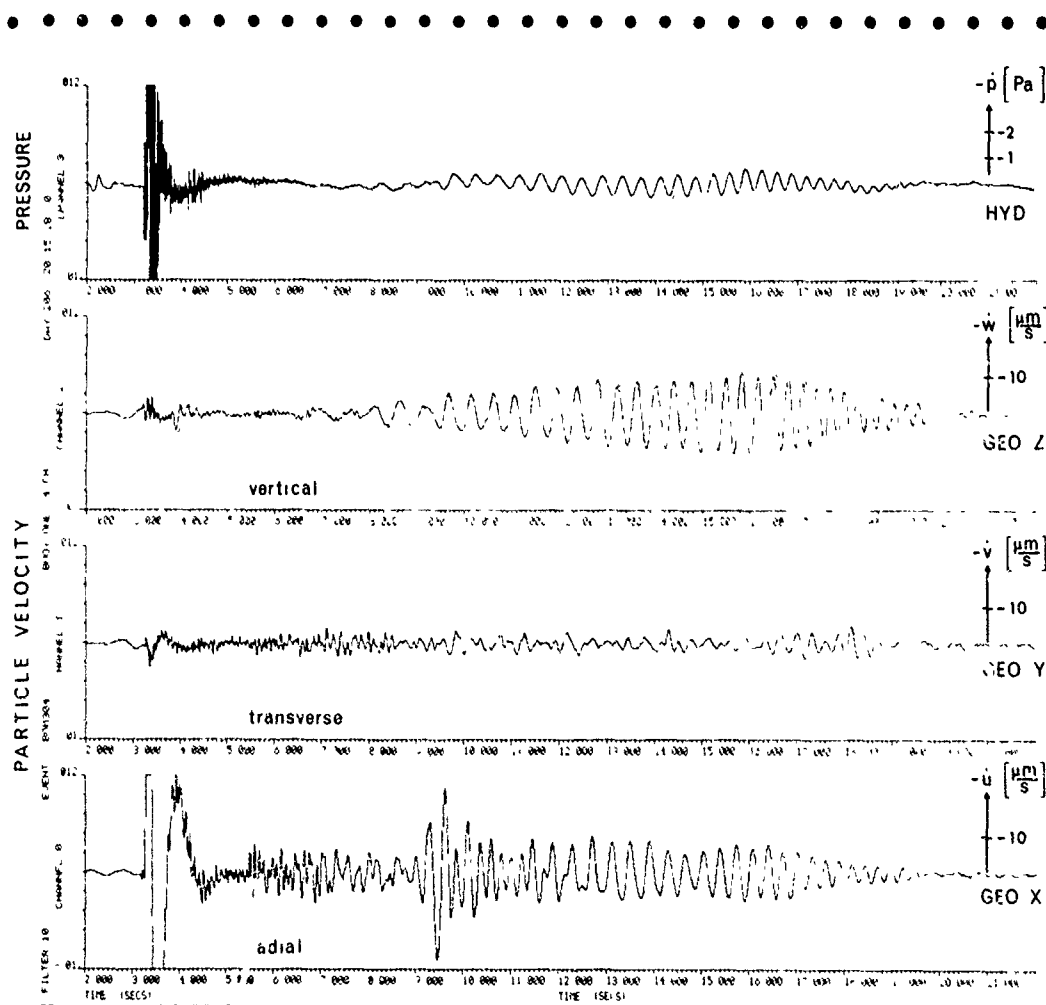


FIG. A4 LINE-PRINTER PLOT OF THE SIGNALS FROM THE FOUR BASIC SENSORS (180 g TNT FIRED AT 1.3 km DISTANCE)

The wavelet itself consists of a long-lasting, narrow-band signal that shows the expected normal dispersion, indicating that the higher frequencies are left behind. Especially at the output of the radial sensor GeoX we realize that the beginning of the main signal is concealed by another superimposed wavelet that has relatively-high amplitudes and an extremely small bandwidth. In agreement with the theoretical predictions, the hydrophone also senses the low-frequency pressure variations created by the interface wave.

As a final check for identification we have displayed the corresponding velocity vector in the radial/vertical X-Z plane using the radial velocity  $u$  as abscissa and the vertical velocity  $w$  as ordinate. At the top of Fig. A5 we have therefore again plotted the appropriate sections (windows) of both signals and below we have displayed the resulting hodographs for 14 successive one-second windows.

Due to the above-mentioned superimposed wavelet, the first four windows A-D are still quite irregular and curve B especially seems to be complicated by the superimposition of a horizontal ellipse. This latter feature could indicate the coexistence of a higher mode. Nevertheless, the following ten hodographs (E to N) form very regular vertical ellipses that are circumscribed clockwise or prograde. Towards the tail of the signals these ellipses fade away and merge into the background noise.

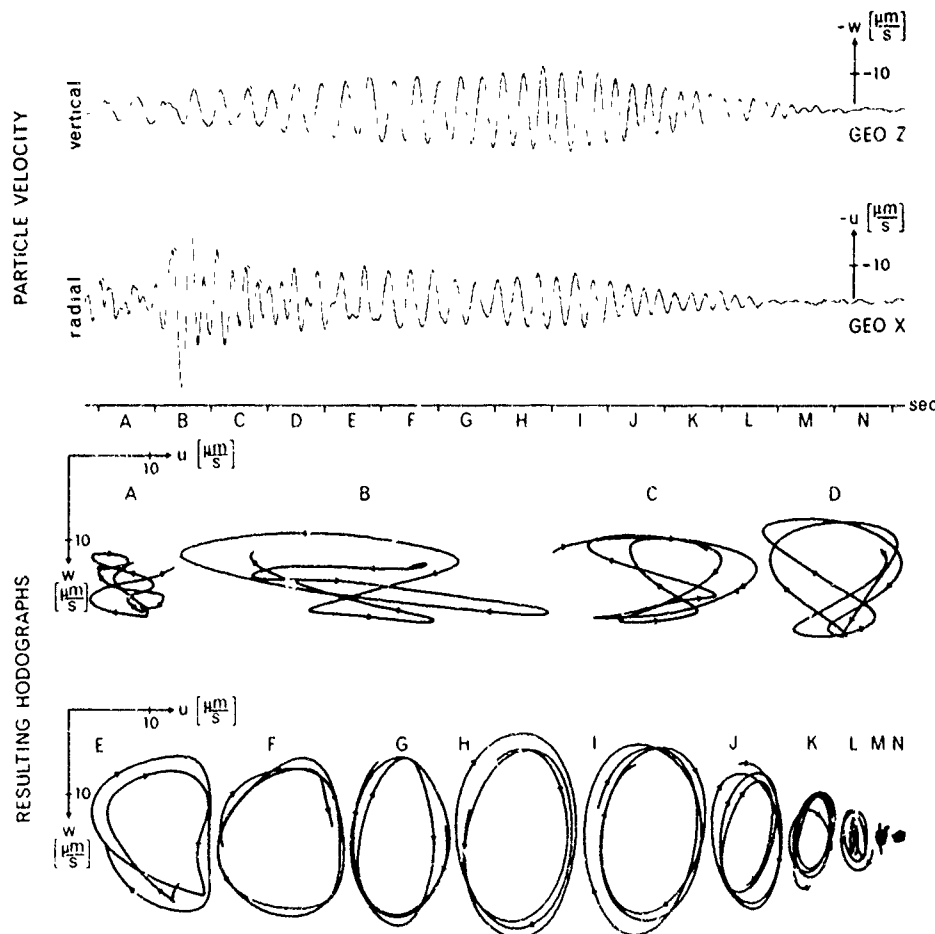


FIG. A5 RADIAL AND VERTICAL PARTICLE VELOCITY OF THE INTERFACE WAVELET IN FIG. A4 WITH THE RESULTING HODOGRAPHS

After this unambiguous identification of the wave type we would like to discuss more carefully some of its propagation characteristics. For this purpose we have stacked in Fig. A6(a) the output of the vertical geophone GeoZ for Run 2, using the same scale for all signals but increasing the actual charge size with growing distance according to the indication on the right-hand side.

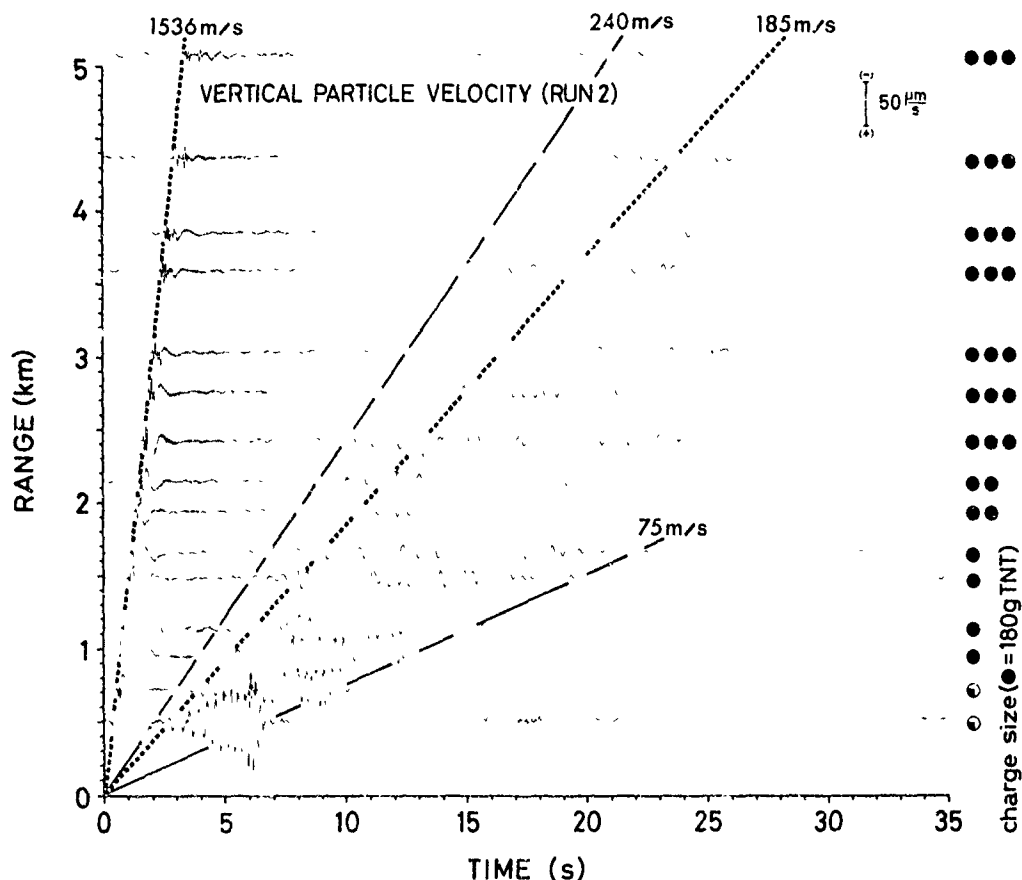


FIG. A6 (a) STACKING OF THE VERTICAL PARTICLE-VELOCITY FOR AN ACOUSTIC RUN OVER A LAYERED SEDIMENT-BOTTOM

As reference quantity, the first dotted line marks the onset of the unavoidable water wave propagating with a velocity of 1536 m/s. The first continuous line indicates the front of the seismic signal, which is roughly characterized by 1.5 to 2 Hz oscillations and a velocity of about 240 m/s, while the second continuous line marks the tail of the signal with 4 to 5 Hz oscillations and a velocity of 75 m/s. In our plot this latter tail of the seismic wavelet disappears at distances of about 1 km due to the frequency-dependence of the attenuation; this dependence may be linear, as is known from P- and S-wave propagation at higher frequencies. The attenuation coefficients for this and several other data sets will be calculated properly and reported separately.

The seismic wave-guide under consideration thus offers optimal propagation conditions for frequencies below 3 Hz. The second dotted line emphasizes the above-mentioned superimposed wavelet, which has a propagation velocity of 185 m/s.

Figure A6(b) shows the stacking of the corresponding output of the radial geophone GeoY. Here the onset of the interface wave is more hidden by some refracted arrivals but the superimposed wavelet is much more pronounced and reveals its very narrow frequency band of 2.5 to 3 Hz.

Modelling this special wave-propagation phenomenon with the Centre's FFP-Program showed that the theory indeed predicts seismograms composed of a long-lasting dispersed wave train (zeroth mode) and a super-imposed, pulse-like, more-or-less monochromatic wavelet (first mode). A more detailed discussion of our measurements and their theoretical aspects was presented <A.2> at the conference on Bottom-Interacting Ocean Acoustics Conference held at SACLANTCEN in June 1980. In a second paper <A.3> at the same conference we demonstrated that in shallow-water areas ambient and ship-induced infrasonic noise is transmitted in the form of Scholte waves and thus offers the possibility of determining the bearing of the source.

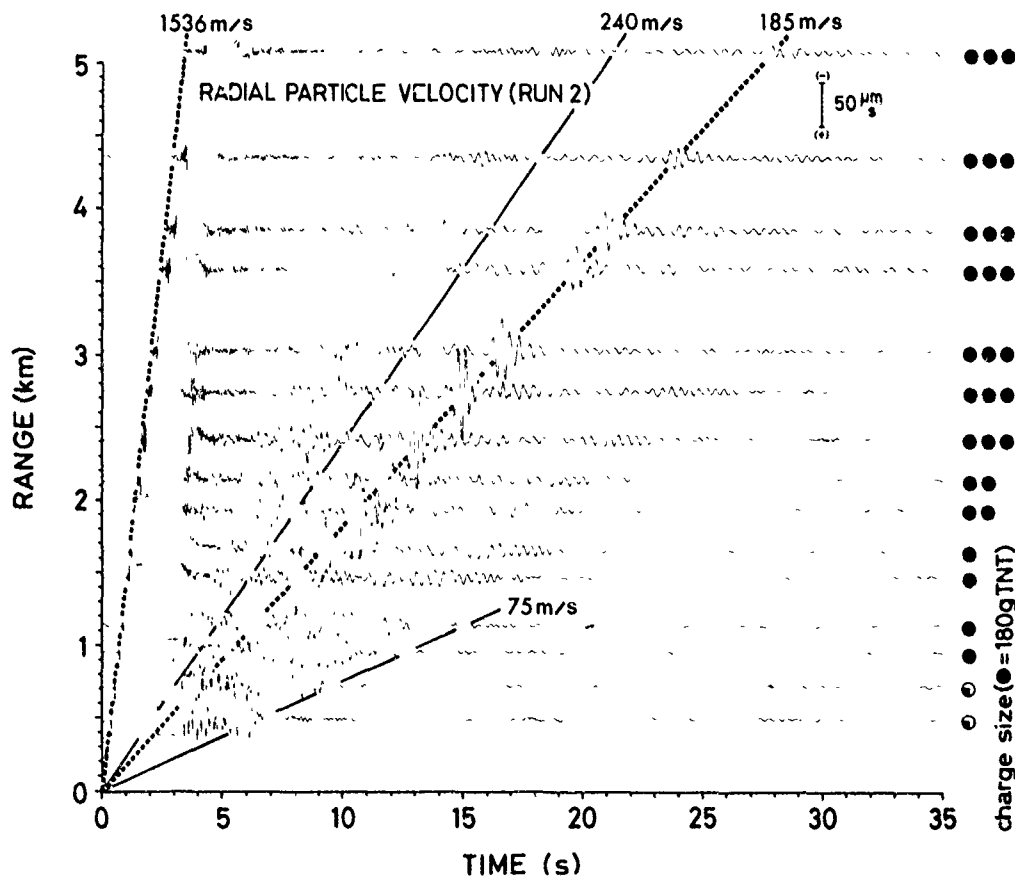


FIG. A6 (b) STACKING OF THE RADIAL PARTICLE-VELOCITY FOR THE SAME ACOUSTIC RUN AS IN A6(a)

REFERENCES

- A.1 BLACKINGTON, J.G. and ODEGARD, M.E. An ocean-bottom seismograph using digital telemetry and floating-point conversion. IEEE Trans. Geoscience Electronics GE-15: 74-82 (1977).
- A.2 RAUCH, D. Experimental and theoretical studies of seismic interface waves in coastal waters. In: KUPERMAN, W.A. and JENSEN, F.B., eds. Bottom-interacting ocean acoustics conference, June 9-13, 1980. SACLANT ASW Research Centre, La Spezia, Italy. (To be published by Plenum Press).
- A.3 SCHMALFELDT, B. and RAUCH, D. Ambient and ship-induced low-frequency noise in shallow water. In: KUPERMAN, W.A. and JENSEN, F.B., eds. Bottom-interacting ocean acoustics conference, June 9-13, 1980. SACLANT ASW Research Centre, La Spezia, Italy. (To be published by Plenum Press).



END

DATE  
FILMED

3-81

DTIC